IPP-Report

Max-Planck-Institut
für Plasmaphysik

Daniel Neuwirth

Erzeugung von Ammoniak in Endladungen mit Stickstoff im Tokamak ASDEX Upgrade

Formation of ammonia during nitrogen seeded discharges at the Tokamak ASDEX Upgrade

IPP 17/33
Februar, 2012

Physik-Department

Technische Universität München

Formation of ammonia during nitrogen seeded discharges at the Tokamak ASDEX Upgrade

Diplomarbeit von Daniel Neuwirth

durchgeführt am Max-Planck-Institut für Plasmaphysik

Contents

1 Introduction **2**
1.1 Nuclear Fusion . . . 2
1.2 Magnetic Confinement and Divertor Setup . . . 3
1.3 Nitrogen Seeding . . . 5

2 Mass spectrometry at ASDEX Upgrade **6**
2.1 Quadrupole mass spectrometer . . . 6
2.2 Measurement setup . . . 9
2.2.1 Mass spectrometry between discharges . . . 13
2.2.2 Mass spectrometry during discharges . . . 14
2.3 Calibration . . . 15
2.3.1 Optimization of the mass filter . . . 16
2.3.2 Optimization of the ion source . . . 17
2.3.3 Determination of the Cracking Pattern . . . 22
2.3.4 Calibration against the total pressure . . . 23
2.4 Cracking Pattern for partly deuterated molecules . . . 28
2.5 Data Evaluation . . . 32

3 Behavior of ammonia in the all tungsten plasma vessel of ASDEX Upgrade **45**
3.1 Measured Intensities . . . 45
3.2 Conclusions . . . 47
3.3 Calibration . . . 56

4 Nitrogen Seeded Discharges **57**
4.1 Global Parameters of evaluated discharges . . . 57
4.2 Discharges with and without nitrogen seeding . . . 57
4.2.1 Discharge 27082 (without nitrogen seeding) . . . 57
4.2.2 Discharge 27169 (nitrogen seeding) . . . 63
4.2.3 Comparison and Discussion . . . 66
4.3 Ammonia inventory in discharges subsequent to discharges with nitrogen seeding . . . 74
4.4 Consecutive discharges with nitrogen seeding . . . 79
4.5 Nitrogen seeding experiments in hydrogen L-Mode plasmas . . . 79
4.5.1 Development of the measured intensities at the methane-water-ammonia group . . 80
4.5.2 Development of the content of ammonia ($^{15}NH_3$) and nitrogen ($^{15}N_2$) in the residual gas . . . 82

5 Summary and Conclusion **84**

A Appendix **87**

Chapter 1

Introduction

While the energy supply of today mainly relies on fossil resources like coal or mineral oil it has become quite clear during the last years that fossil resources are not a viable option for the future. Besides the problematic emission of carbon dioxide and other greenhouse gases, the earth only yields a limited amount of fossil resources. It is foreseeable that the commercial mineral oil reserves will run out within the next century. Therefore alternative energy sources that are reliable, clean and sustainable have to be found. One considered possibility is the use of fusion technologies. A basic goal of the international experiment ITER (International Thermonuclear Experimental Reactor), which is currently being build in France, is to show the feasibility of fusion by magnetic confinement as a future energy supply.

1.1 Nuclear Fusion

The process by which two or more atomic nuclei join together to form a single heavier nucleus is called nuclear fusion. If the mass of the new formed nucleus is smaller than the combined masses of the reactants, energy is released. This is expressed by the concept of nuclear binding energy per nucleon in a nucleus. In figure 1.1 the binding energy per nucleon against the number of nucleons in the nucleus is shown. For light nuclei the binding energy rises with the mass of the nucleus, for nuclei heavier than ^{56}Fe the binding energy declines again. As a direct consequence fission of heavy nuclei and fusion of light nuclei leads to a release of energy. Due to a high cross section at moderate temperatures the formation of helium out of a deuterium and a tritium nucleus is the most accessible fusion reaction for a future fusion reactor on earth.

$$ {}^{2}_{1}D \; + \; {}^{3}_{1}T \quad \rightarrow \quad {}^{4}_{2}He \; + \; {}^{1}_{0}n \; + \; 17,59 MeV \tag{1.1} $$

To fuse the reactants have to get into the range of the strong nuclear force, approximately a few fermi. To do so, the particles have to overcome the repelling coulomb force. Thus two protons would need a relative energy of about 0.50MeV to get close enough to fuse. In today's fusion plasmas with a temperature of about 10 to 20keV only very few particles have such a high energy [1], but tunnel effects already cause a noticeable fusion rate. Unfortunately besides the temperature of the nuclei there are other criteria to be fulfilled in a future reactor. Even at temperatures of about 100keV the probability of an elastic repulsion of the two nuclei due to their positive charges, exceeds the probability of a fusion collision by 5 orders of magnitude[MKa03]. Thus the nucleons have to be confined long enough to execute many elastic collisions. Also the energy of the confined α -particles, 3.52 MeV, has to balance the total energy losses. This criteria defines the following condition for the ignition of a fusion reactor:

$$ n_e \, \tau_E^* \; = \; 2,8 \; \times \; 10^{21} keV \; s \; m^{-3} \tag{1.2} $$

n_e is the electron density, whereas τ_E^* is the energy confinement time. For this simple approach line radiation and bremsstrahlung as well as dilution through the formed helium are neglected.

[1] assuming a Maxwell distribution

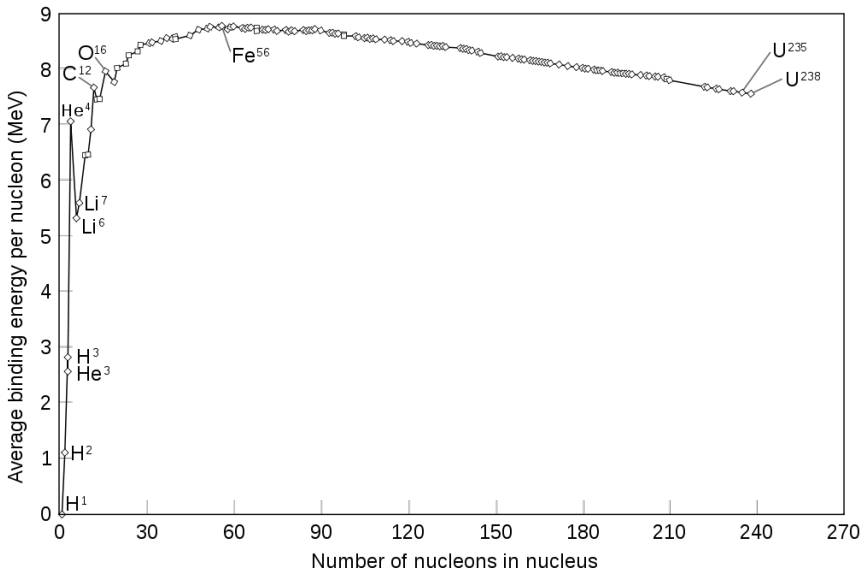

Figure 1.1: *Binding energy per nucleon [WCo]*

1.2 Magnetic Confinement and Divertor Setup

From today's point of view there are two promising ways to achieve the conditions mentioned in equation 1.2: the inertial confinement and the magnetic confinement. In Europe mainly magnetic confinement is pursued. At temperatures of 10 keV all atoms, besides very heavy atoms like tungsten, are completely ionized. The confinement of a plasma is immediately linked to a pressure gradient $\vec{\nabla}p$ which has to be balanced by the cross product of the current density $\vec{j}$ and the magnetic field $\vec{B}$ [ABo04].

$$\vec{\nabla}p = \vec{j} \times \vec{B} = \frac{(\vec{\nabla} \times \vec{B}) \times \vec{B}}{\mu_0} \tag{1.3}$$

The presence of a magnetic field forces the charged particles on spiral traces around the magnetic field lines. While the movement of the particles is strongly suppressed in vertical direction they can move freely along the magnetic field lines. To avoid particle losses at the end of the configuration, the magnetic field lines have to be closed to a torus. But this toroidal structure of the field lines also leads to a gradient of the magnetic field. Thus electrons and ions are separated from each other and are building up an electric field $\vec{E}$ perpendicular to the magnetic field lines. In combination this leads to an $\vec{E} \times \vec{B}$ - Drift, driving the particles out of the configuration. To avoid the separation a helical field configuration is necessary. One option is to apply a toroidal current in the plasma. Such a configuration is called Tokamak, many experiments like ASDEX (axial symmetric divertor experiment) Upgrade (see Figure 1.2), JET (Joint European Torus) or ITER base on the Tokamak principle. Today most Tokamaks base on the so called divertor concept. In figure 1.3 the magnetic flux surfaces during a typical discharge at ASDEX Upgrade with divertor-configuration IIb are shown. Two general types of flux surfaces exist. Closed ones at the center of the torus, at which the last closed flux surface is called seperatrix and open surfaces, which hit the wall of the plasma vessel within the divertor structure, where most of the impurities are released. But due to the geometry of the flux surfaces they can hardly reach the plasma core. Iimpurities are instead neutralized and removed from the divertor via a pumping system. The divertor configuration enabled the discovery of the high confinement mode, or short H-mode, at ASDEX Upgrade in the early 80es [FWa82].

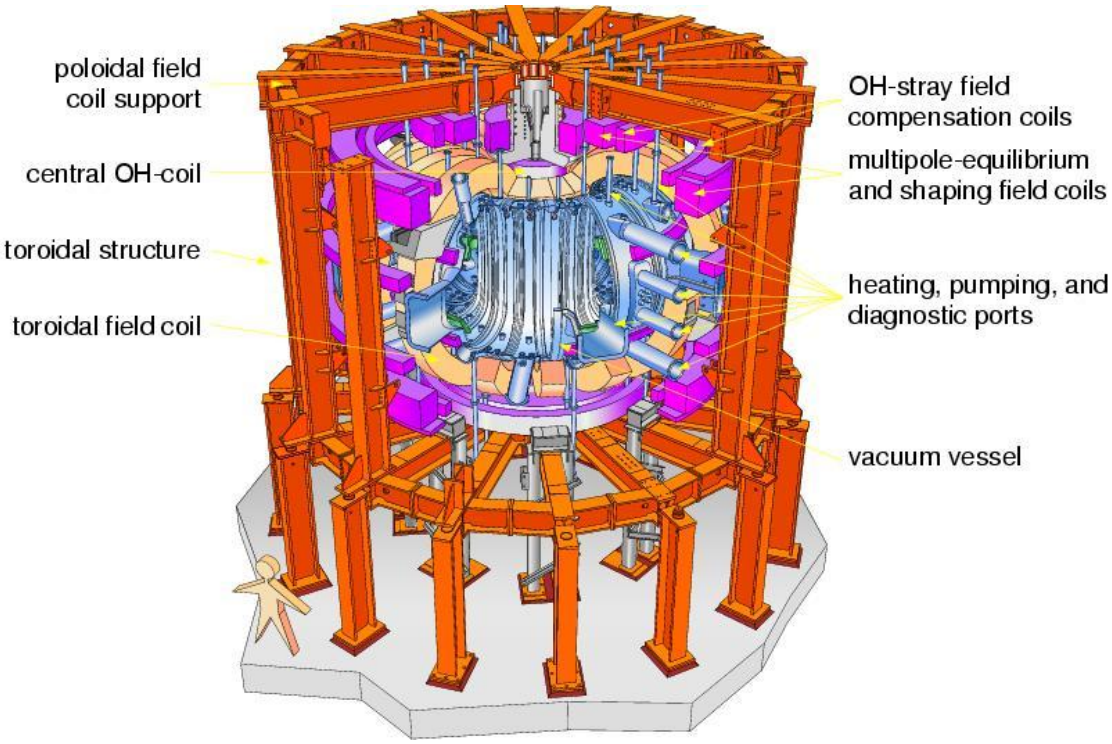

Figure 1.2: *Tokamak ASDEX Upgrade*

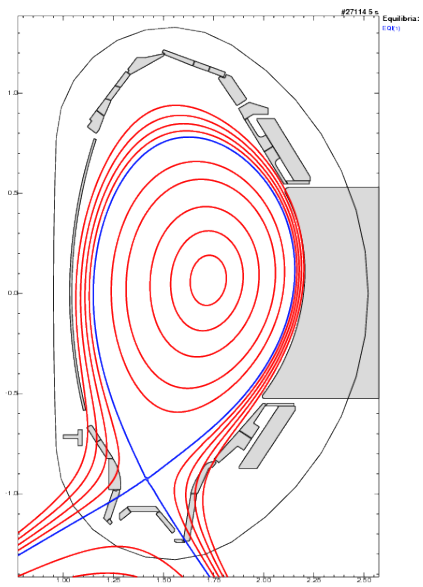

Figure 1.3: *Poloidal view of the divertor configuration IIb at ASDEX Upgrade. The separatrix is shown as blue, the flux surfaces as red lines 5s after the beginning of H-mode discharge 27114.*

1.3 Nitrogen Seeding

The first wall elements of the plasma vessel of ASDEX Upgrade were initially made out of carbon tiles as carbon sustains very high heat loads without damage. The disadvantage of a carbon wall is that, together with eroded carbon atoms, deuterium can form a:CD layers [MMa06]. As long as only deuterium plasmas are used, like in ASDEX Upgrade, this might be acceptable, but as soon as tritium is involved this is no longer the case. For ITER using a plasma out of deuterium and tritium the formation of such layers can lead to an unacceptable high tritium inventory. For this reason other wall materials were discussed. From 1999-2005 ASDEX Upgrade made the stepwise transition to a full tungsten machine, therefore the complete vessel wall was covered with about 4 μm thick tungsten layers. As a consequence the plasma got much cleaner as the amount of carbon in the plasma decreased dramatically. The side effect is that the reduced level of radiation at the edge due to the reduced amount of carbon leads to a higher heat flux onto the divertor. To avoid damaging the divertor, divertor plasma have to be cooled, especially during experiments with high heating power. At a standard plasma pulse, usually called discharge or shot, first deuterium is filled into the vessel then the deuterium molecules are ionized and confined for a few seconds. In order to achieve a cooling of the edge plasma, additional impurities are seeded during the discharge. As it turns out nitrogen seeding does not only reduce the heat flux onto the divertor but also improves the confinement of the plasma. Also there are changes in ELM [2] behavior and in the transport at the core [HMu09]. At present it is not decided if ITER will start operation with a divertor made out of carbon or out of tungsten. Operating a metal divertor will enforce the seeding of impurities in order to protect the divertor [AKa10].

But like carbon nitrogen can also form stable compounds with hydrogen, for example ammonia. An excessive formation of ammonia is a possible issue for the operation of the cryo pumps. As tritium has to be removed from the residual gas of a discharge, it is necessary to know if the gas plants have to deal with a significant amount of ammonia. Additionally if ammonia is retained in the vessel of ITER, ammonia could cause problems for the control of the plasma. Hence within the present diploma thesis subsequent questions are investigated:

- How much ammonia is formed during a typical nitrogen seeded discharge?
- Is there a retention of ammonia in the tungsten plasma vessel of ASDEX Upgrade?
- Is there a interaction between the tungsten wall and ammonia?
- Is there a enrichment of ammonia in the vessel for consecutive nitrogen seeded discharges?

The residual gas of discharges with and without nitrogen seeding are analyzed by mass spectrometry. Hence a quantitative analysis is possible. The huge amount of recorded data calls for an automatized evaluation. Therefore a computer based approach had to be developed that allows a reliable analysis of the composition of the residual gas.

[2] edge localized mode, a disturbance of the plasma

Chapter 2

Mass spectrometry at ASDEX Upgrade

At ASDEX Upgrade there are up to four mass spectrometers analyzing the residual gas of a discharge. During the next chapter the general functionality of the mass spectrometers is handled. Later the necessary measurement setup to overcome the special problems at ASDEX Upgrade is presented. At the end of the chapter a summary of the data evaluation is given.

2.1 Quadrupole mass spectrometer

Mass spectrometry is a standard method to investigate the composition of the residual gas in a vacuum chamber by measuring the atomic mass to charge ratios (m/z) of the particles contained in the residual gas. As shown in figure 2.1 Mass spectrometers usually consist of three parts: the ion source, the mass analyzer and the detector.

The first part of a mass spectrometer is the ion source. As mass spectrometers are using electric fields to separate particles according to their mass to charge ratio, the first step is to ionize the gaseous sample. For this purpose many different options like electron spray ionization, chemical ionization or electron impact exist. The ion sources in the devices used for this thesis are based on the electron impact method. At a hot filament electrons are emitted and then accelerated by an electric field. When an electron hits a neutral particle, often an electron in the outer shell is lost and hence the neutral particle is ionized. In figure 2.2 the cross section of this process is shown as a function of the electron energy for common gases. At electron energies below 10eV almost no ionization takes place. At roughly 70eV the cross section of the most gases has a broad maximum. The maximum cross section varies for different gases by about one order of magnitude. Hence the detection efficiency in a mass spectrometer is different for different samples.

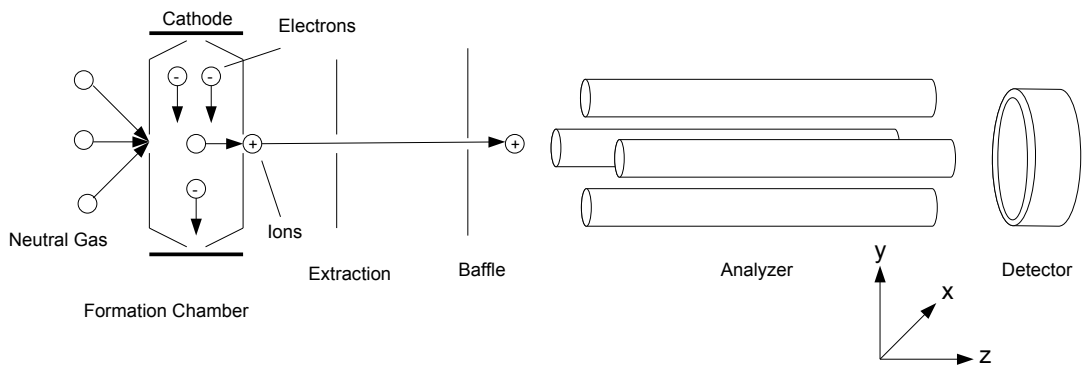

Figure 2.1: *Schematic of mass spectrometer*

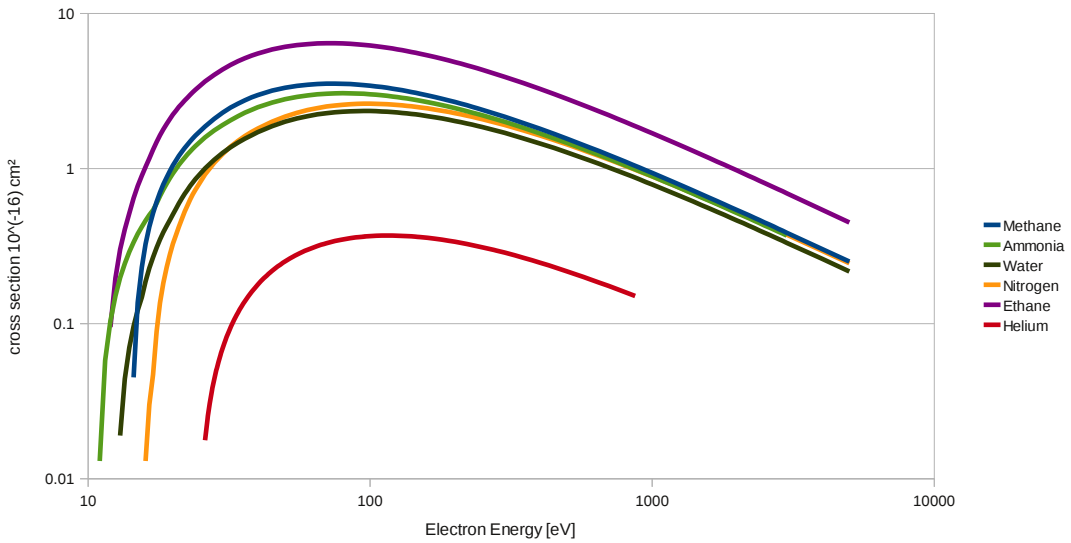

Figure 2.2: *Cross section of the ionization process by electron impact as a function of the energy of the striking electron*

The second part of a mass spectrometer is the analyzer or mass filter. Mass spectrometers are often named after the method used to separate the ions according to their mass to charge ratio. There are four major concepts:

- Sector instruments using electric and magnetic fields
- Time of flight instruments using the different velocities of ions with different masses after accelerating them in an electric field
- Quadrupole ion traps
- Quadrupole instruments using an oscillating electric field

There are various modifications for special applications. As quadrupole spectrometers can be build compactly, handled quite easily while remaining highly flexible and being commercially available, this type is a standard technique in mass spectrometry for residual gas analysis. Consequently quadrupole mass spectrometers are operated at ASDEX Upgrade. In figure 2.3 a schematic of the mass filter is presented. A quadrupole mass filter usually consists of four rods pointing in z-direction. The ions trespass the mass filter in axial direction.

At rods A a positive direct voltage $+U$ is superposed by an alternating voltage with an amplitude $+V$ and frequency ω, at rods B a negative voltage $-U$ is superposed by an alternating voltage with an amplitude $-V$ and the same frequency ω (figure 2.3). Opposite rods have therefore the same potential. The potential at the rods is then given by:

$$\Phi_A = +U + V cos(\omega t) \tag{2.1}$$

$$\Phi_B = -U - V cos(\omega t) \tag{2.2}$$

Superposing the potentials of all 4 rods gives the total potential Φ at a specific place

$$\Phi = [U + V cos(\omega t)] \frac{x^2 - y^2}{2r_0^2} \tag{2.3}$$

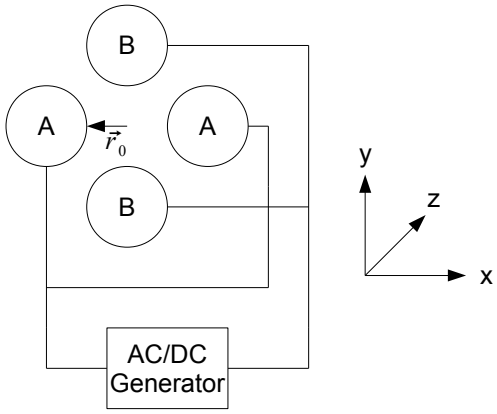

Figure 2.3: *Schematic of the mass filter*

In equation 2.3 r_0 is the inner radius. x and y are the distances of the sample ion from the x and y-axis respectively. Due to the potential Φ in equation 2.3 the ions are accelerated in x and y direction but not in z direction. The equations of motion are:

$$\frac{d^2x}{dt^2} + \frac{ex}{mr_0^2}\,[U + Vcos(\omega t)] = 0 \tag{2.4}$$

$$\frac{d^2y}{dt^2} - \frac{ey}{mr_0^2}\,[U + Vcos(\omega t)] = 0 \tag{2.5}$$

$$\frac{d^2z}{dt^2} = 0 \tag{2.6}$$

m is the mass of the ion, e the elementary charge assuming only ions with one elementary charge and r_0 being the inner radius again. It should be noted that the use of such a potential Φ does not lead to mixed terms containing x and y. By using the parameters a and q

$$a = \frac{4eU}{\omega^2 r_0^2 m} \tag{2.7}$$

$$q = \frac{2eV}{\omega^2 r_0^2 m} \tag{2.8}$$

2.4 and 2.5 can be transformed into a form of the Mathieu's differential equation.

$$\frac{d^2x}{dt^2} + \frac{\omega^2}{4}[a + 2qcos(\omega t)]x = 0 \tag{2.9}$$

$$\frac{d^2y}{dt^2} - \frac{\omega^2}{4}[a + 2qcos(\omega t)]y = 0 \tag{2.10}$$

Two general types of solutions exist. Bound solutions allowing the ion only a finite displacement and thus the ion can reach the detector and unbound solutions with an infinite displacement and consequently leading to a collision between ion and rod. As the stability of a solution only depends on a and q, a two dimensional stability diagram (see figure 2.4) for the movement through the mass filter can be drawn [TWa07]. U and V are completely free parameters but in a mass spectrometer they are usually kept at a fixed ratio. According to 2.9 and 2.10

$$\frac{a}{q} = \frac{2U}{V} = const \tag{2.11}$$

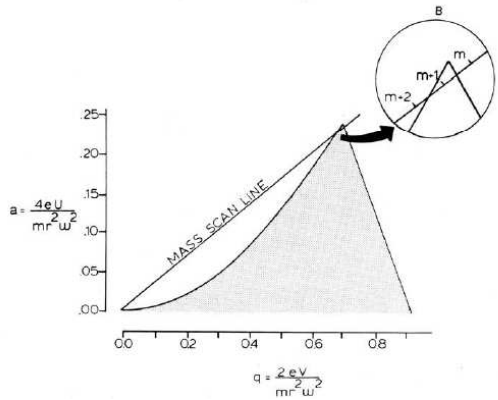

Figure 2.4: *Stability diagram [PMi86]*

is chosen. In figure 2.4 this is shown as the mass scan line. Only ions within the shaded stable area can pass the mass filter. As the choice of U and V are limited to a fixed ratio only ions with parameters a and q belonging to the intersection of mass scan line and shaded area can trespass the analyzer. As the area of stability is fixed regarding a and q, the mass of an ion being able to pass the filter has also to increase if U and V increase. Hence by successive increase of the voltages a complete spectra for a given mass range can be scanned. The mass analyzer as well as the ion source have to be evacuated to avoid collisions of the sample ions with other particles. By increasing the slope of the mass scan line the resolving power of the analyzer improves as the intersection between mass scan line and shaded area decreases, but at the cost of a lower intensity. This allows a quick adjustment of the resolving power and sensitivity according to the actual conditions.

The third part of a mass spectrometer is the actual detector. The devices used for this thesis are equipped with a Faraday Cup detector. It consists of three parts, a collector electrode kept at a constant potential, a high-ohmic resistor and a Faraday cage. Ions hitting the metal surface of the collector electrode are neutralized by electrons drawn from the ground. The voltage drops at the resistor, which is installed between electrode and ground, then it is amplified and measured. Hence the output signal is proportional to the amount of ions neutralized. To prevent reflected ions from leaving the detector a Faraday cage is build around the electrode. The Faraday cup provides a high accuracy and low noise while being stable and reliable but its time constant is rather long [TWa07]. Another type of detector is the secondary electron multiplier (SEM) providing a better time resolution and sensitivity but it cannot be operated at pressures higher then 10^{-4}Pa and does not supply the long term stability of a Faraday Cup.

2.2 Measurement setup

As the pressure at the divertor during typical discharges barely exceeds 10^{-1}Pa the residual gas can be treated as a ideal gas [WAt87]. Thus the absolute pressure p is given by the sum of the partial pressures p_i of the components in the residual gas.

$$p_{tot} = \sum_i p_i \tag{2.12}$$

Hence the partial pressure p_i of a component of the residual gas can be calculated if the absolute pressure of the residual gas and the concentration of this component in the residual gas are known. The absolute pressure is measured by different vacuum gauges, the composition of the residual gas can be determined by mass spectrometry. The residual gas is removed from the vessel continuously by a pumping system

consisting of turbo molecular and cryo pumps. To calculate the amount of molecules of a certain component contained in the residual gas the pumping speed of the pumping system has to be known. In figure 2.5 a poloidal projection of the plasma vessel of ASDEX Upgrade, illustrating the position of the used vacuum gauges and mass spectrometers is depicted. Also the locations of turbo molecular and in-vessel cryo pump are depicted. Two identical mass spectrometers are installed at the lower divertor. The mass spectrometer HPQI is set up at the inner side, the mass spectrometer HPQO at the outer side. Each of the mass spectrometers (MKS HPQO or MKS HPQI) is combined with at least one vacuum gauge (ITR 100, MKS 670, TPR 265 and GP 370 or ITR 090 respectively). Hence gas composition and absolute pressure are known at each mass spectrometer. The used mass spectrometers and vacuum gauges are described below in detail.

Pressure measurement For measuring the pressure of the residual gas three different types of vacuum gauges are operated. Ionization gauges (ionivacs) ionize the molecules in the gas and determine the pressure by measuring the electric conductivity. They can be operated in a pressure range from 10^{-5}Pa to 10^{1}Pa but as shown in figure 2.2 the amount of formated ions depends not only on the pressure but also on the composition of the measured gas. Consequently the measured pressure is not independent of the gas composition. As the composition of the residual gas is not known preliminary, a calibration of the ionization gauges is not possible. Three ionization gauges are operated: ITR 090 and ITR 100 manufactured by Leybold and GP 370 manufactured by Grandville-Phillips. The second type are mechanical gauges. A diaphragm is shaped by the pressure difference between a completely evacuated chamber and the residual gas. The shaping of the diaphragm results in a change of its capacity, which can be correlated to the pressure. A gauge that bases on this method is called capacity gauge. This type of pressure measurement does not depend on the composition of the gas and thus can be calibrated. At the outer divertor one capacity gauge, a baratron by MKS (MKS 670) is installed. The pressure range of the used baratron is between 10^{-3}Pa and 10^{-1}Pa, consequently not the entire ASDEX Upgrade operational pressure regime can be covered. To overcome this problems an ionivac is operated together with a baratron. While the pressure measurement during the discharge remains independent of the gas mixture the entire pressure range is covered. As a third type also Pirani gauges are operated, measuring the thermal conductivity of the gas which depends on the pressure. But similar to ionization gauges Pirani gauges are not independent of the gas composition. One pirani gauge made by Pfeiffer (TPR 265) is installed at HPQO at the outer divertor.

Pumping Speed

At ASDEX Upgrade cryo and turbo molecular pumps are operated to remove the residual gas fromm the plasma vessel. The pumping speeds were determined in 2009 [VRo09(2)] for deuterium only and are shown in table 2.1. Since then some enhancements were done at ASDEX Upgrade, but the pumping speed should roughly be the same.

Pump	Pumping Speed [l/s]
Turbomolecular Pumps	$16100 - 6131 \cdot p_{HPQO} + 1835 \cdot p^2$
Cryo Pump	$11500 + 276000 \cdot p_{HPQO}$

Table 2.1: *Pumping speeds of turbo and cryo pumps determined for deuterium at ASDEX Upgrade in 2009*

The contribution of NBI boxes and diagnostics installed at ASDEX Upgrade are neglected. Consequently the calculated quantities of impurity molecules are too low. Typical pressures at the divertor during discharges are a few 0.1 Pa. At this pressure range the flow of the residual gas towards the pumps is in the transition regime between laminar and molecular flow. Hence the different components of the residual gas are pumped at different speeds. But as deuterium molecules are by far the must abundant molecules in the residual gas it is plausible to assume that all other components are carried along by the deuterium molecules. Hence the pumping speeds for all components are assumed to be equal.

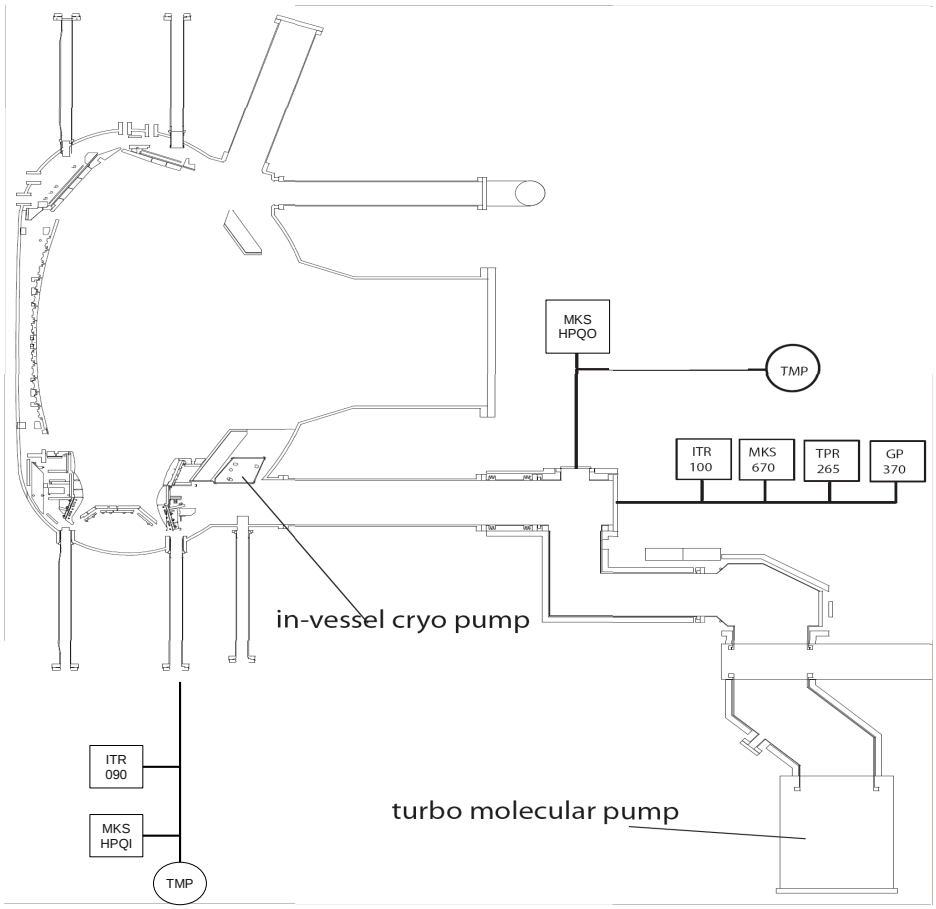

Figure 2.5: *Cross section of the plasma vessel with pumps, pressure gauges (ionization gauges ITR 90 and ITR 100, capacity gauge MKS 670, priania gauge TPR 265 and ionization gauge GP 370) and mass spectrometers (MKS HPQI and MKS HPQO).*

Determination of the composition of the residual gas

As stated above two identical mass spectrometers are operated, one is positioned at the inner divertor (HPQI) and one at the outer divertor (HPQO). Both devices are manufactured by MKS and belong to the high pressure quadrupole (HPQ-2) series. Mass spectrometers of this type are specialized to work at pressures up to 1Pa and can therefore measure during discharges. For the operation of mass spectrometers at ASDEX as well as for the evaluation of the measured data some problems have to be solved.

- High pressures during discharges and rapid pressure changes
- Strong magnetic fields (up to 2.4T)
- Space limitations
- Thermal drifts
- Presence of deuterium

The mass filters of HPQO and HPQI are rather short, hence collisions between the sample ions are avoided. As a drawback the resolving power of the instruments is also limited. Furthermore the influence of magnetic fields on the mass filter is minimized. But the mass spectrometers still require magnetic shielding, limiting size as well as the cooling of the devices. Hence thermal drifts of the mass to charge scale occur during an experimental day (see section 2.2.2).

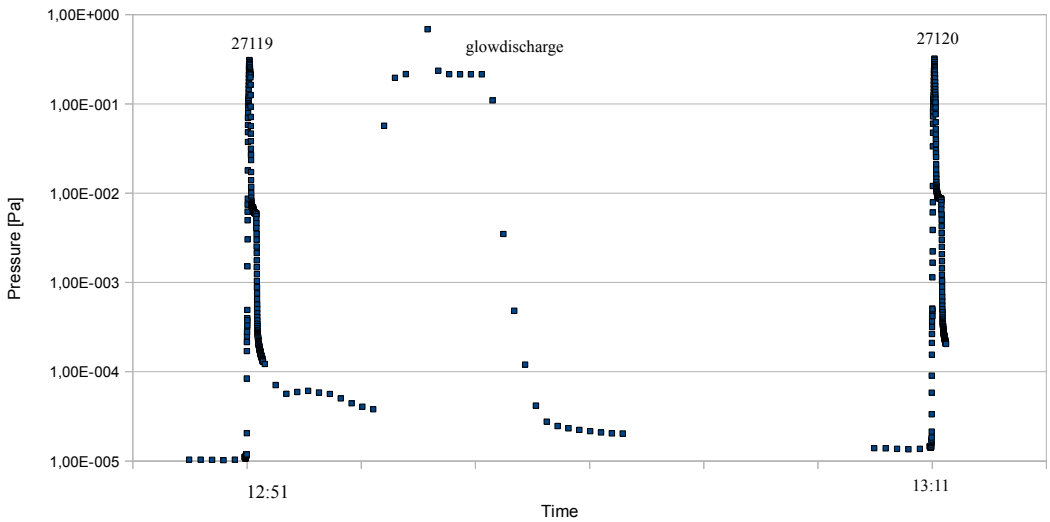

Figure 2.6: *Pressure at the divertor for discharges 27119 and 27120 measured by MKS 670 and GP 370*

Figure 2.6 illustrates the pressure dynamics within and between typical discharges at the divertor. The base pressure of ASDEX Upgrade is roughly 10^{-5}Pa. At the beginning of a discharge the pressure at the divertor rises about four orders of magnitude within a second. A typical discharge at ASDEX Upgrade lasts roughly 5-10s, during this time interval the mentioned pressure remains roughly constant. After the discharge the pressure at the divertor decreases about 3 orders of magnitude during a few seconds, afterward the pressures only changes slowly. After roughly 20 minutes of consecutive pumping the base pressure is reached again. Subsequent to some discharge a glow discharge is performed in order to desorb impurities form the surface of the plasma vessel by ion bombardment. At the beginning and the end of the glow discharge, the pressure changes rapidly.

2.2.1 Mass spectrometry between discharges

As the pressure at the divertor changes only slowly between discharges, beside glow discharges, a time resolution of about one minute is sufficient for the mass spectrometers. Hence they can be operated in Analog Scan mode Thus the intensities from m/z =0.5 to m/z =50.5 are scanned with a step width of roughly m/z =0.15 repeatedly. As the focus lies on a good accuracy one complete scan takes about 50 seconds.

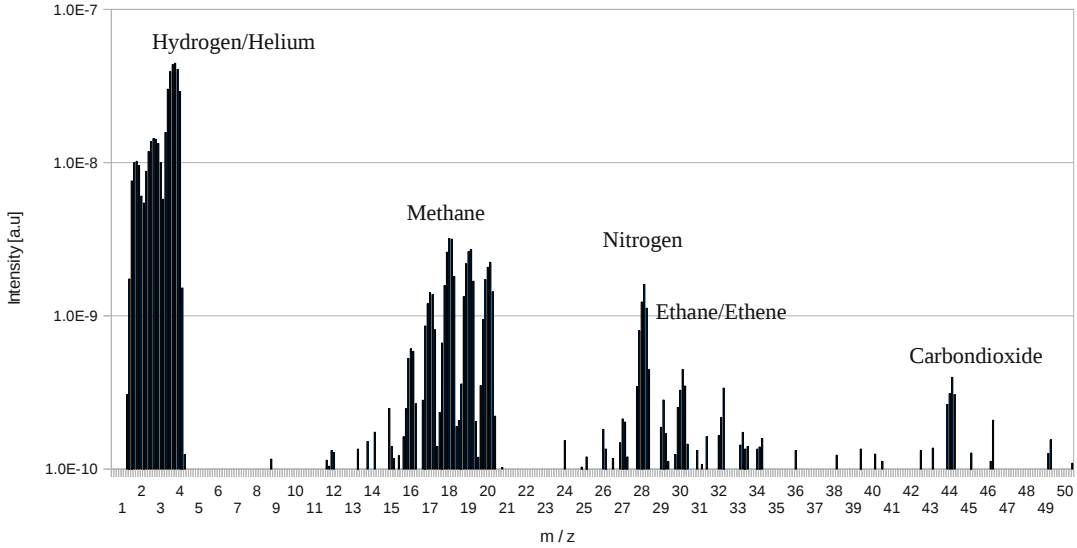

Figure 2.7: *9th Analog Scan after discharge 27114*

In figure 2.7 the measured intensities during the 9th Analog Scan after discharge 27114, performed on 2011-06-09, are shown. This scan was recored roughly ten minutes after discharge 27114. The most prominent peak in the spectrum is located at m/z =4 and is related to deuterium and helium. As deuterium is the working gas of ASDEX Upgrade, deuterium is expected to be the main component of the residual gas. But also intensities at m/z =2 and m/z =3 show up, thus also molecular protium (H_2 m/z =2) and isotopically mixed hydrogen (HD m/z =3) molecules are contained in the residual gas. The most striking peak group is located from m/z =12 to m/z =20. Major contributions are probably made by water (H_2O^+m/z=18 and methane (CH_4^+m/z=16). But also a significant intensity at m/z =20 shows up. This intensity is related to completely deuterated methane (CD_4^+ and water (D_2O^+) molecules.

Often single peaks are directly interpreted as certain compounds e.g. m/z=18 $\rightarrow$ water or m/z=16 $\rightarrow$ methane, but at the deuterium environment of ASDEX Upgrade such a simple interpretation is not possible. Assuming that all hydrogen atoms are replaced by deuterium atoms the molecular peaks of water and methane are both shifted to m/z =20. Therefore a direct interpretation of the spectrum by simple assigning peaks to compounds is not a valid approach.

The sample molecules (e.g CD_4) are ionized in the ion source of the operated mass spectrometers by a bombardment with electrons. As stated earlier the striking electrons can take away an electron of the compound and thus the compound is ionized. This process is called direct ionization and is shown in 2.13

$$e^- + CD_4 \quad \rightarrow \quad CD_4^+ + 2e^-. \tag{2.13}$$

But it is also possible that the striking electron splits the compound into two or more parts. Thus for methane also the formation of four fragment ions CD_3^+ (m/z=18), CD_2^+ (m/z=16), CD^+ (m/z=14) and

C^+ (m/z=12) according to

$$e^- + CD_4 \rightarrow CD_3^+ + \bullet D + 2e^- \quad (2.14)$$
$$e^- + CD_4 \rightarrow CD_2^+ + D_2 + 2e^- \quad (2.15)$$
$$e^- + CD_4 \rightarrow CD_1^+ + D_2 + \bullet D + 2e^- \quad (2.16)$$
$$e^- + CD_4 \rightarrow C^+ + 2D_2 + 2e^- \quad (2.17)$$

is possible. This processes are called dissociative ionization. Consequently within the ionization process of water D_2O^+ (m/z=20), DO^+ (m/z=18) and O^+ (m/z=16) can occur. The abundances of the fragment ions compared to the abundance of the molecular ion (CD_4^+ for deuterated methane and D_2O^+ for deuterated water vapor) is specific for each compound. The relative abundances normalized to the base peak are called fragmentation or cracking pattern, the cracking patterns for methane and water are shown in figures 2.8 and 2.9. CD_4 is referred as the molecular ion, whereas CD_3^+, CD_2^+, CD_1^+, C^+ are called fragment ions.

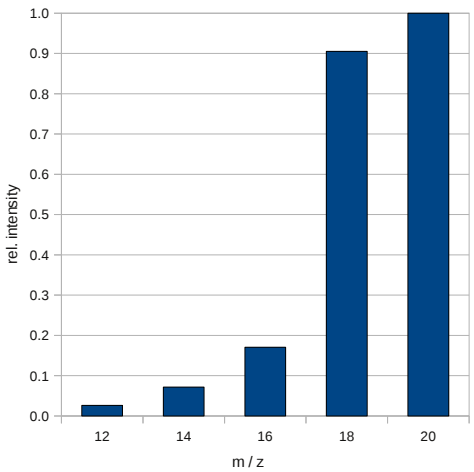

Figure 2.8: *Calculated cracking pattern of completely deuterated methane normalized to m/z =20*

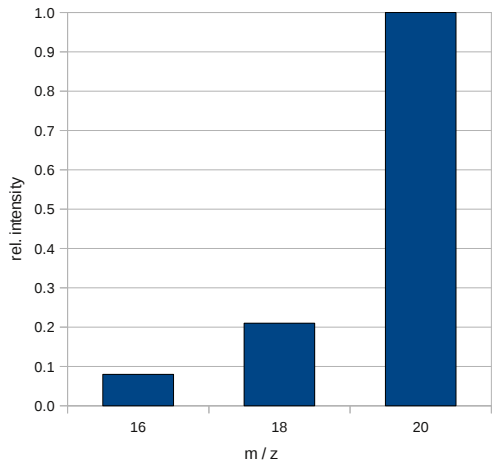

Figure 2.9: *Calculated cracking pattern of completely deuterated water normalized to m/z =20*

Consequently methane and water vapor will also evoke intensities at m/z =18 and m/z =16 but at different ratios. Therefore to distinguish methane from water vapor the intensities at m/z =18 and m/z =16 have to be taken into account additionally. To rely on the intensity at m/z =12 to distinguish between methane and water is not possible as the intensity at m/z =12 is at least one order of magnitude lesser than the intensity at m/z =20 or m/z =18. The intensity at m/z =14 is at least partly evoked by nitrogen, therefore it cannot not be used to distinguish methane from water.

While the interpretation of the peak m/z =44 as carbon dioxide is quite clear, some uncertainties arise at m/z =28. Peak m/z =28 may be caused by nitrogen (N_2^+), carbon monoxide (CO^+) or fragments of deuterated hydrocarbons (e.g. ethane). As also intensities at m/z =24 to m/z =34 show up, hydrocarbons like ethane or ethene are also contained in the residual gas. But they evoke only a part of the intensity at m/z =28. Hence major contributions to the intensity at m/z =28 are made by nitrogen or carbon monoxide.

2.2.2 Mass spectrometry during discharges

As stated above a typical discharge at ASDEX Upgrade lasts about 5-10s. Hence a time resolution of 1s is required. Therefore a continuous scan of the complete mass range is not possible. Instead the intensities at predefined mass to charge ratios are measured. To keep the time resolution at 1s only

4	12	14	16	18	20	28
Deuterium	Methane	Methane	Methane	Methane	Methane	Nitrogen
Helium	-	Ammonia	Ammonia	Ammonia	Ammonia	Ethane
-	-	Nitrogen	Water	Water	Water	Ethene

Table 2.2: *Major contributions to the intensities at m/z =4, m/z =12, m/z =14, m/z =16, m/z =18, m/z =20, m/z =28*

about ten mass to charge ratios are be scanned. Therefore two problems have to be considered. First the devices measure precisely at the predefined integer mass to charge ratios e.g. 16 while the actual maximum of peak m/z =16 is located at e.g. m/z =16.13. Additionally HPQO and HPQI tend to shift the m/z scale during an experimental day. But as the devices are operated in Analog Scan between the discharges the maximum of the peaks is known, and therefore the measured intensities at m/z =16.00 can be corrected with regard to the actual peak maximum (see chapter 2.5). The other limitation is the lack of a complete spectra, as only the intensities at certain mass to charge ratios are measured, there is no information about the intensity at the other mass to charge ratios. Assuming that carbon dioxide is the major component of the residual gas and the intensity at m/z =44 is not measured, as there is no information about the intensity at m/z =44 it is almost impossible to determine the partial pressure of carbon dioxide. As carbon dioxide via the fragments C^+ and O^+ also evokes an intensity at the methane-water-ammonia group, a high undetected amount of carbon dioxide can disturb the distinction between these three compounds. Consequently the scanned mass to charge ratios have to be chosen very carefully. As stated above, the basic goal is the distinction between methane, water and ammonia, hence the focus is set on this group. Additionally fragments of oxygen, carbon monoxide, carbon dioxide, nitrogen and argon can evoke intensities at the methane-water-ammonia group. The probability of forming such a fragment is for all mentioned molecules a few percent (see cracking pattern in the NIST database [NIST(2)]), consequently the intensity measured for the molecular ion would have to exceed the intensity at the corresponding peak at the methane-water-ammonia group by at least one order of magnitude to have a significant effect on these intensities. Assuming that the composition of the residual gas stays roughly the same during and between discharges, the intensities shown in figure 2.7 can be used to find components that could seriously disturb the distinction of ammonia from water and methane. As the intensity at m/z =16 exceeds the intensities at m/z =32 and m/z =44 no severe influence of oxygen or carbon dioxide is expected. The interpretation of m/z =28 is not clear, but during and after a discharge with nitrogen seeding, nitrogen is expected to be the most abundant impurity in the residual gas. Consequently the intensity at m/z =28 has to be measured in Peak Jump mode. To distinguish ammonia from methane and water additionally the intensities at m/z =12 and from m/z =14 to m/z =20 are measured.

Several seconds before a discharge a global trigger signal (TS04) is distributed by the ASDEX Upgrade control system switching automatically the measurement mode of the mass spectrometers from Analog Scan mode to Peak Jump mode. About 50 seconds later the mass spectrometers are switched back to Analog Scan mode.

2.3 Calibration

As stated above in chapter 2.2.1 the interpretation of the measured mass spectra can not be done by simply assigning intensities at certain mass th charge ratios to certain compounds. To determine the composition of the residual gas the cracking patterns of the compounds expected in the residual gas have to be used. Table 2.2 illustrates which compounds evoke major intensities at some chosen mass to charge ratios. Hence at least the cracking patterns of the substances listed in table 2.2 have to be known. The cracking pattern of many substances are listed in archives like NIST [NIST(2)]. But cracking patterns differ from mass spectrometer to mass spectrometer and also depend on the settings of the ion source. Additionally the cracking pattern of deuterated compounds are often not available. Hence the cracking

pattern of deuterium, helium, nitrogen, methane, water and ammonia have to be determined for both mass spectrometers HPQI and HQPO separately. As shown in figure 2.2 the ionization probability via electron impact depends on the sample compound. Also the transmission probabilities through the mass filter are different for different compounds. Hence the product of both probabilities has to be determined in order to calculate the composition of the residual gas. The total pressure at HPQI is not know as only a ionization gauge is operated there. Hence the mass spectrometer have to be calibrated absolutely against a capacity gauge. In order to simulate the pumping characteristics of the residual of a typical discharge, gas mixtures similar to the residual gas were used in all calibration measurement. Therefore subsequent approach was executed to calibrate the mass spectrometers:

- Use a gas mixture similar to the residual gas of an ASDEX Upgrade Discharge
- Optimize the ion source towards a high degree of fragmentation
- Determine the cracking patterns of each compound contained in the gas mixture
- Determine the ionization, transmission and detection probabilities for each compound
- Calibrate the mass spectrometer against a baratron

During all calibration measurements the mass spectrometer were operated in Analog Scan mode.

2.3.1 Optimization of the mass filter

To separate ions with different mass to charge ratios within the mass filter a direct voltage U is superposed by an alternating voltage V. The ratio U/V is kept at a fixed ratio. A standard procedure for operating mass spectrometers is to assign certain values of U/V to mass to charge ratios. Therefore a gas mixture (see table 2.3) is filled into the vessel of ASDEX Upgrade and a full spectrum is recorded (see figure 2.10). As the mass to charge ratios of the measured peaks (m/z =4, m/z =16, m/z =28 and m/z =40) are known, the mass to charge scale can be assigned.

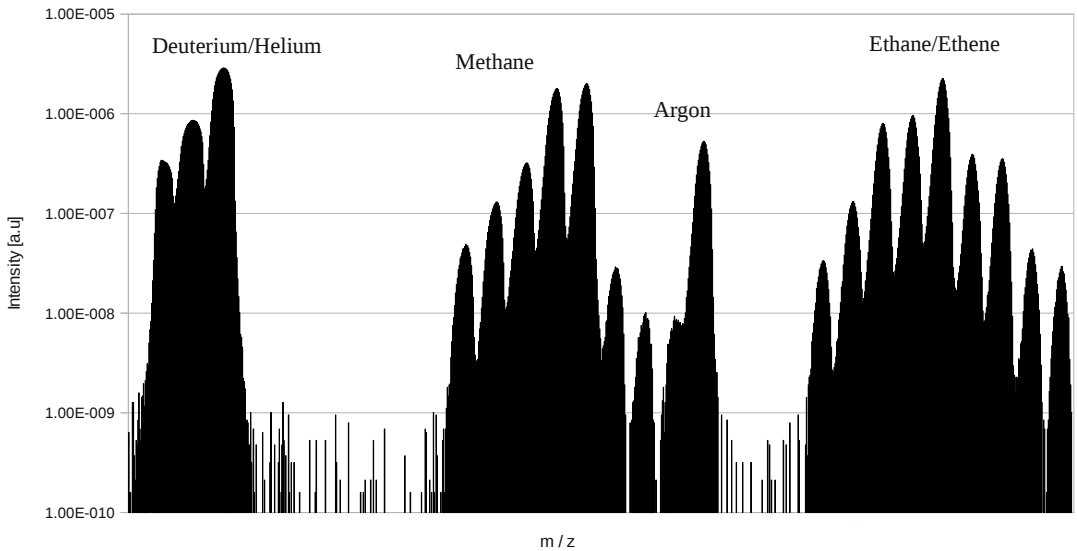

Figure 2.10: *Mass spectrum from HPQI of gas mixture shown in table 2.3 with uncalibrated mass to charge scale (2011-05-30). The total pressure in the plasma vessel was 0.039Pa*

Molecule	Fraction[%]	Base Peak
Helium	10,4	m/z =4
Deuterium(D_2)	58,21	m/z =4
Methane	11,7	m/z =16
Ethane	5,12	m/z =28
Ethene	5,42	m/z =28
Argon	9,45	m/z =40

Table 2.3: *Gas mixture 1 used during the calibrations performed on 2011-02-25 and 2011-05-30*

2.3.2 Optimization of the ion source

As the molecular peaks of completely deuterated methane, water and ammonia are all located at m/z =20, the molecular peak can not be used to distinguish these three compounds. Instead the distinction has to be made by taking the different abundances of fragment ions like ND_2^+ or CD_3^+ into account. Consequently a high degree of fragmentation is desirable. Hence the ion source of each mass spectrometer has to be optimized towards this condition. Three different parameters control the behavior of electrons and ions within the ion source.

- Electron energy: Electrons are emitted from the filament within the formation chamber and subsequently accelerated by a positive potential (see figure 2.11). By varying the potential the energy of the electrons at the collision with the neutral sample atoms can be controlled.

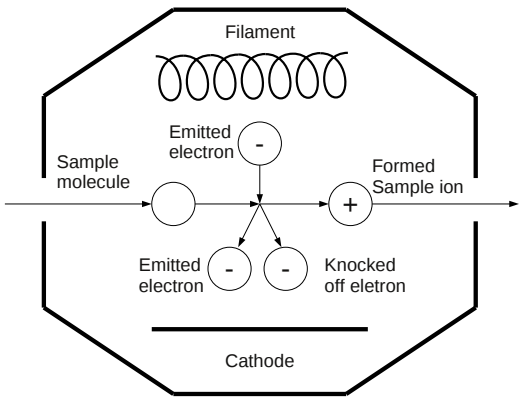

Figure 2.11: *Schematic of the ionization process in the ionization chamber*

- Emission current: By increasing the current through the filament, more electrons are emitted from the filament. But also the filament gets warmer, consequently more chemical reaction at the filament can occur. Addiditionally space charges can occur limiting the effect of a higher emission current.
- Extraction potential: Between the formation chamber and the mass filter a negative potential is applied. Therefore sample ions are accelerated out of the formation chamber whereas electrons cannot leave the chamber. A high extraction voltage removes the ions from the formation chamber quickly and prevents reaction between ions.

To find the optimal setup all three parameters are varied independently from each other. The optimal setup is characterized by a high degree of fragmentation, an overall high intensity while the filament stays quite cool. The behavior of the cracking patterns depending on the three mentioned parameters

was investigated on 2011-02-25 for HPQO and again on 2011-05-30 for both instruments. In contrast to the calibration in May on 2011-02-25 the turbo molecular pumps were operated. As test gas was filled into the vessel continuously the pressure stayed rather constant at 0.13Pa.

Variation of electron energy

Three different electron energies 35eV, 50eV and 70eV are investigated. The extraction voltage is kept at -61V, the emission current at 0.1mA. Now the intensities evoked by methane at m/z =13 to m/z =16 are compared. While a slight increase of the intensities with increasing electron intensities were expected (see figure 2.2), all measured intensities decline with increasing electron energy (see figure 2.12). By normalizing the measured intensities to the intensity measured at m/z =16 an increasing degree of fragmentation with increasing electron energy is visible (see figure 2.13). For example the relative abundance of CH_2^+ m/z =14 normalized to the abundance of CH_4^+ m/z =16 is 9.0% for an electron energy of 35eV and 15.7% for an electron energy of 70eV. To achieve a high degree of fragmentation the highest possible electron energy of 70eV is chosen at the cost of lower overall intensities.

Variation of emission current

The electron energy is kept at 35eV, the extraction potential is fixed at 58V. Three different emission currents are set up. It is expected that the measured intensities are proportional to the emission current. As shown in figure 2.14 the measured intensities increase not linearly with the emission current due to space charge effects at the filament. As just the amount of striking electrons was varied no influence is expected. In figure 2.15 the measured cracking pattern for an emission current of 0.1mA, 0.2mA and 0.4mA are shown. As expected the measured cracking pattern are roughly equal for all depicted emission currents. An emission current of 0.4mA was chosen, yielding a good balance between sufficient intensities and a quite cool cathode.

Variation of extraction voltage

A high extraction voltage suppresses reaction between ions in the formation chamber as the formed ions leave the chamber rapidly. The extraction voltage has almost no influence on cracking patterns and intensities. In standard operation an extraction voltage of 130V is used. The measurements shown in figures 2.16 and 2.17 were carried out by an electron energy of 35eV and an emission current of 0.1mA. The extraction voltage was varied from -70V to -110V.

The ion energy, determining the speed of the ions in the mass filter is kept constant at 5eV, after the second characterization an ion energy of 7eV is chosen. Although hampered by the changing pressure the characterization on 2011-05-30 shows the same tendencies for both devices. The optimized parameters are summed up in table 2.4.

Parameter	HPQI	HPQO
Electron Energy	70eV	70eV
Emission Current	0.4mA	0.4mA
Extraction Potential	-130V	-110V
Ion Energy	7eV	7eV

Table 2.4: *Setup of the mass spectrometers The extraction voltage of HPQI was changed accidentally from -110V to -130V. But as shown in figure 2.16 there should be no huge influence on the data.*

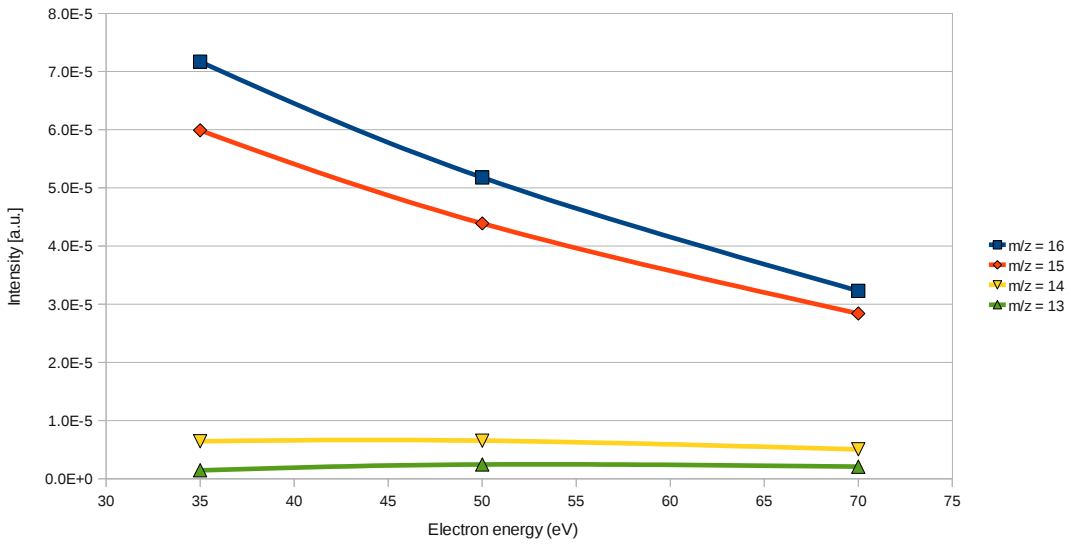

Figure 2.12: *HPQO Total intensities of methane fragments on 2011-02-25 for three different electron energies*

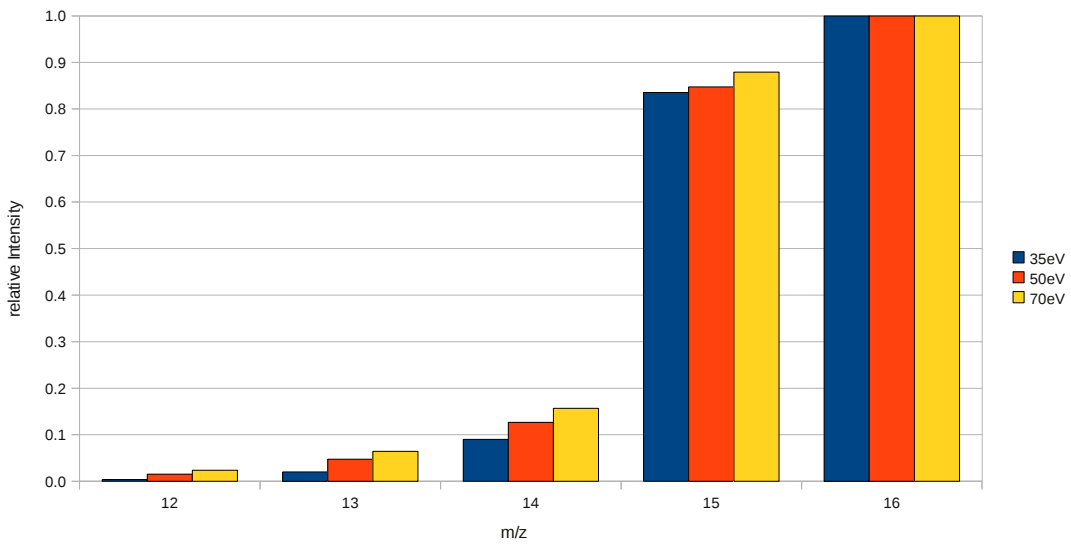

Figure 2.13: *HPQO Cracking Pattern of methane normalized to m/z =16 on 2011-02-25 for three different electron energies*

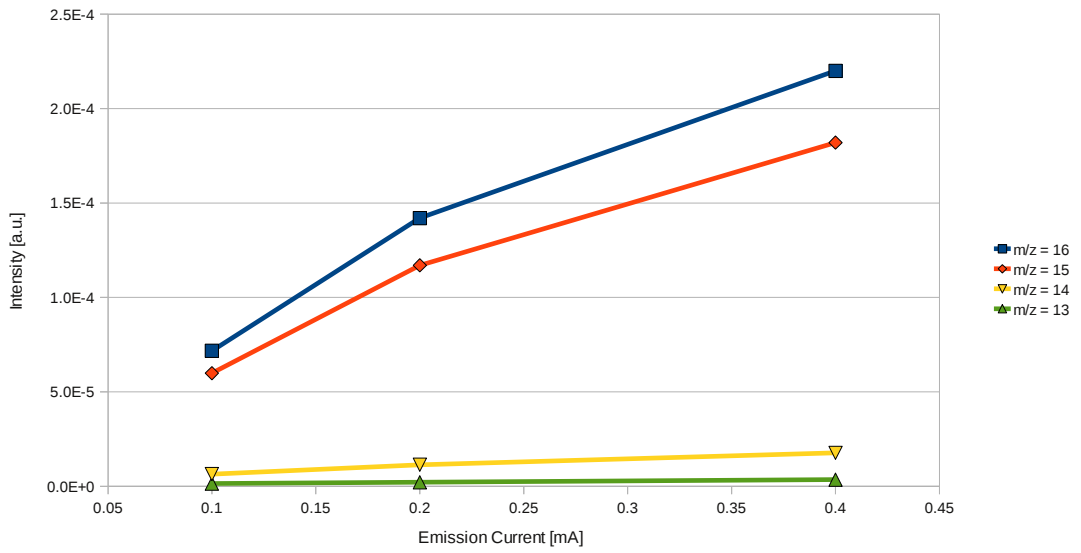

Figure 2.14: *HPQO Total intensities of methane fragments on 2011-02-25 for three different emission currents*

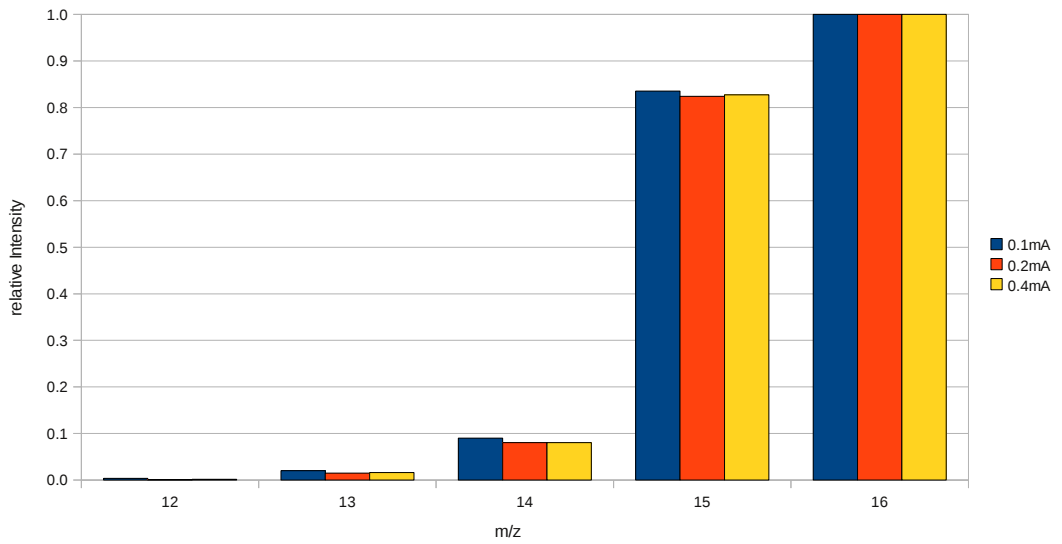

Figure 2.15: *HPQO Cracking Pattern of normalized to m/z =16 methane on 2011-02-25 for three different emission currents*

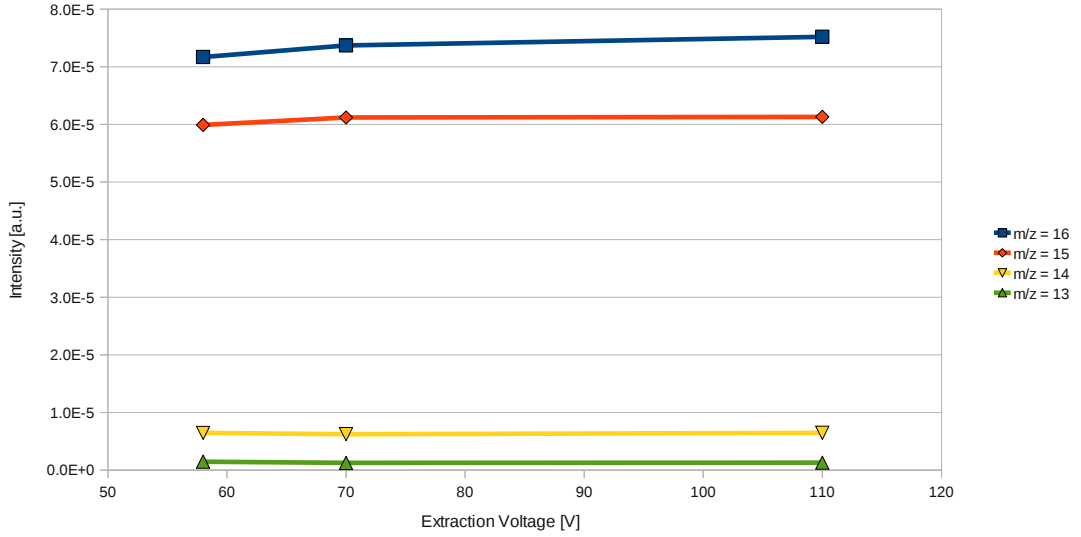

Figure 2.16: *HPQO Total intensities of methane fragments on 2011-2-25 for three different extraction potentials*

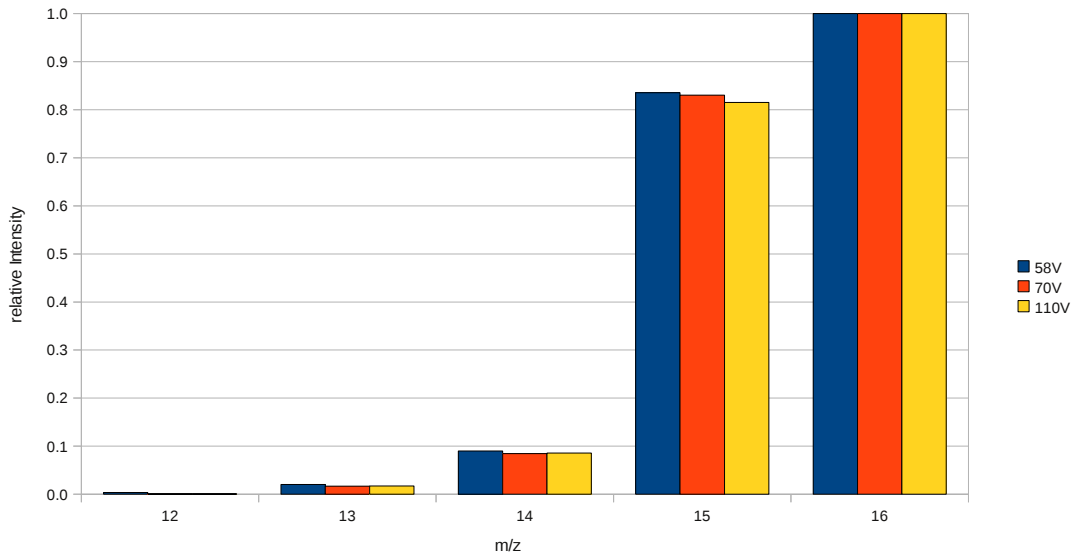

Figure 2.17: *HPQO Cracking Pattern of methane normalized to m/z =16 on 2011-2-25 for three different extraction potentials*

2.3.3 Determination of the Cracking Pattern

In a simple model the residual gas of an ASDEX Upgrade discharge consists mainly of methane, water, nitrogen, hydrogen/deuterium, helium and ammonia. As neon is used to terminate certain discharges before the vessel is damaged, neon can also be part of the residual gas. Hence the cracking patterns of all these molecules have to be known. As stated above the cracking pattern of a certain compound differs from ion source to ion source even at the same setup of the ion source. Therefore the cracking patterns are determined for HPQI and HPQO separately. As it turns out the differences regarding the cracking patterns between HPQI and HPQO are very small (see figure 2.18).

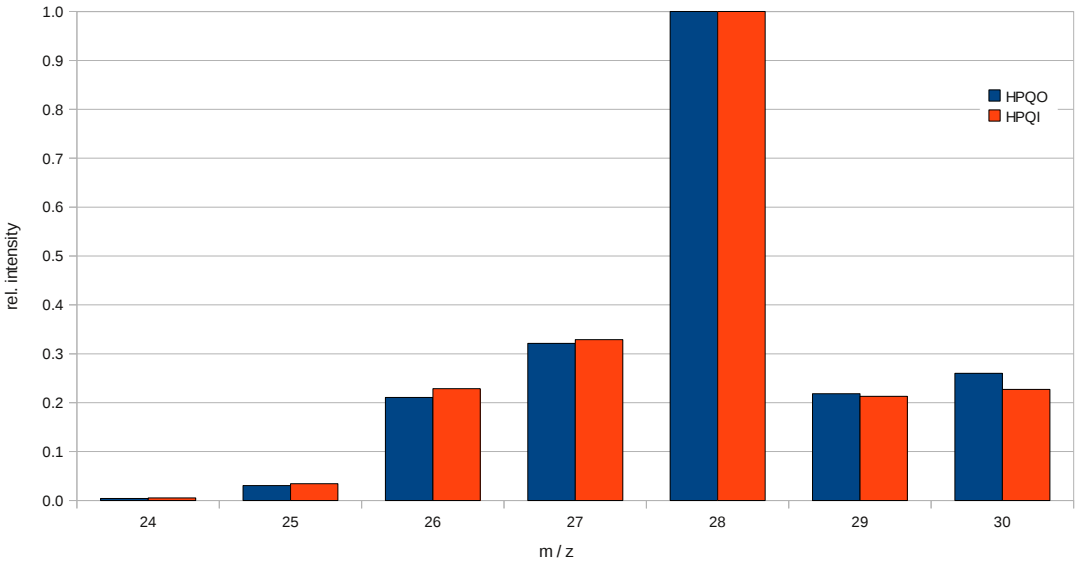

Figure 2.18: *Comparison of the cracking pattern of ethane measured by HPQO and HPQI*

The general approach for the determination of the cracking pattern of a compound is:

- Fill a known gas mixture into the plasma vessel of ASDEX Upgrade
- Measure the intensities at the mass to charge ratios of all possible fragments:
  - CH_4 m/z =12 - m/z =16
  - N_2 m/z =14 and m/z =28
  - $NH3$ m/z =12, m/z =16 and m/z =28

  Hence the components of the used gas mixture have to be chosen in a way that a massive overlapping is avoided.
- Normalize the measured intensities to the intensity of the base peaks

By using two different gas mixtures (see tables 2.3 and table 2.5) the cracking patterns of methane, ethane and ethene could be determined. The intensities evoked by ethane and ethene at m/z =12 - m/z =16 can be neglected. To determine the cracking pattern of ammonia pure ammonia was filled into a stainless steel vessel. HPQO was deinstalled from ASDEX Upgrade and set up at the stainless steel vessel. Hence the cracking pattern of ammonia was only determined for HPQO. As the cracking pattern of other compounds measured by HPQI and HPQO do not differ much, it was assumed that the cracking pattern of ammonia is equal for HPQI and HPQO (see also chapter 3.3). Another problem is to obtain the cracking pattern of water. It is not possible to fill ASDEX Upgrade with water vapor at an adequate level as it is very difficult to remove the water again [VRo09(1)], hence the natural residual gas of ASDEX Upgrade was used. From 2011-06-14 to 2011-06-16 no discharges were performed. Therefore the plasma vessel and also the mass spectrometers were evacuated for 3 consecutive days, as methane is removed much faster from

Molecule	Fraction[%]	Base Peak
Methane	9.79	16
Ammonia	9.88	17
Ethane	10.59	28
Argon	10.09	40
Deuterium(D_2)	15.38	4
Helium	44.37	4

Table 2.5: *Gas mixture 2 used during the calibration performed on 2011-06-20 at ASDEX Upgrade and on 2011-06-28 at a stainless steel vessel*

the walls than water, it was assumed that the signals measured at m/z =16 to m/z =20 are caused by pure water. The retrieved cracking pattern is similar to the cracking pattern of water shown in the NIST database [NIST(2)]. To gain the cracking pattern of nitrogen, oxygen and carbon dioxide a calibration with air was performed again only for HPQO. The obtained cracking patterns for water vapor contained in the air is similar to pattern obtained in the measurement on 2011-06-16. To prevent the vacuum vessel from a contamination with nitrogen and water the calibration was done without a connection between HPQO and the vacuum vessel. Also a calibration on 2011-07-11 with deuterium, hydrogen and helium was done. Neon evokes intensities at m/z =20 and m/z =22, whereas the intensity at m/z =22 is due to the neon isotope ^{22}Ne. Hence the cracking pattern of neon does not depend on the ion source.

2.3.4 Calibration against the total pressure

On 2011-06-20 gas mixture 2 was continuously filled into the vessel of ASDEX Upgrade, two turbo molecular pumps were operated, the cryo pump was at room temperature. Hence the mass spectrometers could be calibrated against the total pressure measured by the capacity gauge MKS670. By increasing the flow of the gas mixture into the vessel the pressure in the vessel also increases. Four different pressures of the gas mixture, from 0.002Pa to 0.131Pa, were set up and kept constant for several minutes each. In figures 2.19 and 2.20 the intensities of the ethane peak group are shown for both instruments. The methane and ammonia data is shown later in chapter 3. The pressures in the vessel measured by the capacity gauge MKS 670 are listed in table 2.6. After timestep 50 [1] and 85 [2] respectively the flow of the gas in the vessel is stopped for a few timesteps and then raised to the level before again (phase VII). After measurement steps 60 and 100 (phase VIII) respectively the flow is stopped entirely and the gas mixture is pumped out of the vessel. The remaining intensity at m/z =28 indicates that nitrogen, probably produced by the decomposition of ammonia, is still present in the vessel.

Measurement steps(HPQI)	Measurement steps(HPQO)	Phase	Pressure [Pa]
10 - 20	05 - 10	I	0.005
20 - 30	12 - 17	II	0.018
30 - 40	20 - 25	III	0.031
40 - 55	27 - 35	IV	0.064
60 - 70	35 - 40	V	0.131
70 - 85	45 - 50	VI	0.067

Table 2.6: *Pressure measured by the capacity gauge MKS 670 during the calibration performed on 2011-06-20 at ASDEX Upgrade*

As long as gas is injected into the vessel the gas composition is known. If the cracking patterns for all components are known, a theoretical spectrum for the gas mixture can be calculated. Ionization, transmission and detection probability for each compound can be determined by simply comparing the measured intensities with a calculated spectrum. As also the absolute pressure is measured by a capacity

[1] 1 timestep is equivalent to a complete scan
[2] The mass resolution of HPQO is set to a higher value, hence one complete scan takes longer

gauge, the mass spectrometers can be calibrated absolutely and therefore act as pressure gauges. In figure 2.21 the correlations between the measured intensity at m/z =28 and the partial pressure of ethane are shown. Whereas for HPQI measured intensity and partial pressure are proportional this is not the case for HPQO. As the pressure is measured directly at HPQO this behavior can not be explained by pressure fluctuations. As HPQO could not be exchanged during the campaign, it was still operated but the data was not evaluated any longer, consequently all data shown in this thesis is taken by HPQI. The different slopes in figure 2.22 correspond to different detection efficiencies for each molecule, but they also contain the different transmission and detection probabilities. Some species like ethane can be easier ionized than others, e.g. helium. Assuming a gas mixture containing the same amount of ethane and helium, the measured intensity at m/z =28 will be much higher than at m/z =4. Consequently the slope of Helium in figure 2.22 is steeper than the slope of ethane. Like the cracking patterns, the detection efficiencies normalized to nitrogen can also be found in standard libraries. As the turbo molecular pump in sector 13 could not be operated since early July no calibration for nitrogen and also water was done. The calibration factors between measured intensities and partial pressures had to be calculated from the known calibration factor of methane and detection efficiencies provided by Hiden Analytical [HAn]. Later the detection efficiency for nitrogen compared to methane was determined showing a good agreement with the value from Hiden Analytical. Furthermore, as shown in table 2.7, also the other detection efficiencies fit quite well.

Species	Calibration Factor	Detection Efficiency	Detection Efficiency (Hiden)
Helium	4390	0.11	0.14
Deuterium(D_2)	1260	0.39	-
Hydrogen(H_2)	1110	0.45	0.44
Ammonia	451	1.1	1.3
Argon	362	1.4	1.2
Methane	310	1.60	1.6
Ethane	241	2.06	2.6

Table 2.7: *Measured calibration factors, calculated detection efficiencies and detection efficiencies provided by Hiden Analytical renormalizedto methane*

During discharges, the pressures at HPQI and HPQO are not the same. Measurements done by manometers in this areas show that the pressure at HPQI is a factor of two to three higher compared to HPQO. As no baratron is installed at HPQI, there is no exact measurement of the pressure at HPQI. Thus a normalization of the partial pressures measured by HPQI against the measured total pressure is not possible. Hence to determine the partial pressure of each component the calibration factors shown in table 2.7 have to be used. To improve the accuracy of the measurements at HPQI the ionivac should be replaced by capacity gauge and more important HPQO has to be exchanged by a mass spectrometer with a better pressure behavior.

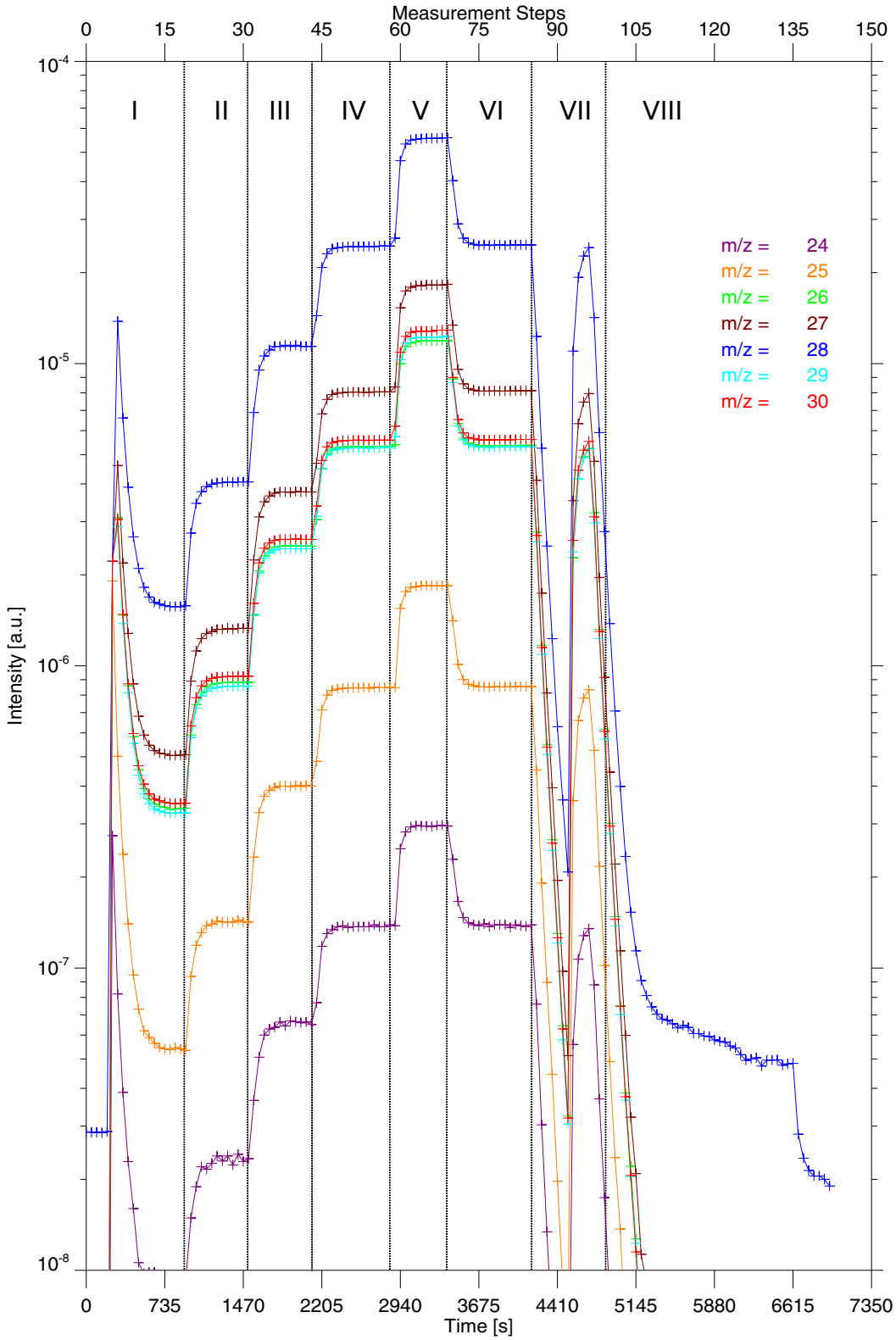

Figure 2.19: *Intensities measured by HPQI evoked by C_2H_x fragments ions of ethane during the calibration on 2011-06-20 at ASDEX Upgrade*

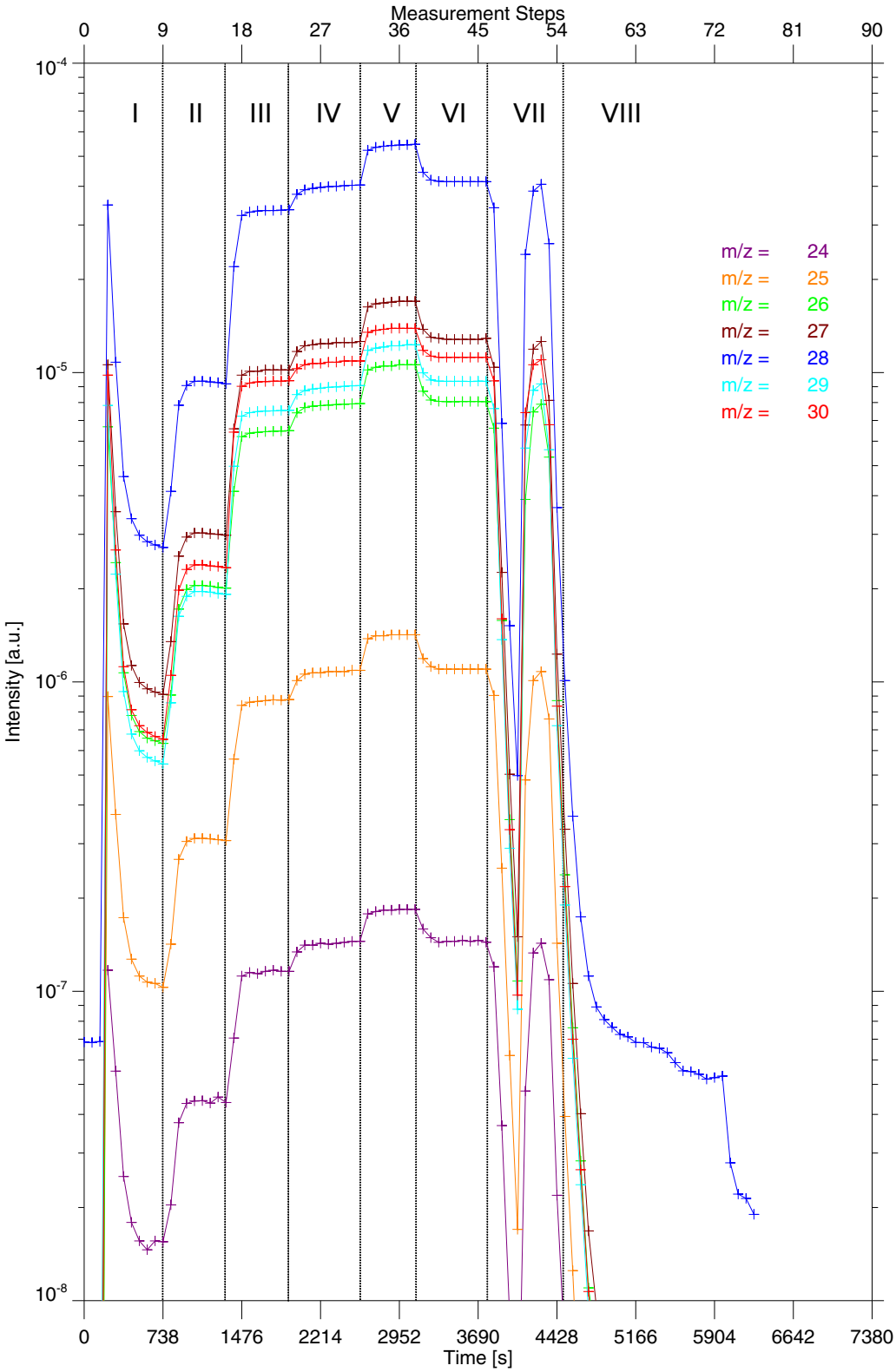

Figure 2.20: *Intensities measured by HPQO evoked by C_2H_x fragment ions of ethane during the calibration on 2011-06-20 at ASDEX Upgrade*

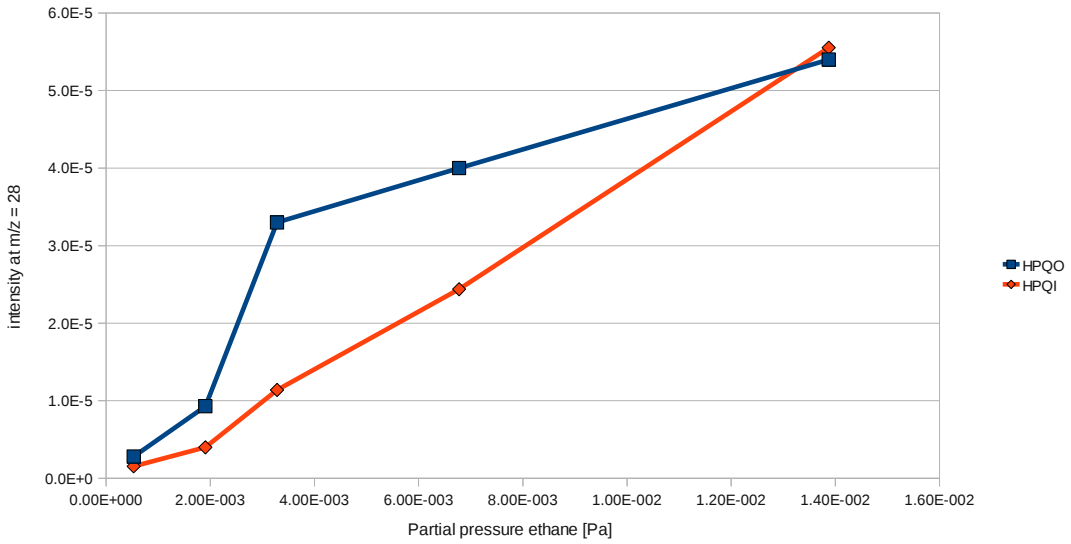

Figure 2.21: *Correlation between partial pressure of ethane and measured intensity at m/z =28 for HPQO and HPQI*

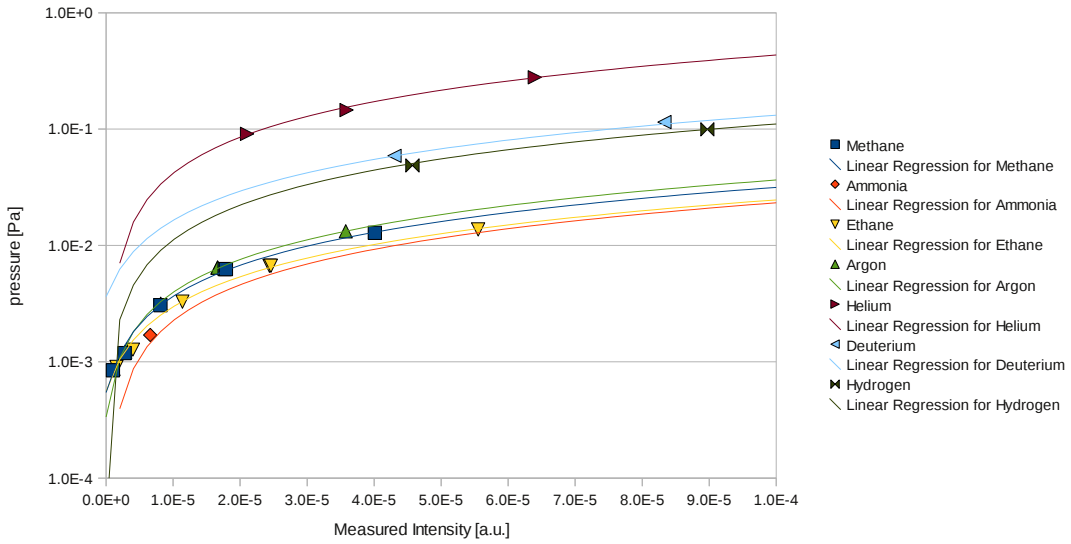

Figure 2.22: *Calibration curves determined for HPQI*

2.4 Cracking Pattern for partly deuterated molecules

As methane is formed within ASDEX Upgrade, it seems reasonable that the atomic distribution of protium and deuterium atoms in the metahne molecules should somehow reflect the atomic distribution of protium and deuterium atoms in the working gas of ASDEX Upgrade. Furthermore the atomic distribution should be roughly equal for two different hydrogen containing compounds formed within ASDEX Upgrade. As shown in figure 2.7 contains the residual gas not only deuterium molecules but also protium and isotopically mixed hydrogen molecules. Hence up to five different methane species (CH_4, CH_3D, CH_2D_2, CHD_3 and CD_4) can be contained in the residual gas. Furthermore also 3 different species of water (H_2O, HDO and D_2O) as well as 4 different species of ammonia (NH_3, NH_2D,NHD_2 and ND_3) can be contained in the residual gas. Two problems have to be considered:

- only the cracking patterns of protonated methane, protonated water and protonated ammonia have been determined
- All methane, water and ammonia species together evoke intensities at 9 different mass to charge ratios (m/z =12 to m/z =20). Hence it is not possible to determine their 12 different partial pressures.

Poschenrieder proposed in [WPo95] and [WPo90] a model that correlates the atomic distribution of protium and deuterium atoms in hydrogen molecules in the residual gas with the the distribution in methane molecules.

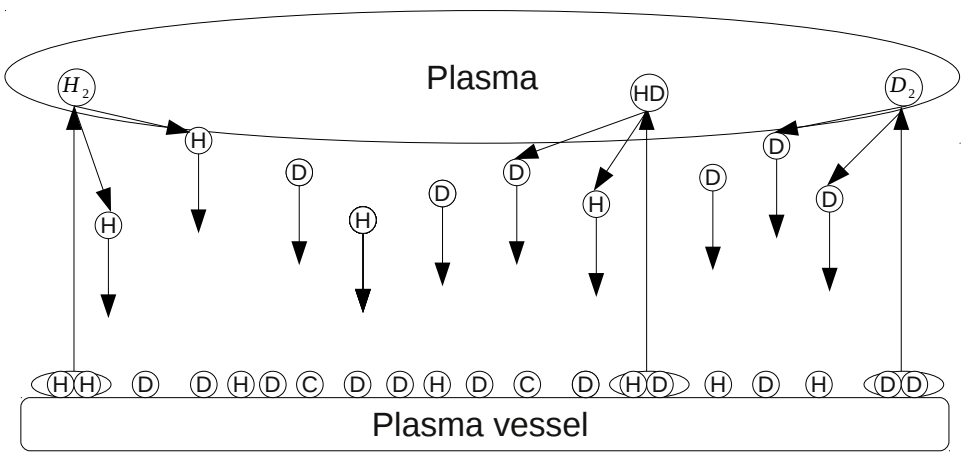

Figure 2.23: *Processes at the surface of the plasma vessel*

Figure 2.23 illustrates some of the processes that take place at surface of the plasma vessel during a discharge. A flux of particles leave the divertor and hit the walls of the plasma vessel and consequently erode carbon atoms. At the end of the discharge carbon atoms are readsorbed at the surface of the wall again. Since the carbon wall of ASDEX Upgrade was covered with a layer of tungsten, the amount of eroded carbon has strongly declined. But the tungsten layer can be destroyed by arcing or edge erosion, hence there is still a certain concentration c_C of carbon atoms at the surface of the plasma vessel. In fact carbon is still the dominant source for impurity production within ASDEX Upgrade. As stated above a flux of particles hits the wall during the discharge. A part of this flux is reflected and enters the plasma again. The other part is adsorbed at the surface. Q_D is the net flux of deuterium atoms that stick at the walls, whereas Q_H refers to the adsorbed protium atoms. Simultaneously adsorbed protium and deuterium atoms tecombine on the surface of the plasma vessel to D_2, HD and H_2. The formation rate F_{D_2} of molecular deuterium is proportional to

$$F_{D_2} \propto K_{DD} c_D^2. \tag{2.18}$$

K_{DD} is a rate coefficient containing collision probability as well as reaction probability for two deuterium atoms whereas c_D is the surface concentration of deuterium atoms. For H_2 and HD similar equations can be formulated:

$$F_{HD} \propto 2K_{HD}c_D c_H \tag{2.19}$$

$$F_{H_2} \propto K_{HH}c_H^2. \tag{2.20}$$

The factor 2 in equation 2.19 derives from simple statistical considerations. The molecules are desorbed from the surface and enter the plasma again. A desorption of hydrogen atoms is not probable as the surface of the plasma vessel is too cold. Once the molecules reach the plasma the binding between the hydrogen atoms can be broken again. Hence the plasma acts like a sink for the molecules. The dissociation of molecular deuterium can be expressed by the dissociation coefficient S_{D_2}, consequently the change of the partial pressure of D_2 is given by:

$$V\frac{dp_{D_2}}{dt} \propto K_{DD}c_D^2 - S_{D_2}p_{D_2}. \tag{2.21}$$

V is volume of the divertor. Again similar equations for isotopically mixed hydrogen and protium molecules can be formulated.

$$V\frac{dp_{HD}}{dt} \propto 2K_{HD}c_H c_D - S_{HD}p_{HD} \tag{2.22}$$

$$V\frac{dp_{H_2}}{dt} \propto K_{HH}c_H^2 - S_{H_2}p_{H_2}. \tag{2.23}$$

Assuming that the fluxes of hydrogen atoms onto the surface of the plasma vessel are dominated by hydrogen atoms produced by the dissociation of D_2, HD and H_2 molecules respectively, the time dependencies of pressures and surface concentrations can be neglected. For the discharge this assumption is a valid approach [WPo95]. Consequently the partial pressures of D_2, HD and H_2 can be expressed as:

$$p_{H_2} = \frac{K_{HH}}{S_{H_2}}c_H^2 \tag{2.24}$$

$$p_{HD} = 2\frac{K_{HD}}{S_{HD}}c_H c_D \tag{2.25}$$

$$p_{D_2} = \frac{K_{DD}}{S_{D_2}}c_D^2 \tag{2.26}$$

As Poschenrieder stated in [WPo95] p_{HD} (equation 2.25) can also be expressed as:

$$p_{HD} = 2\frac{\sqrt{K_{HH}}\sqrt{K_{DD}}}{\sqrt{S_{H_2}}\sqrt{S_{D_2}}} \tag{2.27}$$

The ratio of the partial pressures of the hydrogen species are then given by equations 2.24, 2.27 and 2.26

$$p_{H_2} : p_{HD} : p_{D_2} = R^2 : 2R : 1 \tag{2.28}$$

$$R^2 = \frac{K_{HH}S_{D_2}}{S_{H_2}K_{DD}}\frac{c_H^2}{c_D^2} \tag{2.29}$$

It can be easily seen that R is equal to ratio of protium atoms N_H to deuterium atoms N_D contained in hydrogen molecules.

$$R = \frac{N_H}{N_D} \tag{2.30}$$

Thus the concentration of protium atoms in the hydrogen molecules, called the HDratio, is given by

$$HDratio = \frac{N_H}{N_H + N_D} = \frac{R}{1+R}. \tag{2.31}$$

A HDratio of one is hence equivalent to pure H_2 gas, whereas pure D_2 gas has a HDratio of zero. It should be noted that a HDratio equal to 0.5 within this model is not only equivalent to 50% protium and 50% deuterium atoms in the hydrogen molecules but refers explicitly to a mixture of 25% H_2, 50% HD and 25% D_2.

Analog to the formation of hydrogen molecules also methane can be formed at the surface of the plasma vessel. According to equations 2.18 - 2.20 the formation rate of CH_4 is proportional to

$$F_{CH_4} \propto K_{HC}^4 c_H^4 c_C, \tag{2.32}$$

c_C is the concentration of carbon atoms on the surface of the plasma vessel. The formation rate of CH_4 is according to equation 2.27 proportional to

$$F_{CH_4} \propto K_{HH}^2 K_{CC}^2 c_H^4 c_C. \tag{2.33}$$

The formation rates of CH_3D, CH_2D_2, CHD_3 and CD_4 are therefore given by

$$F_{CH_3D} \propto 4\sqrt{K_{HH}}^3 \sqrt{K_{DD}} K_{CC}^2 c_H^3 c_D c_C \tag{2.34}$$

$$F_{CH_2D_2} \propto 6 K_{HH} K_{DD} K_{CC}^2 c_H^2 c_D^2 c_C \tag{2.35}$$

$$F_{CHD_3} \propto 4\sqrt{K_{HH}} \sqrt{K_{DD}}^3 K_{CC}^2 c_H c_D^3 c_C \tag{2.36}$$

$$F_{CD_4} \propto K_{DD}^2 K_{CC}^2 c_D^4 c_C. \tag{2.37}$$

As the hydrogen molecules also the methane species are desorbed from the walls of the plasma vessel. They enter the plasma where the $C-D$ and $C-H$ bindings respectively are broken up again. According to equation 2.27 the partial pressures of the five methane species can be expressed as:

$$p_{CH_4} = \frac{K_{HH}^2}{S_{H_2}^2} \frac{K_{CC}^2}{S_{CC}^2} c_H^4 c_C \tag{2.38}$$

$$p_{CH_3D} = 4 \frac{\sqrt{K_{HH}}^3}{\sqrt{S_{H_2}}^3} \frac{\sqrt{K_{DD}}}{\sqrt{S_{D_2}}} \frac{K_{CC}^2}{S_{C_2}^2} c_H^3 c_D c_C \tag{2.39}$$

$$p_{CH_2D_2} = 6 \frac{K_{HH}}{S_{H_2}} \frac{K_{DD}}{S_{D_2}} \frac{K_{CC}^2}{S_{C_2}^2} c_H^2 c_D^2 c_C \tag{2.40}$$

$$p_{CHD_3} = 4 \frac{\sqrt{K_{HH}}}{\sqrt{S_{H_2}}} \frac{\sqrt{K_{DD}}^3}{\sqrt{S_{D_2}}^3} \frac{K_{CC}^2}{S_{C_2}^2} c_H c_D^3 c_C \tag{2.41}$$

$$p_{CD_4} = \frac{K_{DD}^2}{S_{D_2}^2} \frac{K_{CC}^2}{S_{C_2}^2} c_D^4 c_C \tag{2.42}$$

Therefore the ratios of the partial pressures of the five methane species are again given by equations 2.38 to 2.42:

$$p_{CH_4} : p_{CH_3D} : p_{CH_2D_2} : p_{CHD_3} : p_{CD_4} = R^4 : 4R^3 : 6R^2 : 4R : 1 \tag{2.43}$$

whereas R is defined as

$$R^2 = \frac{K_{HH} S_{DD}}{S_{HH} K_{DD}} \frac{c_H^2}{c_D^2}. \tag{2.44}$$

Consequently the distribution of atomic protium and atomic deuterium in hydrogen molecules should be the same as in methane molecules. Poschenrieder now proposed to determine the HDratio within methane and consequently all other impurities by measuring the partial pressures of D_2 (m/z =4), HD (m/z =3) and H_2 (m/z =2). This approach is only valid if all impurities are formed by the described process at surfaces with a similar surface concentration of protium and deuterium atoms.

For a mixture of 5 methane species the resulting total cracking pattern CP_{total} is given by a linear combination of the cracking patterns of each species.

$$CP_{total} = CP_{species} \cdot \vec{p}_{part} \tag{2.45}$$

$CP_{species}$ is a matrix containing the cracking patterns of all methane species. The first row contains the cracking pattern of CH_4, the second the cracking pattern of CH_3D and so forth. $\vec{p}_{part}$ contains the relative partial pressures of the methane species. The first entry of $\vec{p}$ is the partial pressure of CH_4, the second entry corresponds to CH_3D. Equations 2.28 and 2.31 define the ratio of partial pressures of the five different methane species normalized to the partial pressure of CD_4 of the methane species as a function of the HDratio. Hence to calculate the total cracking pattern of methane CP_{total} as a function of the HDratio the cracking pattern of all methane species has to be known. As only the cracking pattern of protonated methanes was determined, the cracking patterns of CD_4, CH_3D, CH_2D_2 and CHD_3 have to be calculated out of the measured cracking pattern of CH_4. While Poschenrieder used a very simple model, a more sophisticated approach developed by Price and Iglesia [GPr89] was applied within this thesis. As the cracking pattern of CH_4 is known also the probabilities for the loss of zero (P_0), one(P_1), two(P_2), three (P_3) or four(P_4) hydrogen atoms during the ionization process in the ion source of the mass spectrometer are known. Assuming the loss of a protium atom is equivalent to the loss of a deuterium atom the relative intensities evoked by fragment ions of CH_3D can be calculated. Two different fragment ions, CHD^+ and CH_3^+ evoke intensities at m/z =15. Within the approach proposed by Price and Iglesia the relative abundance A_{CHD^+} of the fragment ion CHD^+ is given by

$$A_{CHD^+} = \frac{1}{2} \cdot P_2 \tag{2.46}$$

P_2 is the probability for the loss of 2 hydrogen atoms and $\frac{1}{2}$ is the probabilty that exactly one protium and one deuterium atom is losst during the ionization process in the ion source. The relative abundance $A_{CH_3^+}$ of the fragment ion CH_3^+ is analog given by

$$A_{CH_3^+} = \frac{1}{4} \cdot P_1 \tag{2.47}$$

The relative intensity at m/z =15 for the methane species CH_3D is hence given by the sum of equation 2.46 and 2.47. The calculated cracking pattern of CH_3D is shown in table 2.8.

m/z	Ions	Relative intensities
12	C^+	P_4
13	C_H^+	$\frac{3}{4} \cdot P_3$
14	CD^+ and CH_2^+	$\frac{1}{4} \cdot P_3 + \frac{1}{2} \cdot P_2$
15	CHD^+ and CH_3^+	$\frac{1}{2} \cdot P_2 + \frac{1}{4} \cdot P_1$
16	CH_2D^+	$\frac{3}{4} \cdot P_1$
17	CH_3D^+	P_O

Table 2.8: *Assumed cracking Pattern of CH_3D*

The calculated total cracking pattern CP_{total} of methane as a function of the HDratio is shown in figure 2.24. From now on this is refered as the cracking pattern of methane as a function of the HDratio.

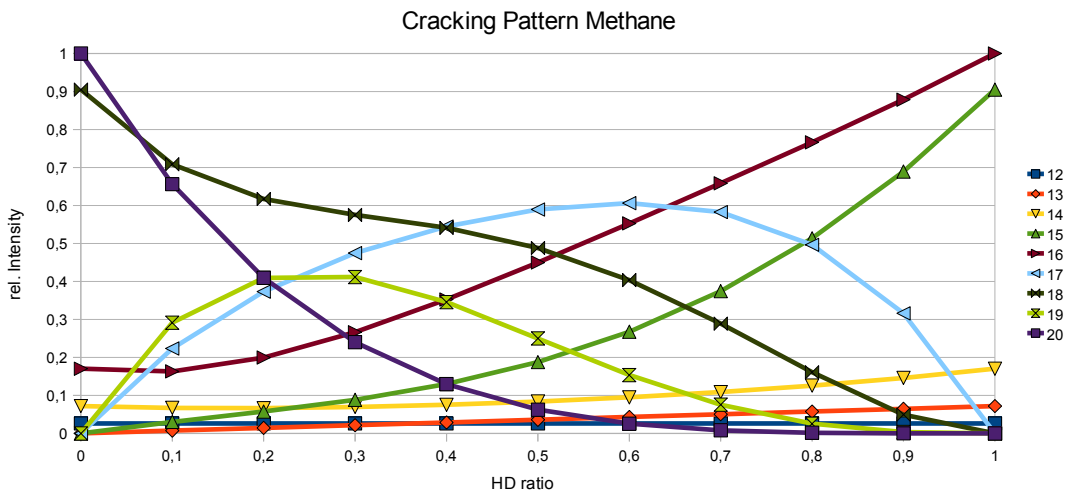

Figure 2.24: *Calculated cracking pattern of methane as a function of the HDratio*

In a similar manner, the cracking patterns for ammonia and water depending on the HDratio are calculated.

D.H. Lenz and WM. C. Conner, Jr. [DLe84] calculated the cracking pattern for CH_3D, CH_2D_2 and CHD_3 based on the measured cracking pattern of CH_4 and CD_4 in analog manner. But in contrast to the approach used for this thesis an isotopic effect in the shattering of and C-D and C-H bond respectively was taken into account. The isotopic factor to describe the difference between a C-D and C-H bond was chosen between 1.1 and 1.25. However the obtained cracking pattern are quite similar to the ones calculated above. Nevertheless assuming a HDratio close to zero during discharges it is not optimal to use purely protonated compounds for calibration.

As stated above the model proposed by Poschenrieder is only valid if all impurities are formed at similar places by similar processes at the same time. Thus different impurity molecules can have a different HDratio if they have different sources. If a impurity molecule is formed within the volume during a discharge a HDratio of roughly zero is expected. If the formation process takes place on the surface of the divertor, the concentration of protium is expected to be a few percent. A much higher HDratio indicates that the impurity is not produced within ASDEX Upgrade but is gassed out by the plasma facing components or produced far away from the divertor. As the source of each impurity is not known preliminary, different HDratios for hydrogen, methane, water and ammonia have to be at least assumed. Consequently it is not sufficient to determine the HDratio for hydrogen by measuring the intensities at m/z =2 to m/z =4. Instead the HDratio for each impurity has to be determined out of the intensity distribution evoked by its fragment ions.

It should be noted the the applied model is not valid if a compound originates from different places. One part of the water vapor is produced within ASDEX Upgrade, therefore the HDratio of this part is almost zero. The other part of the water vapor has an external background and hence a HDratio close to one. This situation can not be addressed by the model described above. However water tends to exchange hydrogen and deuterium atoms, therefore the described model is nevertheless a valid approach.

2.5 Data Evaluation

Once the cracking patterns are calculated the partial pressures of the impurities in the residual gas can now be determined. On a typical experimental day about twenty discharges are performed. Per discharge roughly 60 Peak Jump Scans and 25 Analog Scans are recorded. Hence an automatized evaluation of the measured data is required. Therefore a program package was written in IDL by Felix Reimold in 2008

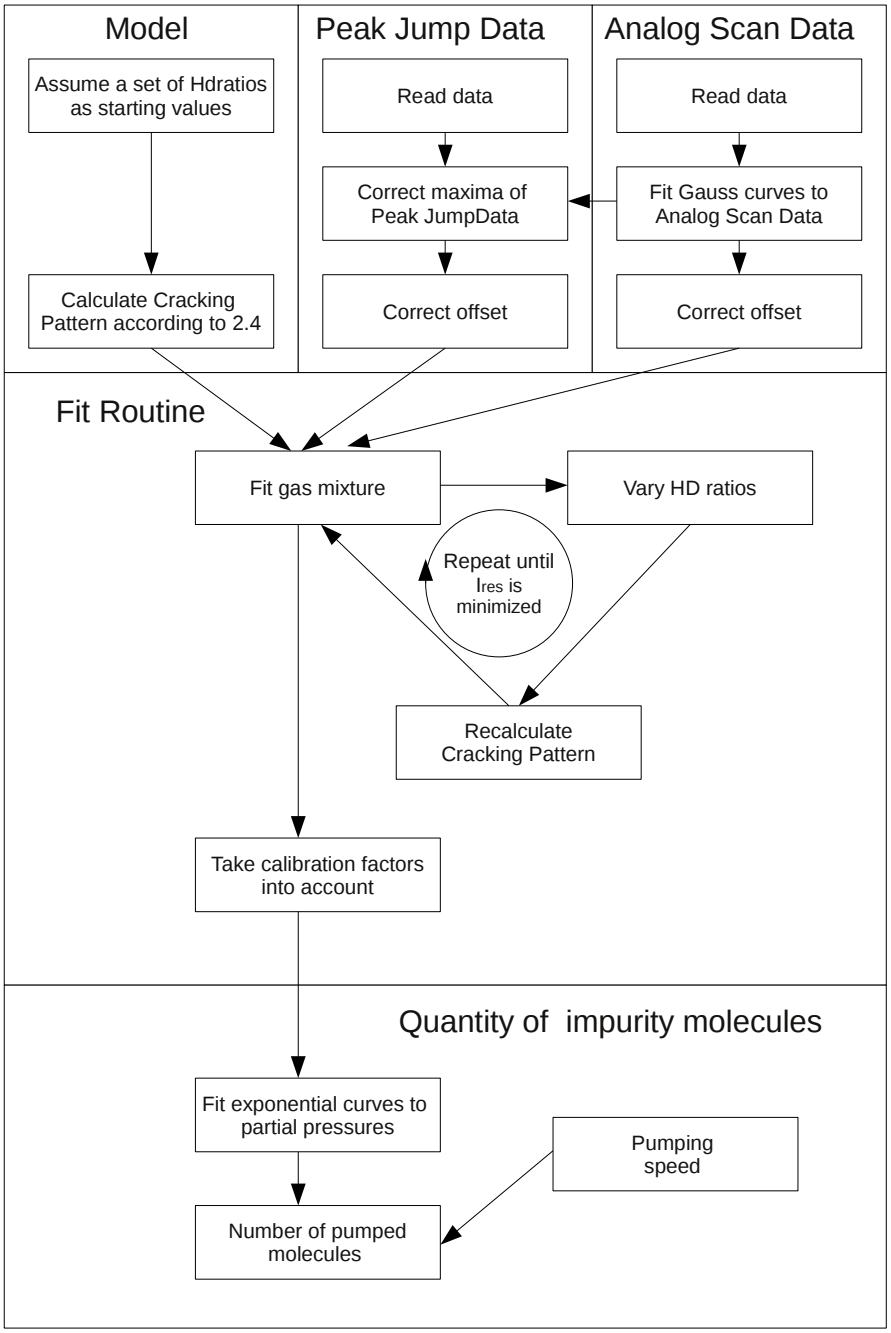

Figure 2.25: *Flow chart of the program package used to calculate the quantity of pumped impurity molecules*

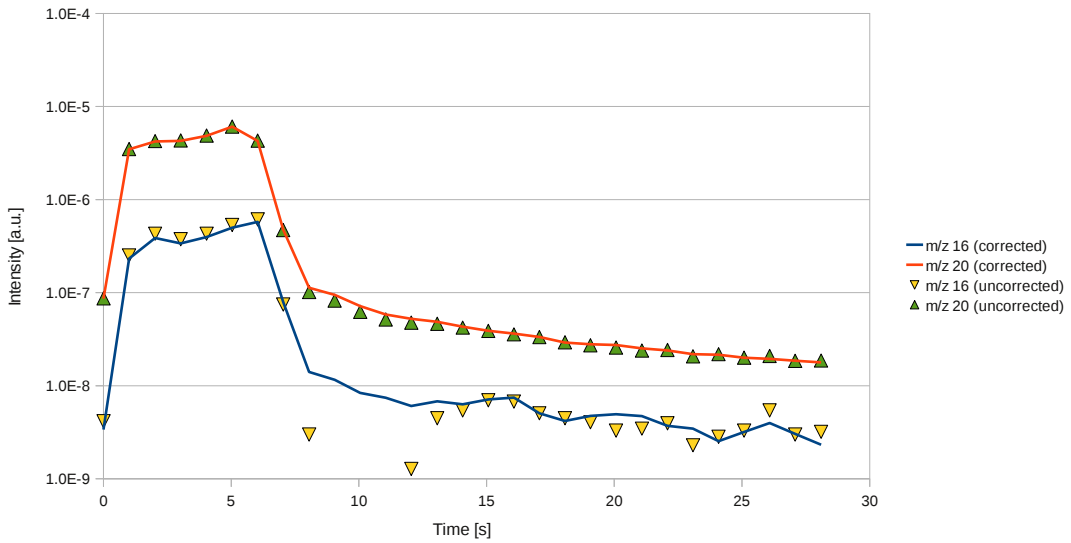

Figure 2.26: *Measured and corrected intensities at m/z =16 and m/z =20 for discharge 27114*

and 2009 [FRe09]. Within this thesis several improvements and extensions like

- an improved offset correction
- an improved routine for the calculation of the cracking pattern according to chapter 2.4
- a combined fit of partial pressures and HDratios of the impurities
- a calculation of the total number of detected molecules

were added to the program package. Figure 2.25 illustrates the main steps in the evaluation. First the corresponding Peak Jump and Analog Scan data for a discharge are put together. As mentioned earlier the m/z scale for the used mass spectrometers is not constant, the peak at m/z =16 e.g. is shifted from 16.00 to e.g 16.22 during an experimental day. Therefore a Gauss curve

$$f(x) \;=\; ae^{-\frac{(x-b)^2}{2\sigma^2}} \tag{2.48}$$

is fitted to each peak measured during the Analog Scan. a is the amplitude, b the center and σ corresponds to the full width at half maximum of the curve. The intensity of a peak is now given by the maximum a of the fitted Gauss curve. While operating in Peak Jump mode only the intensities at defined integer mass to charge ratios are measured. As the centers of the peaks are not mandatory at these mass to charge ratios, the data obtained during this phase has to be corrected. To ensure a good time resolution it was not possible to determine the peak maximum by the mass spectrometers themselves during the Peak Jump measurement. The gauss curves are fitted to every peak for every Analog Scan, thus the parameters b and σ can be averaged over to the total Analog Scan Data for each peak. Assuming an averaged gauss curve with parameters $\bar{b}$ and $\bar{\sigma}$ the measured intensities at the predefined whole mass to charge ratios can be corrected to the intensity at the actual maximum of the peaks. As the shift in the m/z =scale is very slow, b will not differ hugely from Analog Scan to Peak Jump mode.

In figure 2.26 the measured and the corrected intensities at m/z =16 and m/z =20 respectively are shown. Shortly after the discharge, roughly from 8s to 12s, the intensities of some mass to charge ratios like m/z =16 get strongly negative others have a sort of dent (m/z =20). Mass spectrometers of the MKS HPQ series have an internal offset correction. Assuming no real signal at m/z =5, the intensity measured there is used to approximate the offset of the measurement and more important to remove the

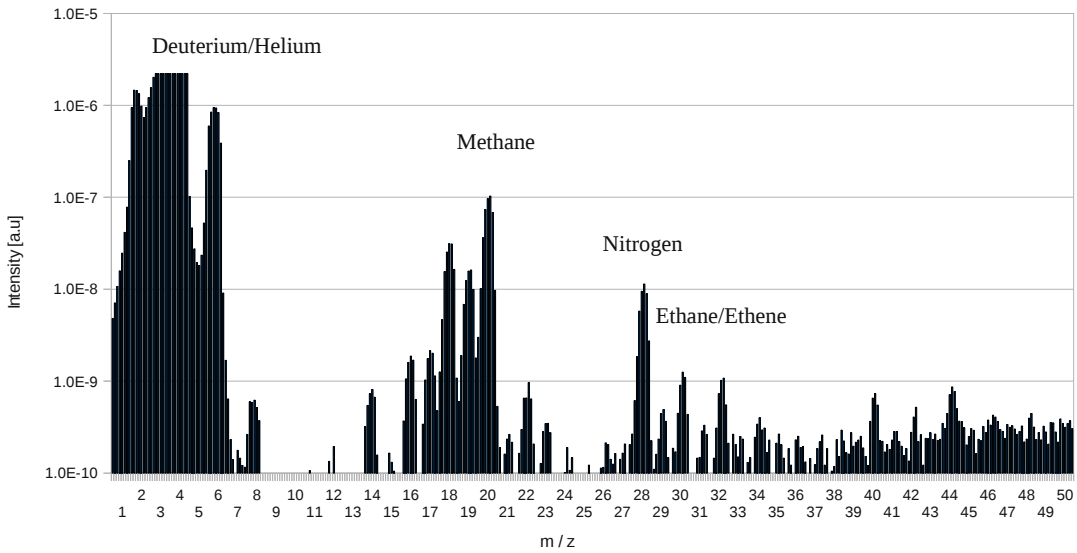

Figure 2.27: *Measured intensities during deuterium injection into the plasma vessel of ASDEX Upgrade without plasma operation*

offset from the measured data. Under typical conditions in a vacuum apparatus m/z =5 might be a good choice, but not at ASDEX Upgrade. As the plasma mainly consists of deuterium, the measured intensity at m/z =4 is very high compared to other mass to charge ratios. The peak at m/z =4 even leads to an intensity at m/z =5 (see figure 2.27). Also an intensity at m/z =6 due to D_3^+ shows up. Consequently the approximated offset is far too big. To overcome this behavior the internal noise correction is set to m/z =23. Additionally the intensity at m/z =23 is measured and subtracted from the other intensities (figure 2.26). Negative intensities therefore do not show up any longer. However by simply filling deuterium into the plasma vessel of ASDEX Upgrade hydrocarbons seem to be produced, but also a small peak at m/z =23 shows up (see figure 2.27). Therefore the applied correction should be a bit to large, but during a discharge there should be no severe influence on the measured data quality. From now on the noise corrected intensities are referred as the 'measured intensities'. In figure 2.28 the combined data for Peak Jump measurement and Analog Scan of discharge 27114 is shown.

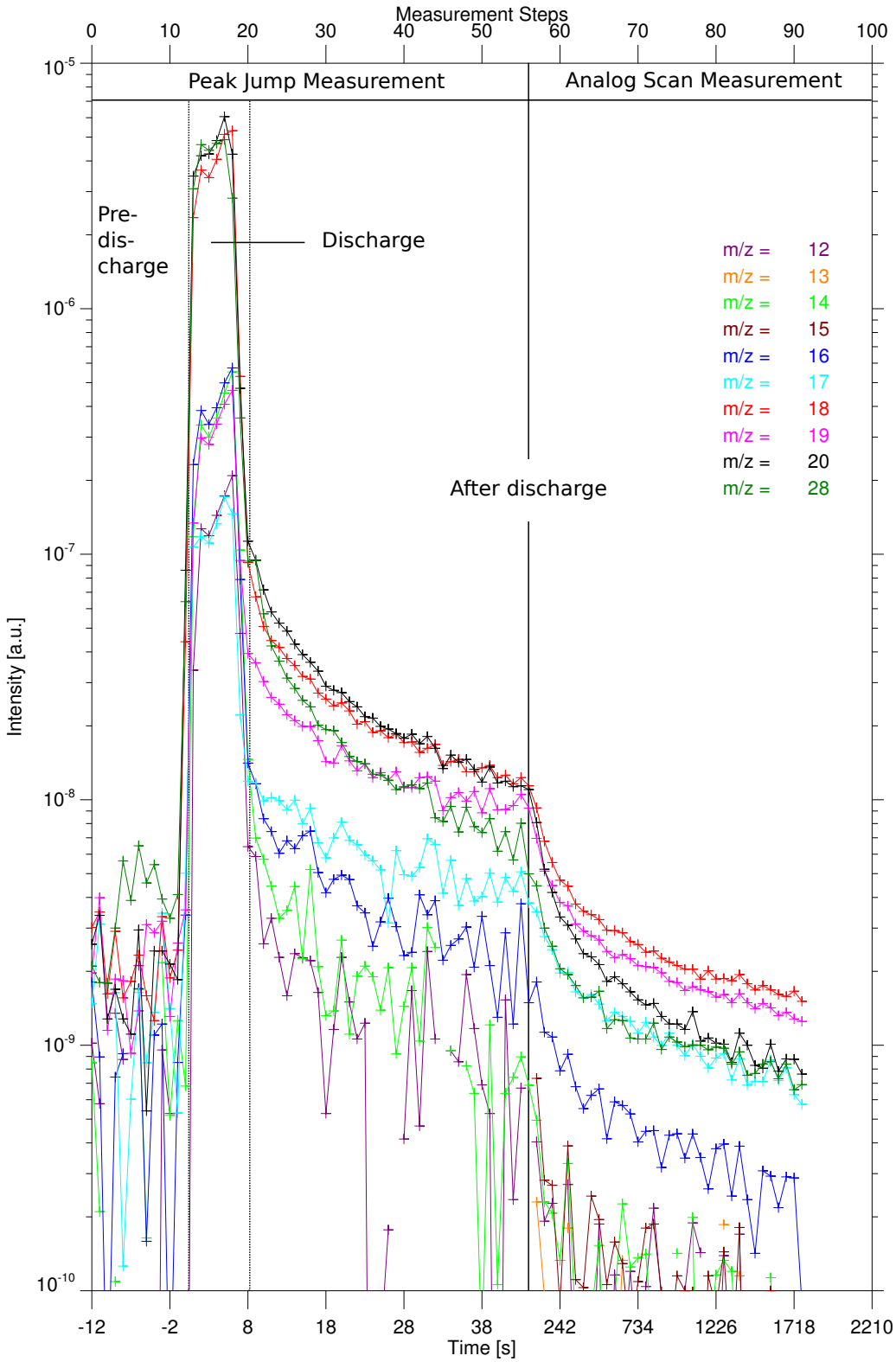

Figure 2.28: *Noise corrected intensities measured by HPQI before, during and after H-mode discharge 27114*

Table 2.9 sums up the different phases and time resolutions of the measurement before, during and after discharge 27114.

Phase	Timespan [s]	Measurement steps	Time Resolution [s]
Peak Jump measurement	-12 - 45	0 - 57	1
Analog Scan measurement	46 - 90	58 - 90	50
Pre discharge	-10 - 0	0 - 10	1
Discharge	0 - 10	0 - 10	1
After discharge	11 - 90	11 - 90	1 or 50

Table 2.9: *Measurement phases during discharge 27114 for HPQI*

The next step is to determine the partial pressures of the impurities contained in the residual gas. Within the program for each measurement step four different HDratios corresponding to hydrogen molecules , water molecules, ammonia molecules and methane molecules can be defined. As stated earlier these HDratios are not known preliminary but they have to be determined out of the measured data.

The spectrum $\vec{I}$, containing the measured intensities of all mass to charge ratios, measured at a certain measurement step is given by

$$\vec{I}_{meas} = CP \cdot \vec{p} \tag{2.49}$$

where CP is a matrix containing the cracking patterns of all impurities and $\vec{p}$ represents the partial pressures of the impurities. Thus the determination of $\vec{p}$ is equal to find the matrix inverse of CP. The size of CP is defined by the number of measured mass to charge ratios and the number of expected impurities. The intensities at 29 mass to charge ratios are measured in order to determine the partial pressure of up to 13 impurities. The measurement of 'surplus' intensities is necessary due to measurement errors. Consequently CP can not be inverted easily. To determine the partial pressures $\vec{p}$ of the impurities the predefined IDL routine 'AMOEBA' is used. AMOEBA bases on the least squares method. To a fitted $\vec{p}_{fit}$ belongs a calculated spectra

$$\vec{I}_{fit} = CP \cdot \vec{p}_{fit}. \tag{2.50}$$

Consequently $\vec{p}$ is determined by minimizing the residual norm I_{res}.

$$I_{res} = ||\vec{I}_{meas} - \vec{I}_{fit}||. \tag{2.51}$$

In figures 2.29 to 2.30 an exemplary evaluation of the 65th measurement step after discharge 27114 is shown. Therefore the measured intensities (blue) are compared to the calculated spectra for pure completely deuterated methane and water (red). The partial pressures of methane and water are $9.3 \cdot 10^{-7}$Pa and $3.9 \cdot 10^{-6}$Pa respectively. The agreement between measured spectrum and calculated spectrum for pure and completely deuterated methane is better than the agreement between measurement and D_2O. Hence methane is preferred by the described fit routine. The fit routine also takes also mixtures of methane and water into account, but pure methane shows the best agreement and hence the smallest residue I_{res}.

As shown in figure 2.7 the spectrum is dominated by m/z =18, m/z =20 and m/z =28 or by m/z =4. Therefore the residual norm is also dominated by the errors made at this mass to charge ratios. To address this problem the partial pressures of hydrogen and helium are fitted separately. For the methane-water-ammonia group it is not possible to separate one component and fit it first. To force the fit to take smaller intensities, e.g. at m/z =12, more into account their contribution to $\vec{I}_{res}$ can be normalized to the intensities measured at other mass to charge ratios like m/z =18. Another intrinsic weakness of this method is that the HDratios and their time dependencies have to be known which is basically not the case. As stated above completely deuterated compounds (e.g. pure CD_4) have a HDratio of zero. Deuterated methane and water cannot evoke intensities at odd mass to charge ratios, but as shown in figures 2.29 and 2.30 there are significant intensities measured at these mass to charge ratios. Hence the partial HDratios of water and methane cannot be equal to zero. In order to address this problem a combined fit of partial pressures and HDratios was developed. The fit routine starts with a basic set of HDratios for

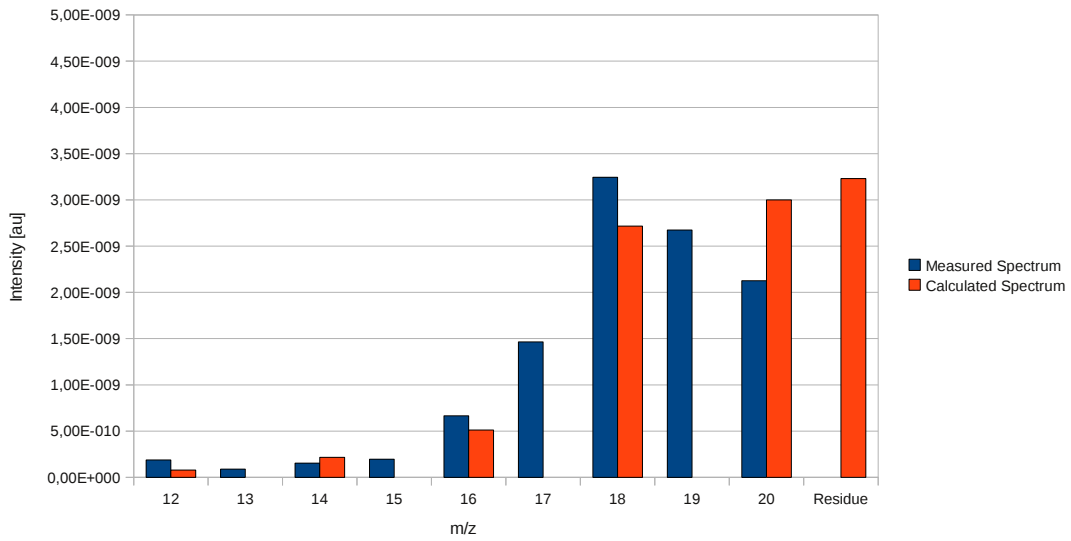

Figure 2.29: *Comparison of measured (65th measurement of discharge 27114) and calculated spectrum for* $9.3 \cdot 10^{-7} Pa$ *of pure* CD_4*. Residue as defined in equation 2.51.*

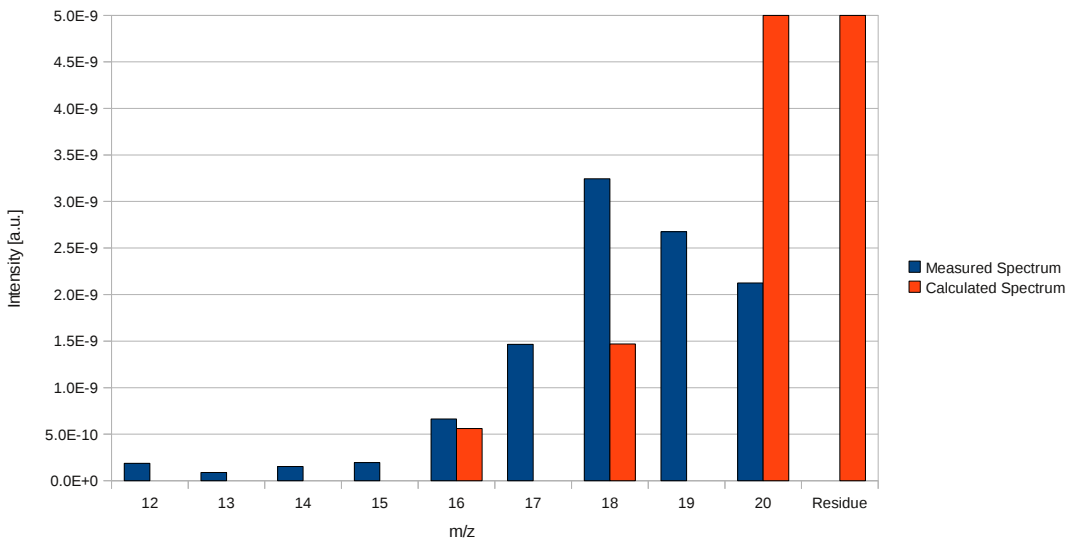

Figure 2.30: *Comparison of measured (65th measurement of discharge 27114) and calculated spectrum for* $3.9 \cdot 10^{-6} Pa$ *of pure* D_2O

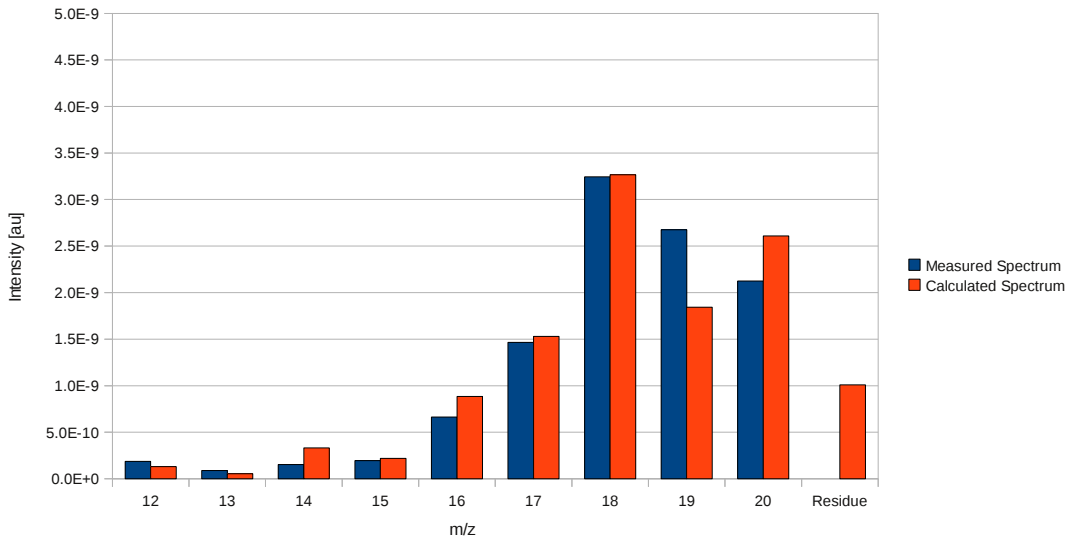

Figure 2.31: *Comparison of measured (65th measurement of discharge 27114) and calculated spectrum for pure methane assuming a HDratio equal to 0.15*

all compounds containing hydrogen (e.g. HDratio for methane and water). For this specific HDratios $\vec{p}$ is fitted again by minimizing the residual norm (see figures 2.29 and 2.30). Now the HDratios are varied in order to find the HDratios which correspond, after fitting $\vec{p}$, to the smallest residual norm. In figures 2.31 and 2.32 the calculated spectra for pure methane with a HDratio of 0.15 and pure water with a HDratio of 0.50 are shown. Again pure methane (partial pressure $1.6 \cdot 10^{-6}$Pa) shows a smaller residual spectrum I_{res} and hence a better accordance bettween measured and calculated spectrum than water (partial pressure $3.86 \cdot 10^{-6}$. But also a possible combined presence of methane and water in the residual gas is taken into account. The calculated spectrum of a combination of $8.5 \cdot 10^{-7}$Pa methane and $1.9 \cdot 10^{-6}$Pa water is shown in figure 2.33. The agreement of the calculated spectrum with the measurement is better than the agreement of the pure compounds. The variation of the HDratios is again realized by an AMOEBA fit routine. However main focus is laid on the distinction between methane, water and ammonia. This group is located between m/z =12 and m/z =20 and hence consists of 9 peaks. In standard operation during Peak Jump mode 8 of this 9 mass to charge ratios are scanned. Additionally m/z =28 is scanned as nitrogen has an impact on m/z =14 and therefore cannot not be neglected like the influence of carbon monoxide or carbon dioxide (see figure 2.7). Consequently while the fit routine is capable to take up to 13 impurities into account, only the partial pressures of nitrogen, water, methane and ammonia are fitted during the discharge. After the discharge additionally hydrogen and helium are fitted. To get information about the abundance of e.g. ethane or argon during the discharge other mass to charge ratios have to be scanned but at the cost of a slower measurement. As their influence on the methane-water-ammonia group is rather small they are completely neglected. Besides the abundances of methane water and ammonia also their HDratios plus the abundance of nitrogen are fitted, so there are 7 free parameters and 9 measured intensities within the model described in chapter 2.4. To evaluate the data of a discharge, first the most probable HDratios are determined by a combined fit of partial pressure and HDratios. On the base of the calculated HDratios the evolution of the HDratio for each compound is fitted (see continuous line in figure 2.35). The abundances of the impurity compounds in the residual gas are now recalculated by using the fitted evolution of the HDratio within the course of a measurement. This procedure leads to smooth partial pressure curves and small residual norms I_{res} between 0.5% and 5% of $||I_{meas}||$. This procedure is necessary as a combined fit gets distracted quite easily due to a relative high number of free parameters. The Peak Jump Scan mode is optimized towards measuring during the discharge thus the data at the end of the Peak Jump measurement when the pressure at the mass spectrometers is already low, the ratio between noise and signal is quite bad. Fits are chosen under two considerations:

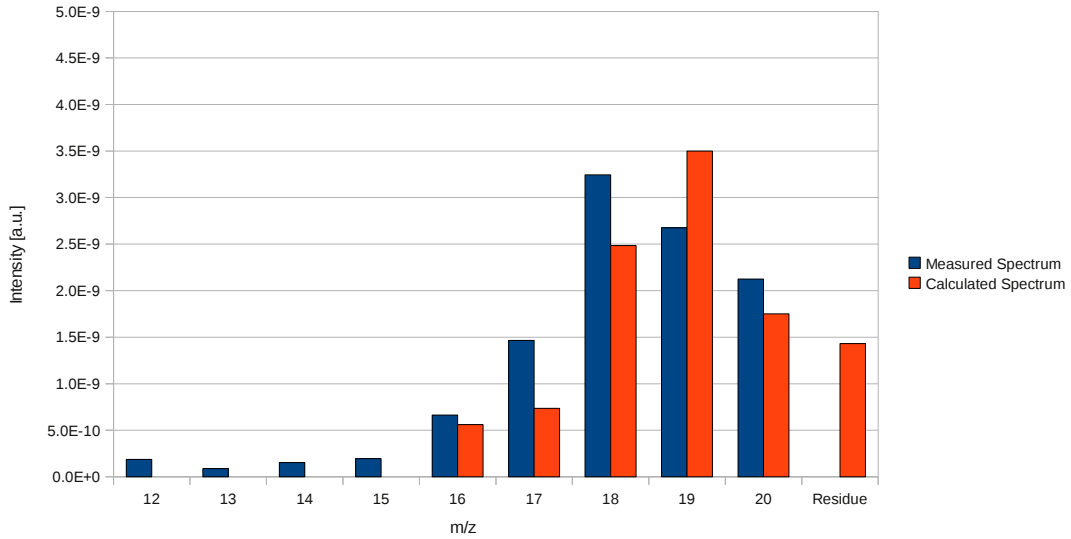

Figure 2.32: *Comparison of measured (65th measurement of discharge 27114) and calculated spectrum for pure water assuming a HDratio equal to 0.50*

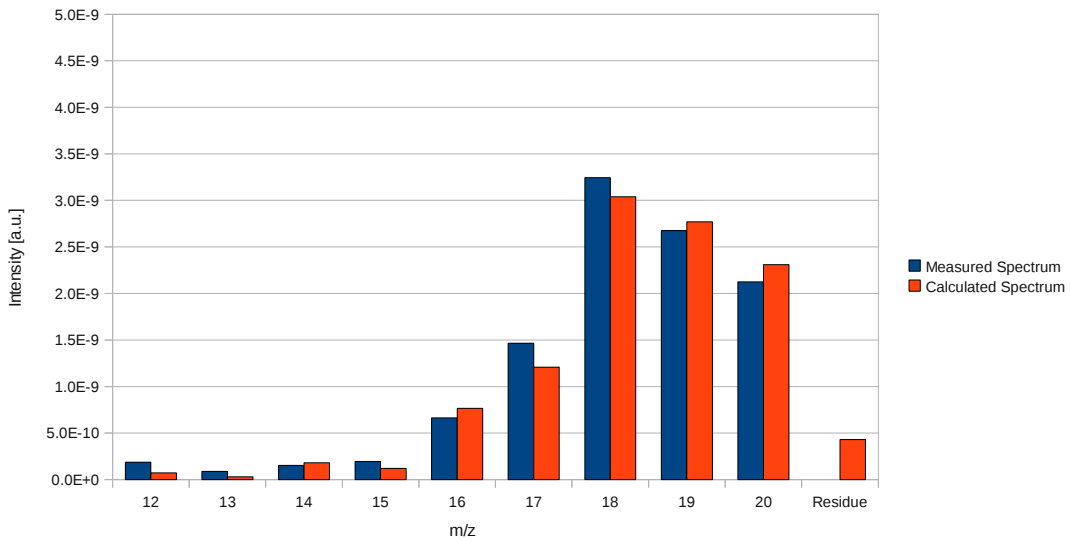

Figure 2.33: *Comparison of measured (65th measurement of discharge 27114) and calculated spectrum for* $2.5 \cdot 10^{-9}$*a.u. methane (HDratio 0.15) and* $3.5 \cdot 10^{-9}$*a.u. water (HDratio 0.55)*

first their residual norm should be minimal, second their partial pressure curves and HDratios should be rather smooth as it is unlikely that the composition of the residual gas changes rapidly. Now the calibration factors shown in table 2.7 are used to convert the fitted abundances into partial pressures. Therefore the calibration factors are multiplied with the fitted abundances of each compound. Typical results for partial pressures and HDratios determined by the procedure described above for discharge 27114 are shown in figure 2.34 and 2.35. For discharge 27114 56 Peak Jump scans and 32 Analog Scans were recorded. Hence measurement steps 1 to 56 represent Peak Jump Scans lasting each about 1 seconds and measurement steps 57 to 89 represent Analog Scans lasting each about 45 seconds, consequently the timescale changes for measurment step 56 to measurement step 57. In figure 2.34 the partial pressures determined by the procedure describe above are shown. The residual norm of the fit is about 4 % of $||I_{meas}||$ throughout the measurement. During the discharge, roughly from 0s to 8s methane and nitrogen are the dominating impurities in the residual gas (see figure 2.34). The partial pressure of nitrogen and methane is roughly $10^{-3}Pa$. It was shown above that the influence of carbon monoxide on the intensities measured at the methane-water-ammonia group can be neglected. Measurements done during discharge 27112 indicate the presence of ethane and ethene. Their combined partial pressure should be about one fifth of the partial pressure of methane. Consequently higher hydrocarbons have no significant influence of the intensities measured between m/z =12 and m/z =20. The partial pressure of water vapor is about $10^{-4}Pa$ and therefore one order of magnitude smaller compared to the partial pressure of methane. As the content of oxygen in the plasma vessel is rather small, the formation of water is not as likely as the formation of methane. As fitting the measured data without ammonia does not corrupt the quality of the fit, the presence of a significant amount of ammonia in the residual gas is not very likely. Before the discharge (-10s - 0s) the ratio between noise and measured intensities is too high for descent evaluation. Consequently the determined partial pressures, as well as HDratios, are not valid. After the discharge water is the dominating impurity followed by methane and nitrogen. Throughout the measurement hardly any ammonia is found in the residual gas. After measurement step 57 the operation mode of the mass spectrometer is switched from Peak Jump mode to Analog Scan mode, consequently the buckles in the partial pressure curves at measurement step 56 exist due to the change in the time scale and hence are not related to a real physical effect. In Analog Scan mode also the partial pressures of deuterium and helium can be determined, but they are not shown in subsequent figures. In figure 2.35 the calculated HDratios for methane and water are shown. The HDratio of ammonia could obviously not be determined. During the discharge the HDratio of methane is almost equal 0, the HDratio of water roughly 0.1. After the discharge both ratios began to rise. However the rise of the HDratio of water is much steeper than the rise of the HDratio of methane (see section 4.2.1). The linear regression for the HDratios of water and methane shown in figure 2.35 are used for the simple fit of the partial pressures mentioned above. In summary the residual gas of discharge 27114 consists roughly of 90% hydrogen(deuterium), 4% helium, 4% water, 1% methane and 1% nitrogen at the end of the Analog Scan phase and thus right before the next discharge. The HDratio of methane is about 0.15 and the HDratio of water about 0.55.

During nitrogen seeded discharges a certain amount of nitrogen molecules is injected into the vessel. To compare the amount of pumped nitrogen atoms contained in ammonia and nitrogen molecules with the amount of nitrogen atoms seeded as nitrogen molecules, the amount of pumped nitrogen molecules and ammonia molecules has to be calculated. The quantity of pumped molecules N is given by

$$N = k \cdot \int_{t1}^{\infty} p(t)S(t)dt \tag{2.52}$$

$p(t)$ is the partial pressure of the impurity and $S(t)$ is the pumping speed for the impurity. Assuming a temperature of 293K at the pumps k is given by

$$k = 2,55 \cdot 10^{17} \frac{molecules}{Pa \cdot l}. \tag{2.53}$$

The used pumping speeds were shown in table 2.1. The effective pumping speed at HPQI is limited by the conductance L between HPQO and HPQI. This conductance was determined to $L = 66\frac{m^3}{s}$ [ASc11]. The effective pumping speed S_{eff} then is given by

$$S_{eff} = \frac{L}{1 + \frac{L}{S}} \tag{2.54}$$

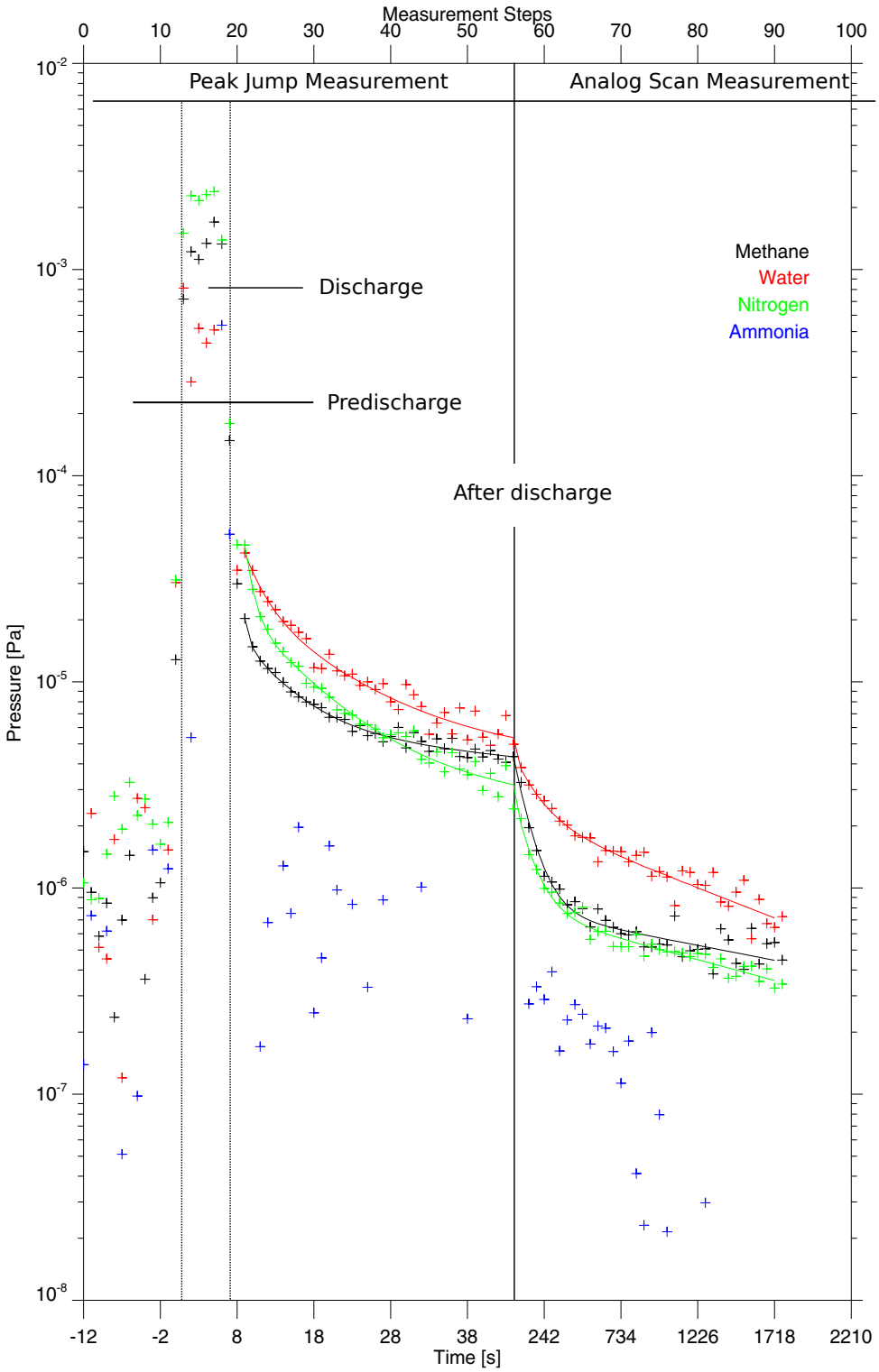

Figure 2.34: *Calculated partial pressures of H-mode discharge 27114 on 2011-06-09*

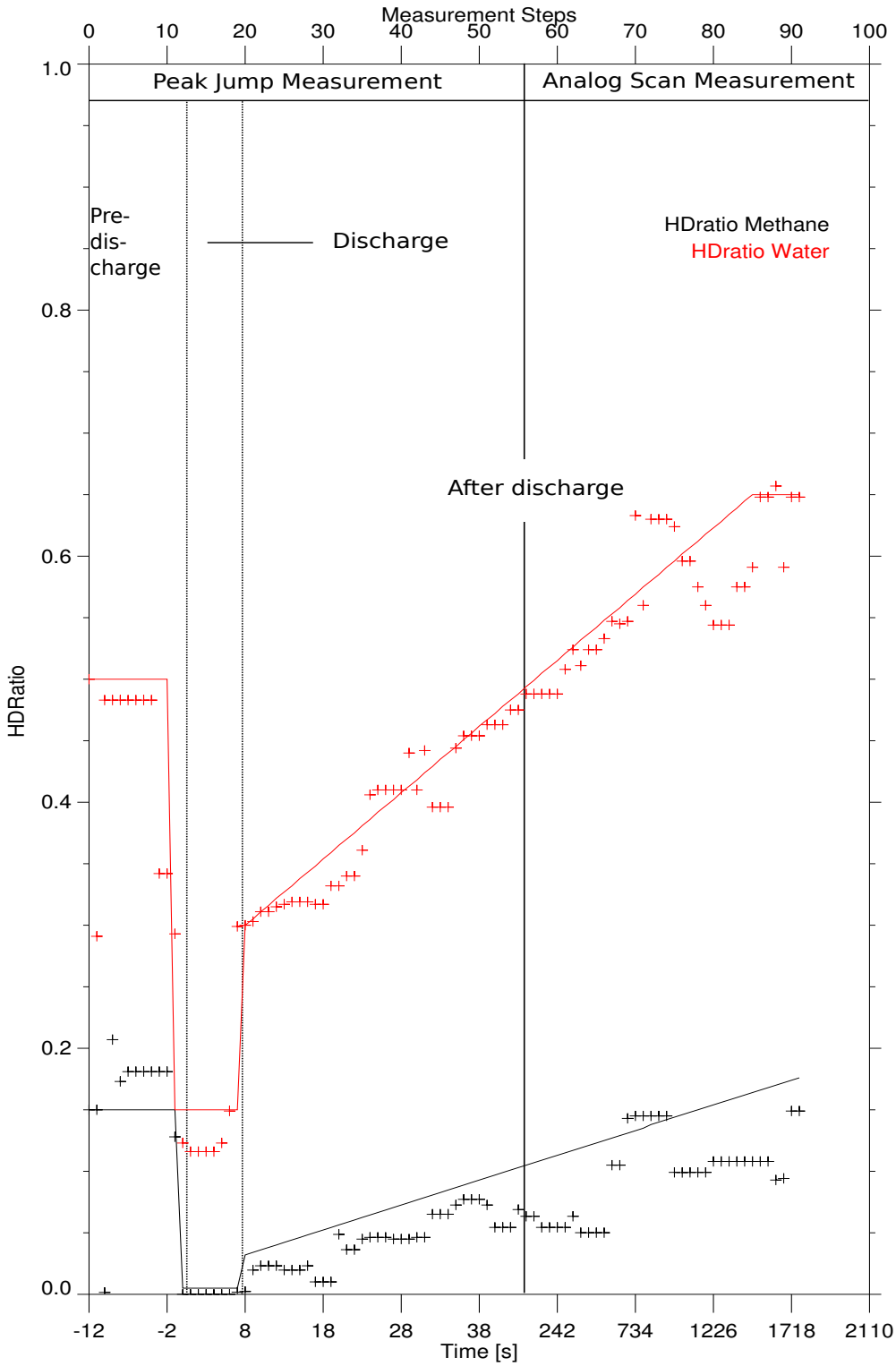

Figure 2.35: *Calculated HDratios of H-mode discharge 27114 on 2011-06-09*

The actual pumping speed for each timestep is calculated for HPQI and HPQO. In standard operation the plasma vessel is pumped out for 20 minutes before the next discharge is performed. Consequently also the partial pressures of the impurities can be measured during this time span. In order to calculate the number of molecules contained in the complete inventory, infinite pumping would be necessary. Consequently exponential curves are fitted to the partial pressure curves and integrated till infinity. After the discharge the pumping speed stays approximately constant, therefore the integration is rather simple. The number of detected molecules during the actual discharge is calculated separately. To calculate the total number of pumped molecules the measured pressure at HPQO was used. The results are shown in table 2.10.

Impurity	After Discharge	Percentage	During Discharge	Percentage	Total	Percentage
Methane	$2,47 \cdot 10^{19}$	1.7%	$7.11 \cdot 10^{19}$	0.5%	$9.58 \cdot 10^{19}$	0.6%
Water	$5,49 \cdot 10^{19}$	3.8%	$1.68 \cdot 10^{19}$	0.1%	$7.17 \cdot 10^{19}$	0.5%
Nitrogen	$2.43 \cdot 10^{19}$	1.7%	$1.28 \cdot 10^{19}$	0.1%	$1.52 \cdot 10^{20}$	1%
Residual gas	$1.43 \cdot 10^{21}$	100%	$1.41 \cdot 10^{22}$	100%	$1.55 \cdot 10^{22}$	100%

Table 2.10: *Composition of the residual gas of discharge 27114*

During the discharge the impurity concentration is below 1% , after the discharge roughly 7% . It should be noted that other impurities like ethane or carbon dioxide are contained in the residual but not fitted and consequently are not shown in table 2.10. The maximal combined partial pressure of ethane and ethane was estimated to be roughly one fifth of the partial pressure of methane. Other impurities can be neglected too (see figure 2.7). Hydrogen and helium are not shown as information about their partial pressures is only available in the Analog Scan phase. As impurity concentration is below 1% , during the discharge their partial pressure is almost equal to the absolute pressure at the divertor measured by the capacity gauge. This results show that ASDEX Upgrade is a well conditioned device.

A rough calculation shows that about $1.02 \cdot 10^{21}$ hydrogen and $5.01 \cdot 10^{19}$ helium atoms were pumped during the Analog Scan phase. It should be noted that 'Analog Scan phase' is not identical to 'after discharge'. The 'after discharge' data includes all scans recorded after the actual discharge and therefore containing Peak Jump scans as well as Analog Scans. As the pressure at HPQO is known, the total number of pumped molecules during the Analog Scan phase can be calculated. Unfortunately the pressure values are only measured for about 10 minutes, consequently only partial pressures measured by the mass spectrometers during this time span are taken into account. It shows up that about $7.70 \cdot 10^{20}$ molecules are pumped in total. Assuming an infinite long pumping $9.40 \cdot 10^{20}$ molecules in total and $1.23 \cdot 10^{21}$ hydrogen molecules are pumped. Maybe this difference is caused by the negligence of the pumping speed of the NBI boxes. Nevertheless an error of 30% has to be expected for total quantities. Molecular nitrogen is usually seeded from valves positioned in toroidal symmetry at the roof baffle of ASDEX Upgrade. The number of seeded nitrogen molecules can be calculated from the electron flow measured by the UVD diagnostic for each valve.

Chapter 3

Behavior of ammonia in the all tungsten plasma vessel of ASDEX Upgrade

In order to determine the cracking pattern as well as the calibration factor of ammonia a gas mixture (see table 2.5) containing ammonia among other gases was filled into the plasma vessel of ASDEX Upgrade on 2011-06-20 as described in chapter 2.3.4. During the measurement the pressure of the gas mixture in the vessel was varied stepwise. The mass spectromters were operated in Analog Scan mode. Due to the corrosive nature of ammonia the gas mixture could not be inserted via the standard gas inlet system of ASDEX Upgrade. Instead it had to be injected from the valve in sector 3. During the measurement two turbo molecular pumps (TMP5 and TMP13) equipped with a thermal decomposer to get rid of the ammonia were operated. The cryo pump was at room temperature. Further information about the general measurement setup was given above in section 2.3.4.

3.1 Measured Intensities

The gas mixture used for calibration only contained undeuterated compounds. Hence methane is expected to evoke intensities from m/z =12 to m/z =16 and ammonia from m/z =14 to m/z =17. Consequently the measured intensities at m/z =12 and m/z =13 are specific for methane and the intensity at m/z =17 for ammonia. Thus a simple separation of methane and ammonia is possible. The influence of isotopes like ^{13}C (relative abundance $\approx 1\%$) and ^{15}N (relative abundance $\approx 0.5\%$) is neglected. Furthermore the background of nitrogen and water can be neglected.

The measured intensities at the m/z =12 to m/z =19 are shown in figure 3.1, the intensities measured for ethane were shown above in figure 2.19. While the intensities at methane specific mass to charge ratios (m/z =12 and m/z =13) follow the applied total pressure quite fast, this is not the case for the ammonia specific intensity at m/z =17. The intensity at m/z =17 does not reach a constant value within several minutes of constant gas flow during each measurement phase (see table 2.6). Nevertheless a trend towards saturation is clearly visible. The intensities at m/z =14 to m/z =16 show a kind of mixed behavior as these intensities are evoked by methane and ammonia. Almost immediately after the flow of the gas mixture into the vessel was stopped (phase VII) hardly any intensity at m/z =12 and m/z =13 can be measured, whereas the intensities at m/z =16 and m/z =17 decrease only slowly. The same behavior can be observed during phase VIII, when the gas flow is stopped and the plasma vessel is again evacuated. As soon as the gas mixture is injected again (phase VII), the intensities at methane related mass to charge ratios are equal to the intensities measured during phase VI. As long as the gas mixture is inserted into the vessel the intensity measured at m/z =16 is the highest within the depicted group. When the gas flow is stopped, the highest intensity is instead measured at m/z =17 which relates to NH^+. As stated above the gas mixture contains only undeuterated compounds therefore it is quite

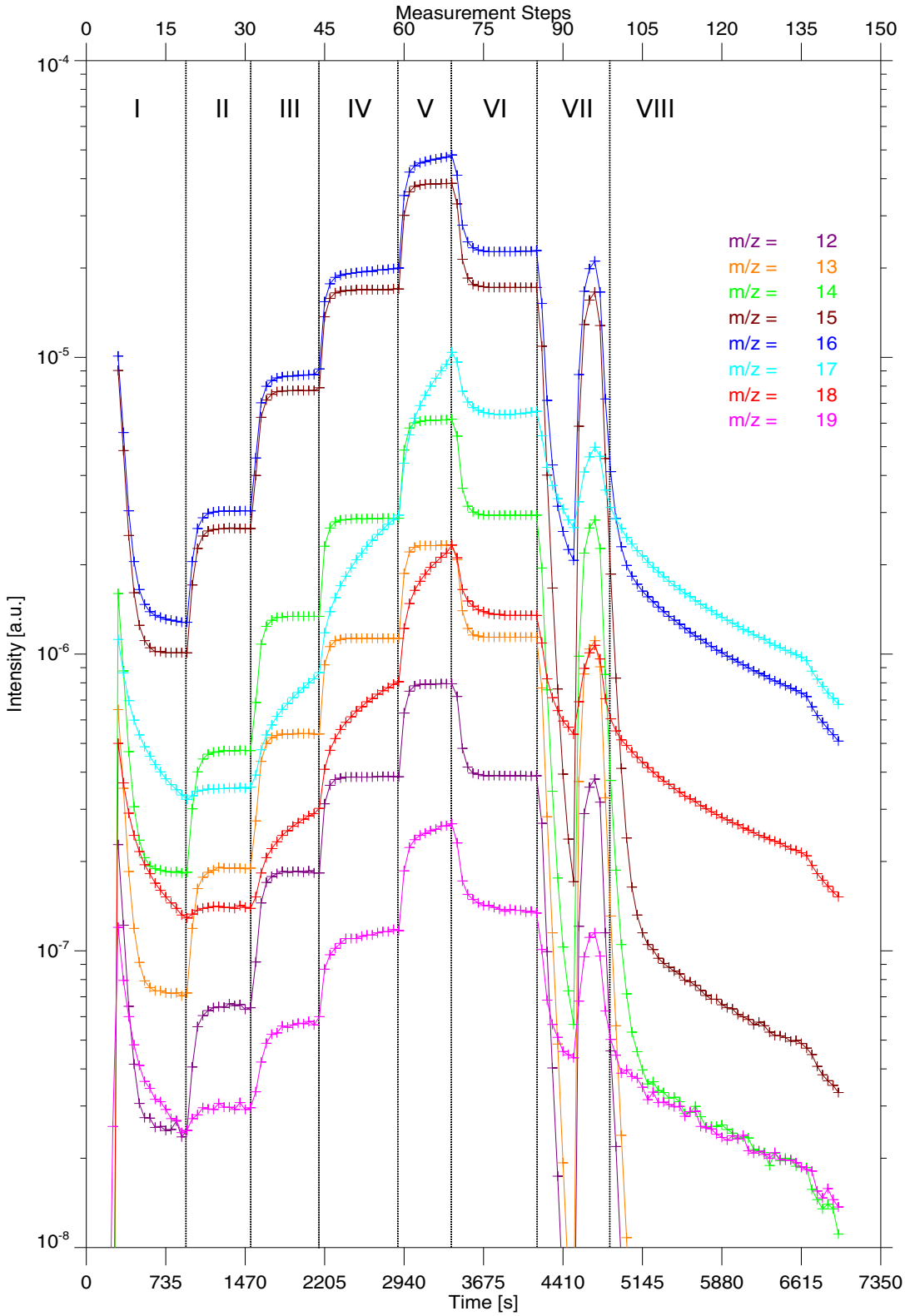

Figure 3.1: *Intensities measured by HPQI at m/z =12 to m/z =19 for a ammonia and methane containing gas mixture injected into in the plasma vessel of ASDEX Upgrade*

Phase	Pressure [Pa]
I	$4.3 \cdot 10^{-3}$
II	$8.9 \cdot 10^{-3}$
III	$1.8 \cdot 10^{-2}$
IV	$3.4 \cdot 10^{-2}$
V	$4.2 \cdot 10^{-4}$
VI	$1.8 \cdot 10^{-4}$

Table 3.1: *Pressures during the measurement performed for an ammonia and methane containing gas mixture injected into a stainless steel vessel*

surprising that significant intensities at m/z =18 and m/z =19 show up. They show roughly the same behavior as m/z =17 and are therefore probably related to ammonia. The intensities measured by HPQO at m/z =12 to m/z =19 are shown in the appendix (see figure A.6). They show a similar evolution as the intensities measured by HPQI.

The surface of the plasma vessel of ASDEX Upgrade consists of carbon covered by a layer of tungsten. The tungsten layer is additionally covered by layers of boron and amorphous hydrocarbon layers. During a campaign deuterium atoms are adsorbed at the surface, even on non experimental days like 2011-06-20. The surface is furthermore plasma activated. To study the influence this surface on the observed effects, the measurement done on 2011-60-20 at the plasma vessel of ASDEX Upgrade was repeated under simplified labor conditions. Therefore the same gas mixture was filled into a stainless steel vessel on 2011-06-28. The mass spectrometer HPQO was deinstalled from ASDEX Upgrade and set up at the stainless steel vessel. Hence all data shown for the 2011-06-28 was measured by HPQO. The flow of the gas mixture into the stainless steel vessel was controlled by the MKS flow controller MKS 647B. A gas washer was used to clean the gas outlet from ammonia. A single turbo molecular pump was operated to keep the pressure in the vessel constant for a constant gas flow. The pressure in the stainless steel vessel was varied from $4.0 \cdot 10^{-3}$ Pa to $4.0 \cdot 10^{-2}$Pa (see table 3.1). Beside the intensity at m/z =18 all measured intensities show roughly the same evolution as the applied absolute pressure (see figure 3.2). Whereas the intensity at m/z =18 follows the applied pressure changes in phases I and II it remains almost constant during phases III - VI. As long as gas in injected the highest intensity is measured at m/z =16. In phases without gas injection (before I and VII) the highest intensity is measured at m/z =18. As soon as the gas flow is stopped (VIII) hardly any intensity can be measured at m/z =12 and m/z =13, whereas the intensities at m/z =14 to m/z =17 only decline slowly. The intensity at m/z =18 even stays roughly constant.

3.2 Conclusions

During the measurements on 2011-06-20 and 2011-06-28 an ammonia and methane containing gas mixture was filled into the plasma vessel of ASDEX Upgrade and a stainless steel vessel respectively. As the relative abundance of ammonia (9.88%) and methane (9.79%) in the gas mixture was almost equal it was expected that also the partial pressures of both compounds in the plasma vessel and stainless steel vessel respectively would be almost equal. During the ionization process in the ionsource of a mass spectrometer fragmentation of the sample molecule can occur. The relative abundance of the fragments is given by the cracking pattern of each compound. As stated above the cracking patterns differ from ion source to ion source but for HPQO and HPQI they are rather similar. Therefore ratios of intensities measured at two mass to charge ratios are roughly equal for both devices. The measured cracking patterns of methane and ammonia (see chapter 3.3) show that the abundance of CH_3^+ (m/z =15) normalized to CH_4^+ is roughly 0.9. The abundance of NH^+ normalized to NH_3^+ is about 0.1. Furthermore the ionization probability of methane is by a factor of 1.2 higher than the ionization probability of ammonia. Hence it is expected that, as long the gas mixture is injected, the intensity at m/z =15 is slightly higher than the intensity

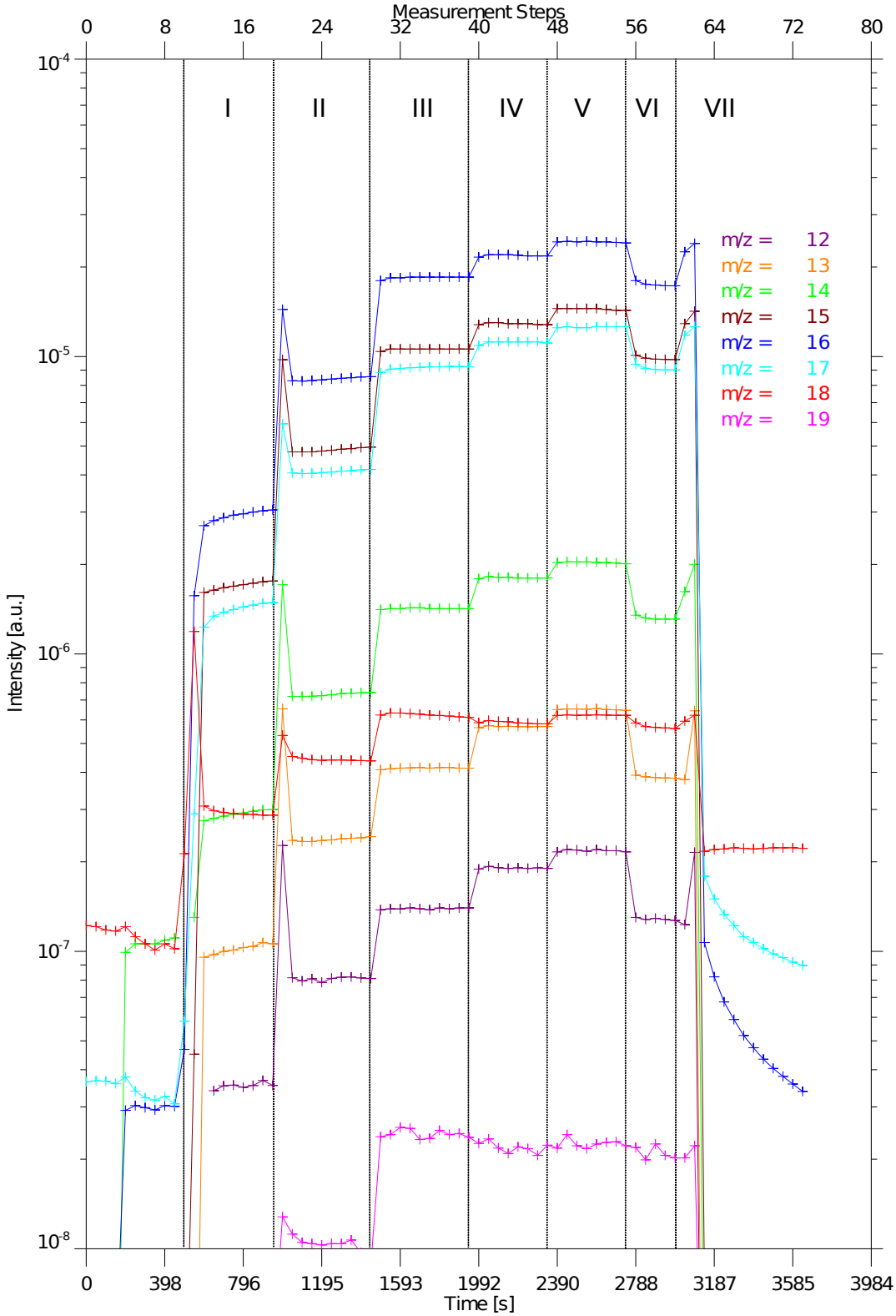

Figure 3.2: *Intensities measured by HPQO at m/z =12 to m/z =19 on 2011-06-28 in the stainless steel vessel*

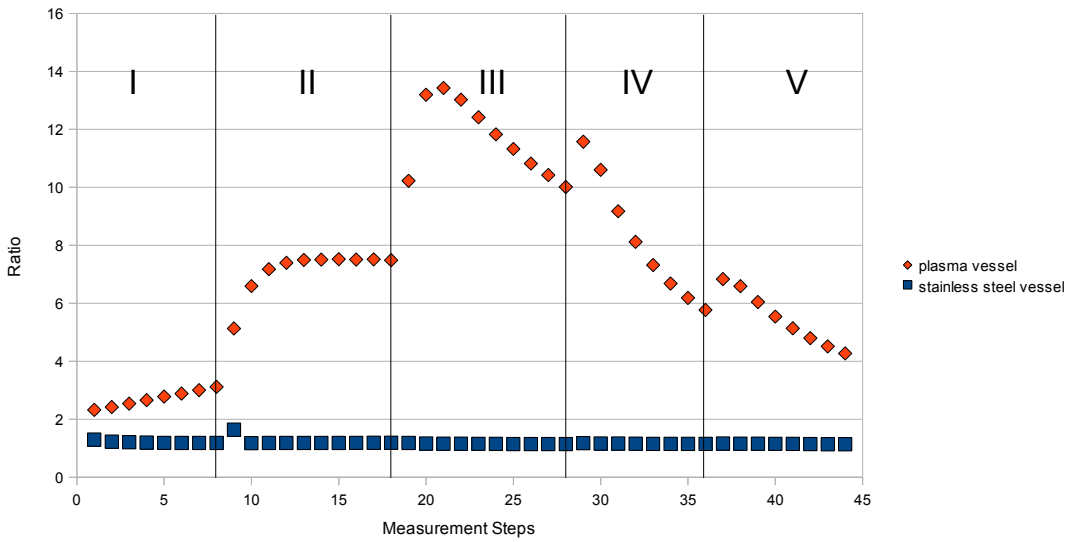

Figure 3.3: *Ratio of the intensities measured at m/z =17 to m/z =15 representing the partial pressure of ammonia and methane respectively*

measured at m/z =17. In figure 3.3 the ratios of the intensities measured at m/z =15 to m/z =17 are shown for the experiments performed at ASDEX Upgrade and at the stainless steel vessel. The phases shown in figure 3.3 are equal to the phases shown in figures 3.2 and 3.1. Hence the absolute pressures increase from phase I to V. Some measurement steps of the experiment at ASDEX Upgrade have been left out in order to show an equal amount of measurement steps for both experiments. During the experiment in the stainless steel vessel the expected ratio of roughly one is measured throughout the experiment. However this is not the case for the measurement done at the plasma vessel of ASDEX Upgrade, instead ratios between 2 and 15 are determined. As undeuterated compounds are used, the intensity at m/z =17 is specific for ammonia and the intensity at m/z =15 roughly for methane. Hence a significant part of the injected ammonia is missing and probably adsorbed at the surface of the plasma vessel. No significant adsorption was observed during the experiment performed in the stainless steel vessel. For a further investigation the partial pressures are determined by the fit routine described in chapter 2.5. The results are shown in figure 3.4. Like the intensity at m/z =17 also the partial pressure of ammonia shows during phases II to V a trend towards saturation. Hence the determined time evolution of the partial pressures of ammonia supports the assumption that ammonia is adsorbed at the surface of the plasma vessel.

As stated above the used gas mixture consisted out of 9.88% ammonia and 9.73% methane. Hence the percentage of adsorbed ammonia can be estimated by simply comparing the measured partial pressures of methane and ammonia. (see figure 3.5, blue curve) A significant part of the ammonia, up to 90% during phase III, is adsorbed at the surface of ASDEX Upgrade. From phase III to phase V two clear trends are visible. At the beginning of each phase when the gas flow is increased also the percentage of adsorbed ammonia increases. During the adjacent time interval with constant gas flow the percentage decreases again. The evolution of the partial pressure of ammonia during phase I is dominated by the gas injection at the beginning of phase I. Hence the partial pressure of ammonia decreases throughout the phase, resulting in an increasing percentage of adsorbed ammonia.

During both experiments an intensity at m/z =18 showed up. The intensity measured during the experiment at ASDEX Upgrade seems to be linked to the intensity at m/z =17. A simple explanation would be the production of NH_4^+ in the ion source of the mass spectrometer. As this effect did not show up during the experiment in the stainless steel vessel this explanation can be excluded. During calibration measurements at ASDEX Upgrade using a gas mixture without ammonia (see table 2.3) such an effect

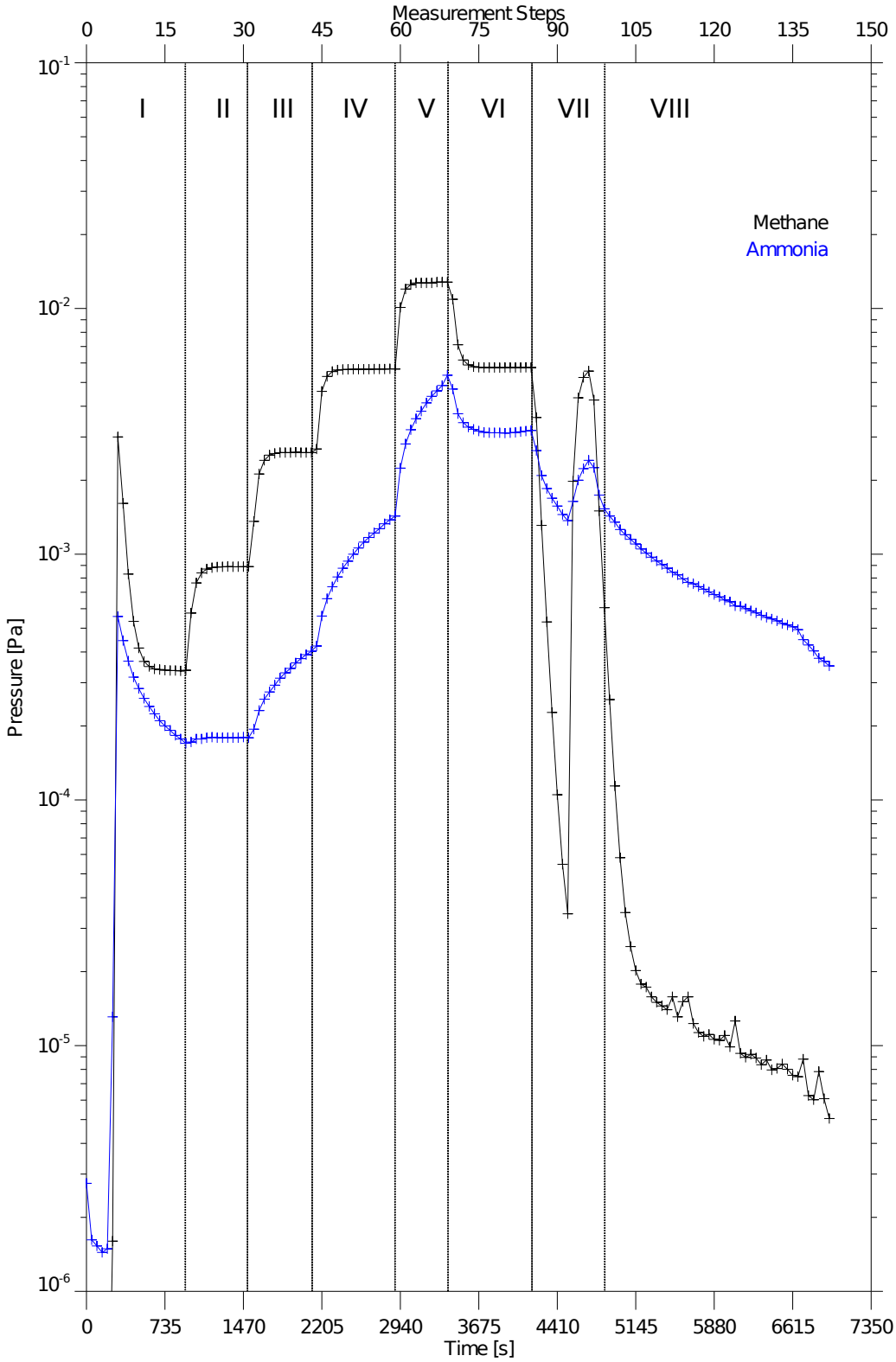

Figure 3.4: *Calculated partial pressures for methane and ammonia injected into ASDEX Upgrade*

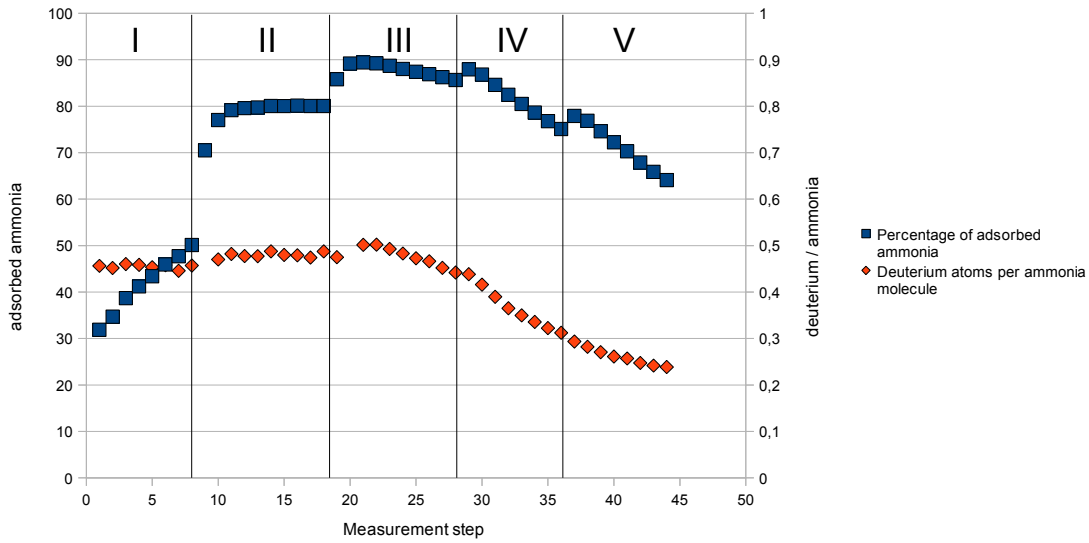

Figure 3.5: *Percentage of adsorbed ammonia (blue curve) and deuterium atoms per ammonia molecule (red curve) for the experiment in ASDEX Upgrade*

was never observed. In figure 3.6 the ratios of the intensities measured at m/z =17 to m/z =18 are shown. As the stainless steel vessel as well as the inlet pipe used on 2011-06-28 were not baked before the experiment, a background of water (m/z =18) has to be expected (see figure 3.2 before phase I and also during phase VIII). Thus by increasing the pressure in the vessel also the intensity measured at m/z =18 will increase slightly. But the extent of the increase of the intensity at this mass to charge ratio at the begin of phases I and II can not be explained by an enhanced desorption of water molecules from the surface of the stainless steel vessel into the volume. Instead this effect is expected to be due to water molecules adsorbed at the inlet pipe. By increasing the gas flow more water molecules are carried away by the streaming gas mixture. This effect seems to saturate during phases III and VI. By comparing the intensity at m/z =18 before the measurement and during phase VIII a net flux of water into the vessel is visible. The described effect induces an increasing ratio of the intensity at m/z =17 to the intensity at m/z =18 throughout the measurement (see figure 3.6). This effect can not be seen in the data obtained from the experiment at ASDEX Upgrade. As this measurement was done during campaign 2010/2011 the plasma vessel was conditioned and evacuated for several weeks. Hence the influence of water is not relevant at the applied pressures. The ratio of the intensity measured at m/z =17 to the intensity at m/z =18 remains roughly constant throughout the measurement, only during phases IV and V (highest pressure) a slight increase of the ratio is visible. This indicates that the intensity measured at m/z =18 is related to ammonia.

As stated above deuterium atoms are adsorbed at the surface of the plasma vessel. Hence an isotope exchange of adsorbed ammonia molecules seems possible. A hydrogen atom of the NH_3 molecule (m/z =17) is replaced by a deuterium atom, resulting in a NH_2D molecule (m/z =18). As shown in figure 3.5 the percentage of adsorbed ammonia decreases with increasing pressure. Hence a lesser part of the ammonia molecules can execute the proposed isotope exchange, resulting in the slight increase of the ratio of the intensity at m/z =17 to the intensity at m/z =18 shown in figure 3.6. The HDratio of ammonia is determined by the fit routine described above, the results are shown in figure 3.7. It shows up that the HDratio of ammonia increases from phase III to V. As the HDratio of ammonia is known the amount of deuterium atoms per ammonia molecule r can be easily calculated

$$r = 3(1 - HDratio). \tag{3.1}$$

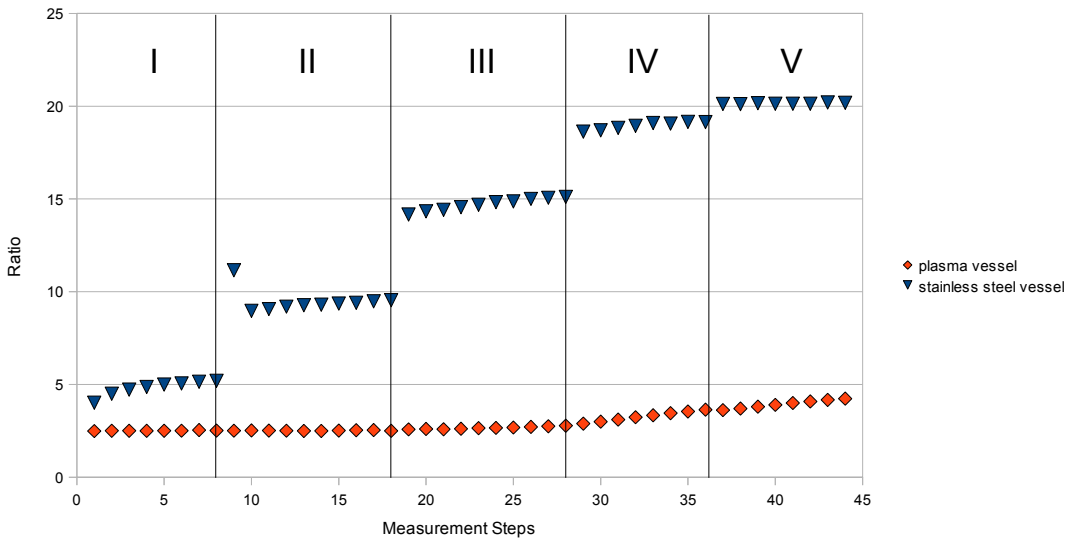

Figure 3.6: *Ratio of the intensities measures at m/z =17 to m/z =18 measured at ASDEX Upgrade and the stainless steel vessel*

The result is shown in figure 3.5. It should be noted that for the calculated HDratios of about 0.85 roughly one of two ammonia molecules has exchanged hydrogen atoms by deuterium. For phases III to V the amount of deuterium atoms per ammonia and adsorbed percentage of ammonia seem to be directly connected.

After the gas flow into the vessel was stopped at the beginning of phase VIII (figure 3.4) during the experiment on 2011-06-20 still significant intensities at m/z =14 to m/z =19 can be measured. Hence ammonia is retained in the plasma vessel of ASDEX Upgrade. The presence of significant intensities at m/z =18 and m/z =19 indicate once more that they are linked to ammonia. A similar effect (intensities at m/z =14 to m/z =17) is visible for the experiment done on 2011-06-28, indicating that ammonia is also adsorbed at the wall of the stainless steel vessel. For the measured intensities in phase VIII of the experiment at ASDEX Upgrade another effect is visible. The ratio of the intensity at m/z =17 to the intensity at m/z =18 declines throughout phase VIII (see figure 3.8). Thus also the HDratio of ammonia decreases (see figure 3.7). The longer an ammonia molecule is retained in the vessel the more probable becomes a replacement of one ore more protium atoms by deuterium atoms.

As the measured effects seem to be connected to the adsorption of ammonia the adsorption mechanism of ammonia on the surface of the plasma vessel of ASDEX Upgrade has to be investigated in detail. Due to the interest in tungsten acting as a catalyst for the synthesis of ammonia out of nitrogen and hydrogen the interaction between tungsten and ammonia has been studied widely. For the adsorption of ammonia on tungsten Estrup and Anderson [PEs68] proposed, based on their results from flash desorption and low energy electron diffraction, an adsorption mechanism involving the formation of WNH_2. Dawson and Handson [PDa68] on the other hand described the adsorption of ammonia on tungsten with a three step model: The first ammonia molecule is decomposed to nitrogen and hydrogen. The nitrogen atom is chemisorbed forming a surface nitride (W_2N). The next ammonia molecule reacts with the chemisorbed nitrogen to $W_2N_2H_2$. The adsorption mechanism therefore could be summarized as:

$$2W \ + \ 2NH_3 \quad \rightarrow \quad W_2N_2H_2 \ + \ 2H_2 \tag{3.2}$$

With a growing surface concentration of hydrogen, an adsorption of undecomposed ammonia was assumed within this model. D.P.Mason et al. [DMa95] proposed a three state model for the adsorption of ammonia on tungsten. The first state refers to a chemisorbed ammonia molecule, the third state to a complete decomposition into nitrogen and hydrogen. D.P Mason et al. proposed that the second state

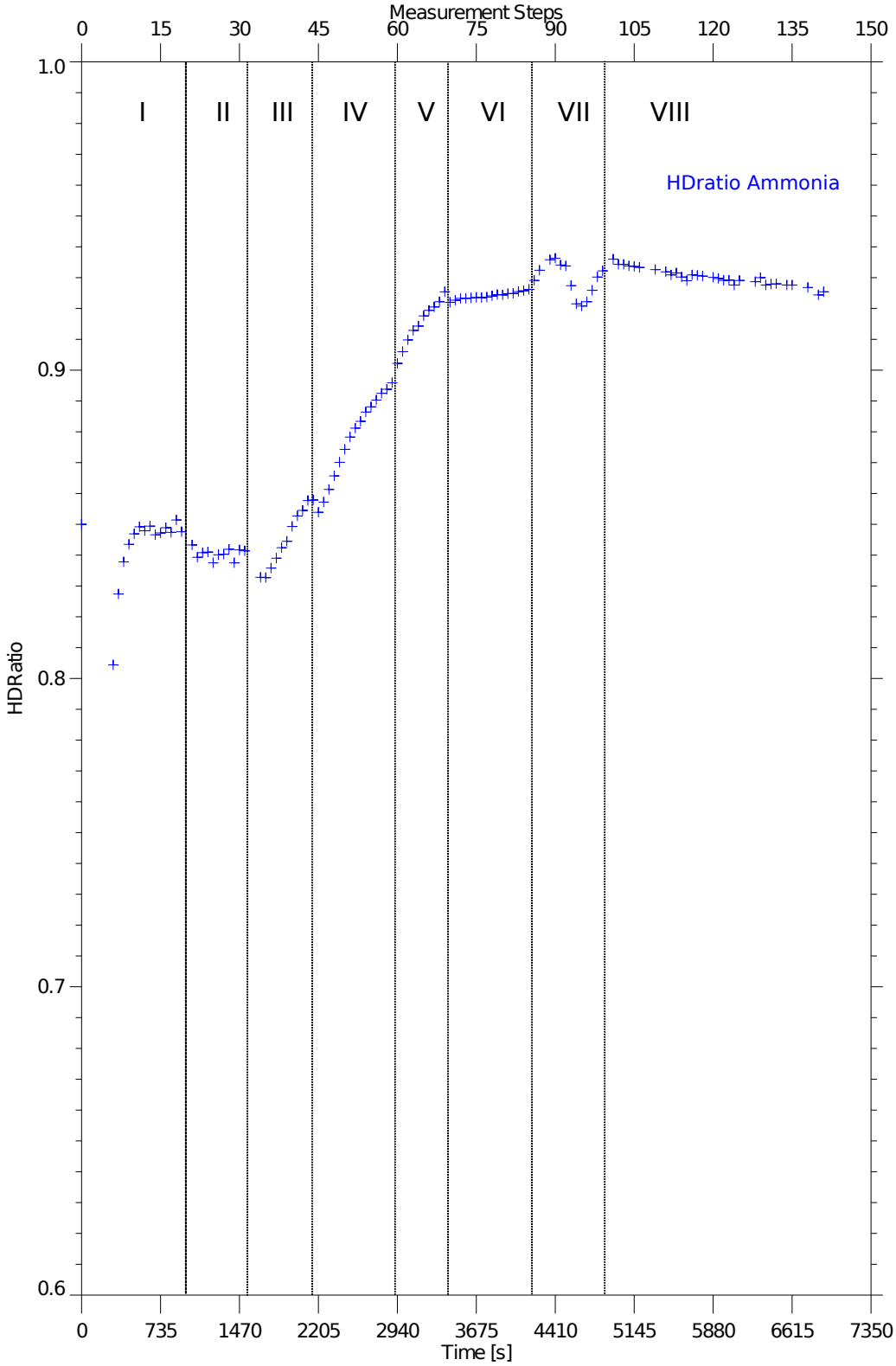

Figure 3.7: *Calculated HDratio of ammonia on 2011-06-20 at ASDEX Upgrade*

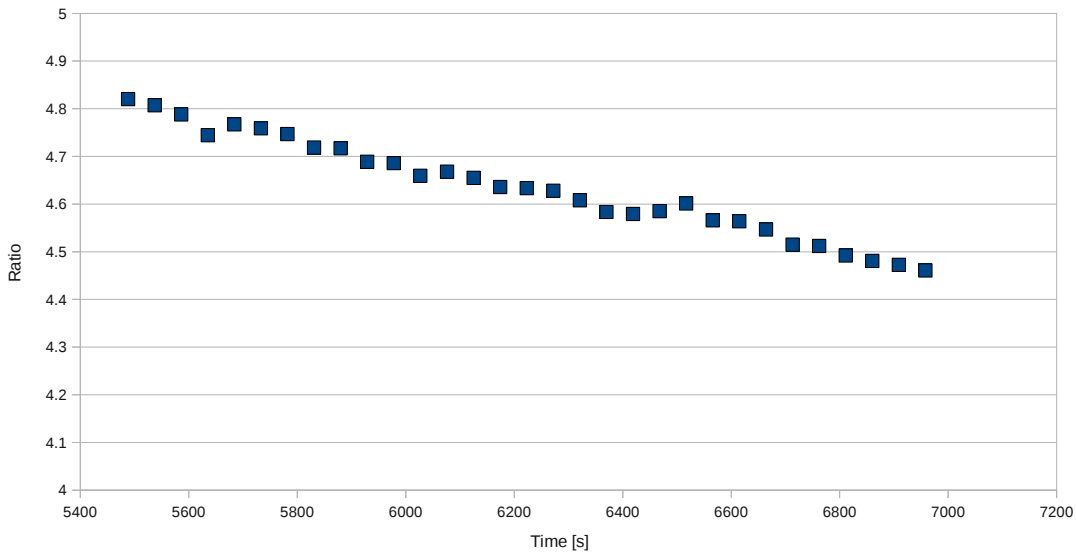

Figure 3.8: *Ratio of the intensities measured at m/z =17 to m/z =18 during phase VIII on 2011-06-20*

refers to a partly dissociated ammonia molecule. As deuterium atoms are present on the tungsten surface of the plasma vessel a recombination to NH_2D seems possible from all proposed intermediate states. Hence deuterium is removed from the surface of the plasma vessel of ASDEX Upgrade. As at the surface of the plasma vessel of ITER tritium will be adsorbed, the removal of tritium seems possible.

As stated above the formation of tritium containing hydrocarbon layers is still an issue for the tritium inventory of ITER. Tabarés [FTa10] recently proposed that the injection of ammonia acts as a scavenger for methyl radicals and therefore prohibits the formation of hydrocarbon layers.

$$NH_3 + \bullet CH_3 \quad \rightarrow \quad HCN + 2H_2 + H \tag{3.3}$$

$$\bullet NH_2 + CH_4 \quad \rightarrow \quad HCN + 2H_2 + H \tag{3.4}$$

Under the assumption that the HCN molecules are not dissociated in the plasma again it would offer a way to remove carbon atoms from the vessel and therefore prohibit the growth of hydrocarbon layers. However the measurements performed in the present work at ASDEX Upgrade indicate that even the pure injection of ammonia without plasma is sufficient to remove deuterium atoms from the walls of the vessel, thus also the removal of tritium atoms seems possible. The quantity of removed deuterium atoms per second is given by:

$$\frac{D}{s} = S(p)p_{NH_3}(t) \cdot r \tag{3.5}$$

The product of pumping speed $S(t)$ and partial pressure of ammonia $p_{NH_3}(t)$ results in the quantity of pumped ammonia molecules, this value has to be multiplied with the quantity of deuterium atoms per ammonia molecule r. As stated above only two turbomolecular pumps were operated during the measurement on 2011-06-20, the cryo pump was at room temperature. Hence the pumping speed $S(p)$ is roughly given by (see table 2.1):

$$S(p) = 2683 - 1021p + 306p^2 \tag{3.6}$$

In figure 3.9 the calculated removal rate of deuterium is shown. The maximal removal rate obtained was roughly $8 \cdot 10^{17}$ deuterium atoms per second. Measurements done by T. Wauters at al. at TEXTOR yield a removal rate for Ion Cyclotron Wall Conditioning of about $5 \cdot 10^{18}$ deuterium atoms per second

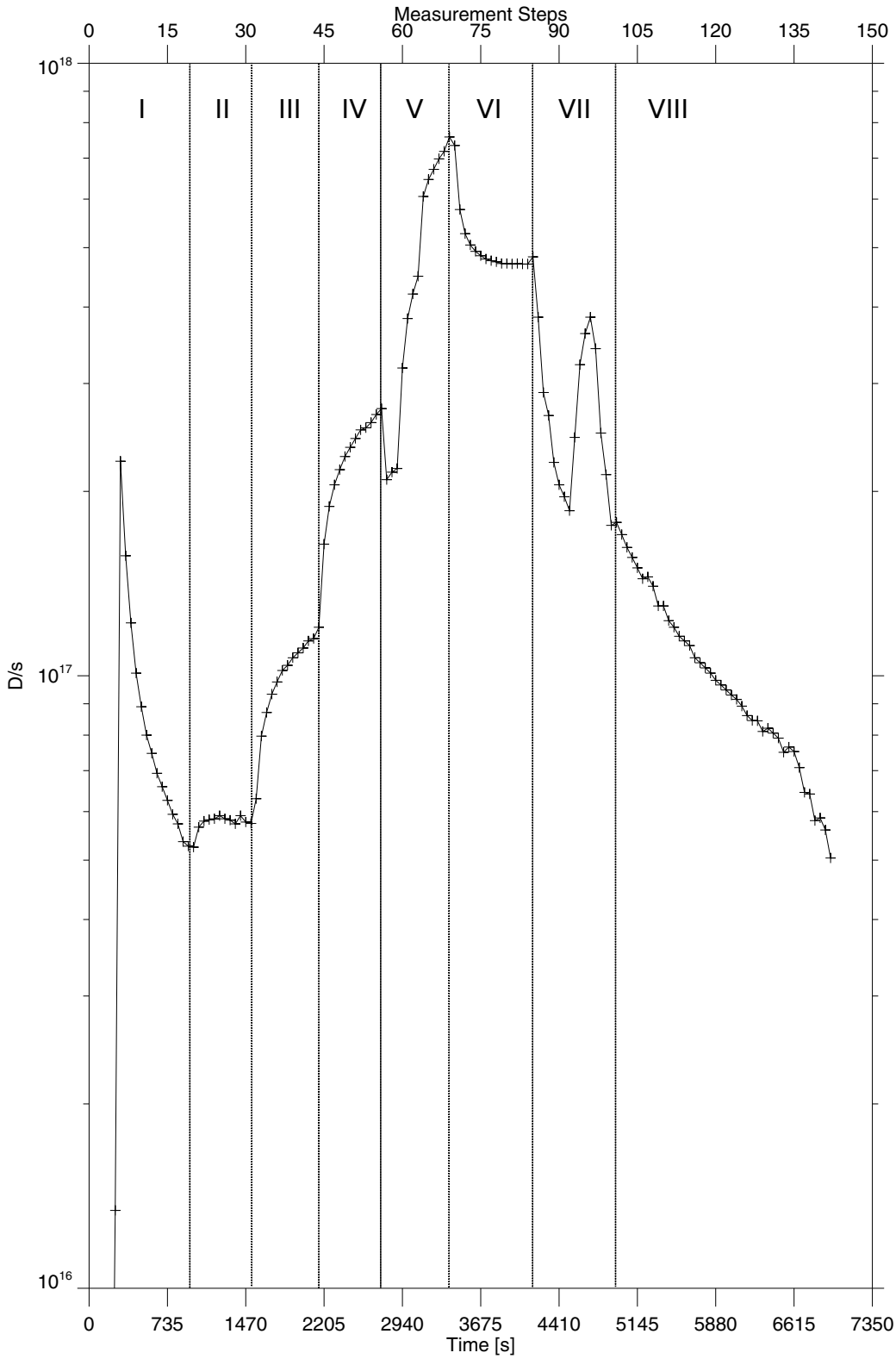

Figure 3.9: *Removal rate of deuterium atoms from ASDEX Upgrade with a flowing ammonia containing gas mixture*

[TWa10]. Oxygen glow discharges performed at ASDEX Upgrade show a removal rate for carbon atoms of about $5 \cdot 10^{18}$ per second [CHo06]. The removal rate of deuterium observed by the injection of ammonia depends on the partial pressure of ammonia. Therefore the removal rate can easily be increased by simply increasing the partial pressure of ammonia. But the HDratio of ammonia also increases with increasing partial pressure. Thus the concentration of deuterium atoms within the ammonia molecules declines, resulting in a lower removal rate. Also pumping speed $S(p)$ decreases with increasing absolute pressure. A further optimization of these three parameters would probably lead to a higher removal rate of deuterium.

3.3 Calibration

The described behavior of ammonia (adsorption, isotope exchange) yields two problems for the calibration. First a straightforward determination of the cracking pattern of ammonia is not possible as a preliminary unknown part of the hydrogen atoms within the ammonia molecules is replaced by deuterium atoms. Therefore pure ammonia gas was injected into the stainless steel vessel, as described above, hence the cracking pattern could be determined for HPQO. Assuming pure ammonia in the vessel during phase VIII, cracking pattern and HDratio of ammonia during this phase could be determined. Both calculated cracking patterns were quite equal. The second problem regards the determination of the calibration factor of ammonia. As am unknown part of the ammonia is adsorbed at the walls of the plasma vessel, the exact gas composition is in principle not known any longer as a unknown sink for ammonia exists that changes with the absolute pressure. While this effect can be neglected for the calibration factor of all other components of the gas mixture, the calibration factor of ammonia can not easily be calculated. The flow of the gas mixture into the vessel is equal during phases IV and VI, consequently the partial pressures of methane and the other components beside ammonia are also equal in both phases (see figures 3.1 and 2.19). Only the calculated partial pressure of ammonia differs. Therefore it is assumed that the difference in the absolute pressure is completely due to the different partial pressure of ammonia (see figure 3.4) Therefore the measured intensity differences during this time span could be roughly assigned to a difference in the partial pressure of ammonia. The determined calibration factor was shown above in chapter 2.3.4. For a better calibration the flow of the gas mixture into the plasma vessel of ASDEX should be kept constant until now further ammonia is adsorbed and the partial pressure of ammonia remains constant.

Chapter 4

Nitrogen Seeded Discharges

If ITER uses a tungsten divertor the seeding of impurities, probably nitrogen, will be mandatory to reduce the local heat flux onto the divertor tiles. As stated above in section 1.3 a massive formation of ammonia out of nitrogen and tritium can become a serious issue for plasma control. Therefore two questions have to be investigated.

1. Is there a significant production of ammonia during or after discharges with nitrogen seeding? If yes, how much ammonia is formed?
2. How does ammonia behave in a tungsten vessel between discharges? Is there a retention of ammonia and consequently a enrichment of ammonia for consecutive discharges with nitrogen seeding?

To investigate a possible production of ammonia one discharge without nitrogen seeding (27082) is compared to a discharge with nitrogen seeding (27169). Partial pressures as well as HDratios of methane, water, ammonia and nitrogen are determined for both discharges by the fit routine described in section 2.5. As also the pumping speed at the mass spectrometers was known, additionally the number of formed ammonia molecules can be calculated. In a next step discharges without nitrogen seeding but subsequent to discharges with nitrogen seeding are investigated. Finally a series of successive discharges with nitrogen seeding (27092, 27093, 27095) are evaluated in order to investigate a possible enrichment of ammonia in the plasma vessel of ASDEX Upgrade.

4.1 Global Parameters of evaluated discharges

For deuterium plasmas the residual gases of 10 discharges are evaluated in detail. They were all performed between 2011-06-01 and 2011-06-21. All discharges reached the high confinement regime and featured a stable flattop phase for several seconds. The last boronization before these discharges was done in May on the 2011-05-16. The global parameters of all presented discharges with deuterium plasma are shown in table 4.1. P_{aux} is the applied auxiliary heating power provided by neutral beam injection (NBI), electron cyclotron resonance heating (ECRH) and ion cyclotron resonance heating (ICRH), n_e is the line averaged density. As stated above for experiments with a high heating power the seeding of impurities like nitrogen is mandatory to protect the divertor. Discharges 27094, 27170, 27173, 27174 and 27175 were not successful and can be therefore neglected.

4.2 Discharges with and without nitrogen seeding

4.2.1 Discharge 27082 (without nitrogen seeding)

Figure 4.1 a) and b) illustrate the evolution of the plasma current I_p and the toroidal magnetic field respectively. Both stay rather constant throughout the discharge at 1.2MA and -2.4T respectively. Also the line averaged density n_e, depicted in figure c), remains almost constant. As shown in figure d) significant auxiliary heating power P_{aux} of at least 5MW is applied throughout the discharge. The evolution

Discharge	Date	n_e $[\frac{10^{19}}{m^2}]$	P_{aux}[MW]	Flattop[s]	Seeded nitrogen molecules
27082	2011-06-01	8.5	7.2	5.8	-
27092	2011-06-07	9.1	12.6	3.3	$2.80 \cdot 10^{21}$
27093	2011-06-07	10.3	12.9	3.3	$2.78 \cdot 10^{21}$
27095	2011-06-07	9.4	13.0	3.3	$2.78 \cdot 10^{21}$
27114	2011-06-09	7.0	6.5	5.4	-
27169	2011-06-21	8.7	14.5	6.5	$4.20 \cdot 10^{21}$
27171	2011-06-21	7.1	3.6	2.8	-
27172	2011-06-21	10	13.7	3.8	$2.79 \cdot 10^{21}$
27176	2011-06-21	9.2	7.8	2.8	-
27177	2011-06-21	8.1	12.6	4.4	-

Table 4.1: *Global Parameters of evaluated discharges*

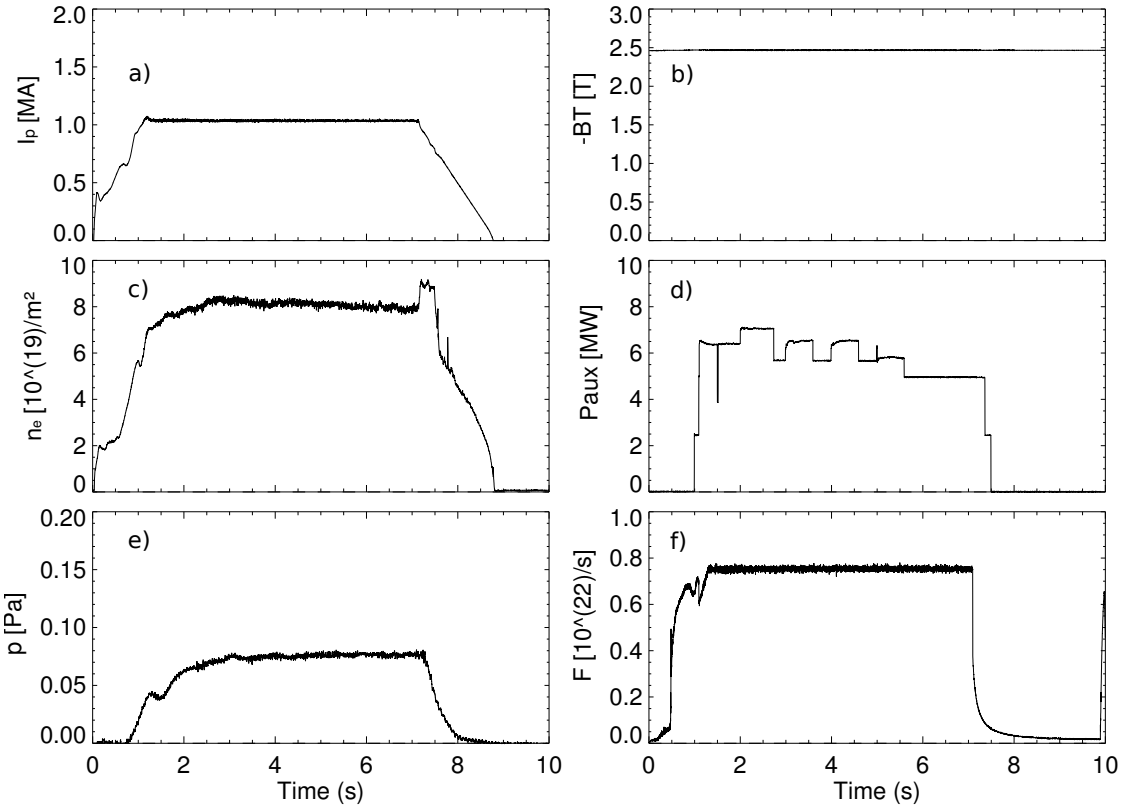

Figure 4.1: *a) Plasma current I_p, b) Toroidal magnetic field BT, c) line averaged density n_e, d) auxiliary heating power P_{aux}, e) Pressure at the divertor p and f) Injected deuterium flux F during non nitrogen seeded H-mode discharge 27082*

of the pressure at the divertor illustrated in figure e) reveals a stable phase of about 4s, also a constant flow of roughly $8 \cdot 10^{21}$ deuterium atoms per second was applied.

In figure 4.2 the measured intensities at m/z =12 - m/z =20 and m/z =28 before, during and after discharge 27082 (without nitrogen seeding) are shown. Three different groups of intensities can be seen. The intensities measured at m/z =20, m/z =18 and m/z =28 are at least one order of magnitude higher than the other impurities. The second group consists of the intensities of m/z =16, m/z =19 and m/z =14. The lowest intensities are measured at m/z =17 and m/z =15. All intensities remain during the discharge (0s-10s) roughly constant and are fairly equal to the intensities measured during discharge 27114. After the discharge all measured intensities decline as the plasma vessel is gas flow of deuterium is stopped. The highest intensity between 10s and 60s is measured at m/z =20 followed by m/z =18, m/z =19, m/z =28, m/z =17 and m/z =16. Later (500s-2000s) the intensity at m/z =18 is the highest in the measured spectrum, furthermore the intensities at m/z =19 and m/z =28 also exceed the intensity at m/z =20.

The next step is to determine the partial pressures of methane, water, ammonia and nitrogen. The calculated values are shown in figure 4.3. During the discharge the partial pressures of nitrogen and methane are roughly $2 \cdot 10^{-3}$Pa, the partial pressure of water is $5 \cdot 10^{-4}$Pa and hence about a factor of 5 lower. At the end of the discharge the partial pressures of nitrogen and methane decline by two orders of magnitude within a few seconds. Throughout the measurement the partial pressure of methane shows the steepest descent. Consequently about 15 minutes after the discharge, the partial pressure of methane is roughly $4 \cdot 10^{-7}$Pa and therefore at least a factor of two lower than the partial pressure of water and nitrogen. The partial pressure of water declines slower than methane and also nitrogen, hence water is the dominating impurity in the residual gas 15 minutes after the discharge. Except during the discharge ($5 \cdot 10^{-5}$Pa) there can be hardly any ammonia found in the residual gas. Consequently only the HDratios of water and methane could be determined and shown in figure 4.4. The HDratio of methane is roughly zero during the discharge (0s-10s). Assuming that almost the entire content of methane in the residual gas is formed within the plasma vessel by the formation mechanism described in section 2.4 this result fits with the expectations. The HDratio of water is roughly 0.1 and therefore only slightly higher, indicating that also water is formed out of oxygen and hydrogen/deuterium during the discharge. With the end of the discharge the HDratio of methane starts to rise slowly from 0 right at the end of the discharge to 0.1 about 20 minutes later. As shown in figure 2.27 the pure presence of deuterium in the plasma vessel of ASDEX Upgrade induces the formation of hydrocarbons and probably also water. As the walls of the plasma vessel are activated by the bombardment of energetic particles during the discharge there is probably an enhanced production of impurities shortly after a discharge. As more and more molecular hydrogen compared to molecular deuterium can be found in the residual gas, also more and more hydrogen atoms should be contained in methane and water molecules. Therefore the slight increase of the HDratio is plausible, but the much steeper increase of the HDratio of water cannot be explained by this mechanism. A possible explanation is the presence of two different sources for water in the residual gas. Both assumed processes are shown in figure 4.5. The first source is the production of water out of hydrogen and oxygen atoms adsorbed at the surface of the plasma facing components (PFCs). The distribution of protium and deuterium atoms within the formed water molecules should roughly be the same as in the methane molecules. The second source is the out gassing of natural water contained in the bulk of the PFCs. It is known that water can hardly be removed from the PFCs as the vessel can only be heated up to 420°K [VRo09(1)]. This water has a HDratio close to to one. During the discharge a HDratio of roughly 0.1 is determined for water, hence the production out of adsorbed oxygen and hydrogen seems to be the dominant process. After the discharge the out gassing gets more and more important, resulting in a steeper increase of the HDratio of water compared to the HDratio of methane.

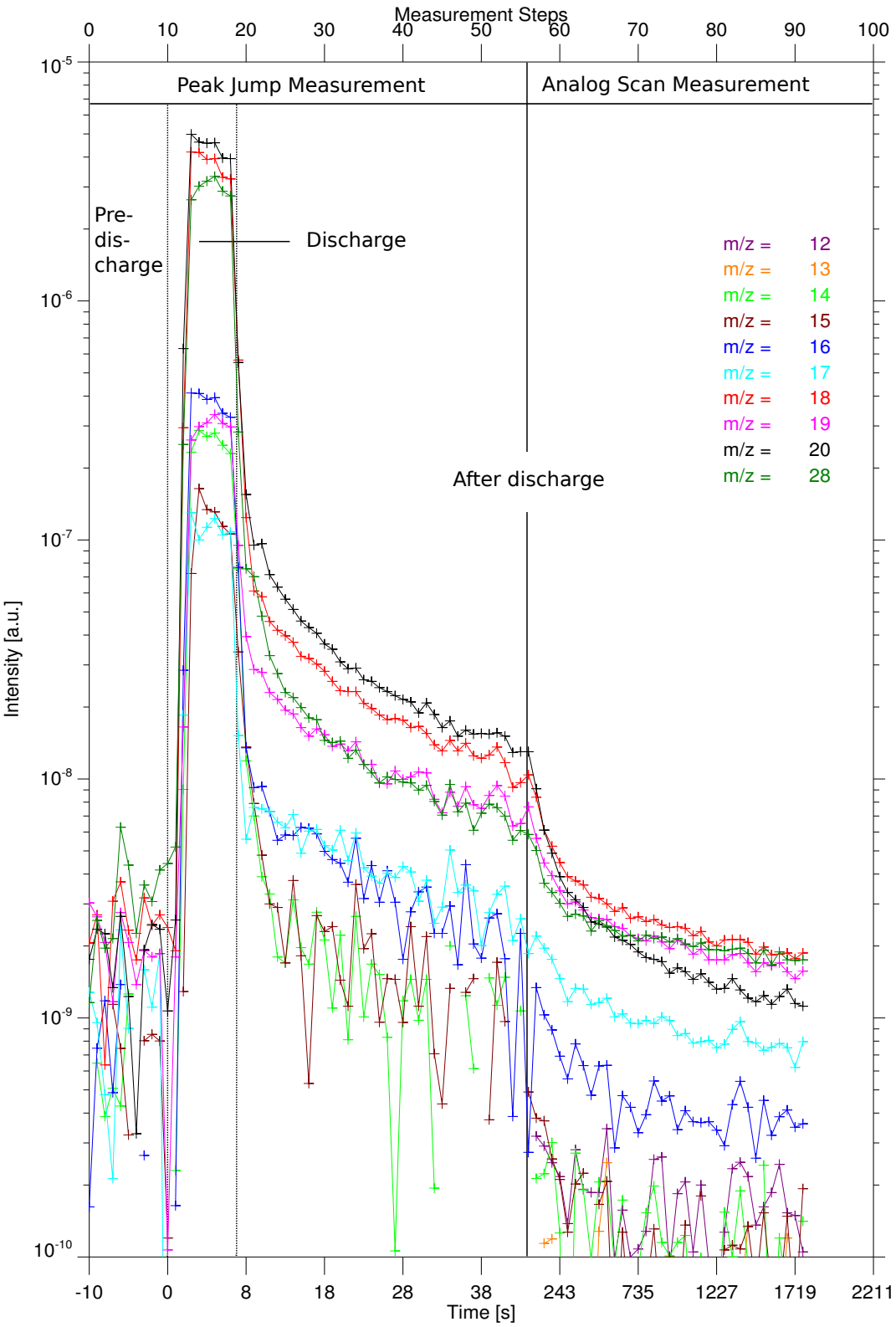

Figure 4.2: *Intensities measured by HPQI before during and after non nitrogen seeded H-Mode discharge 27082 (without nitrogen seeding)*

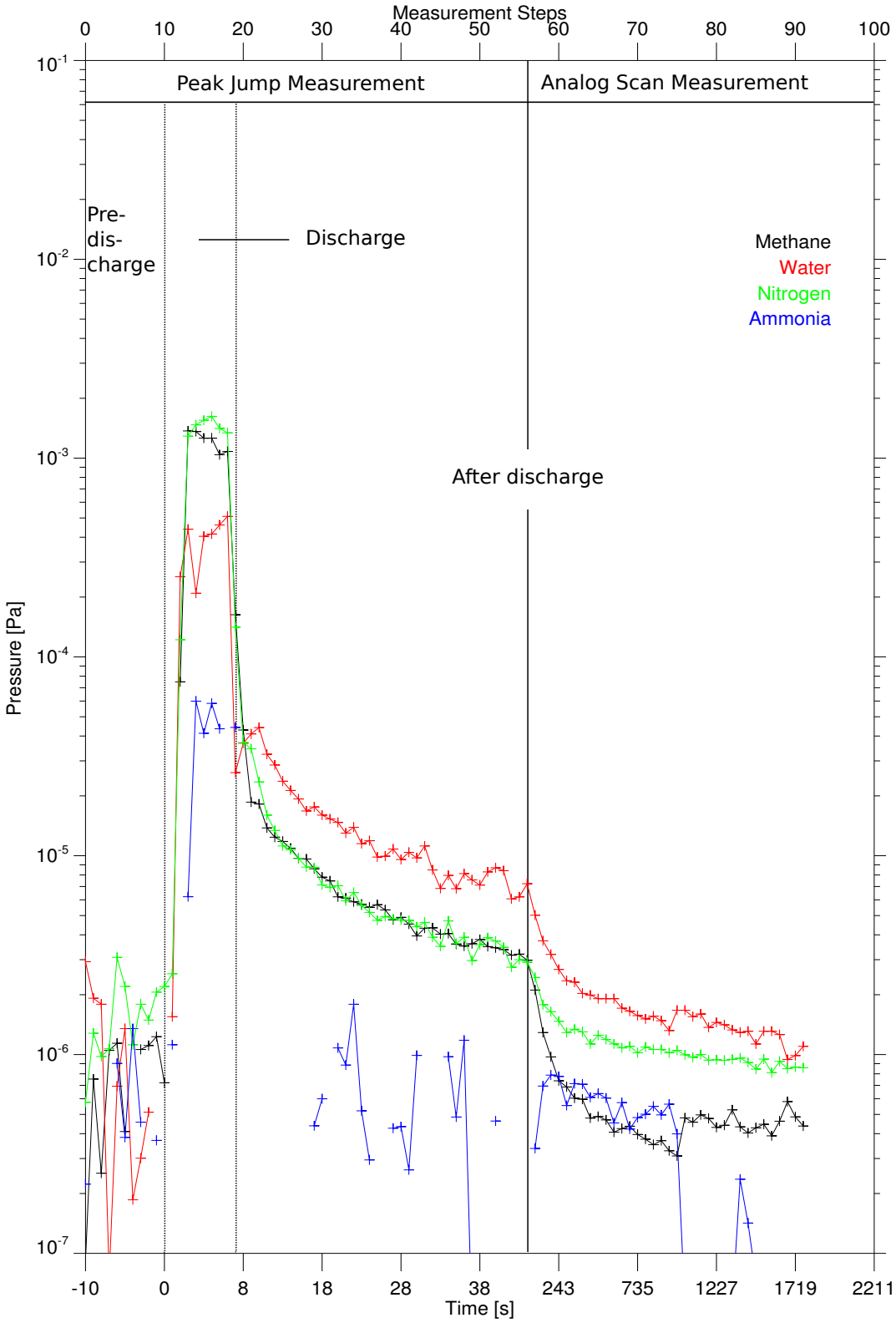

Figure 4.3: *Calculated partial pressures before, during and after non nitrogen seeded H-mode discharge 27082*

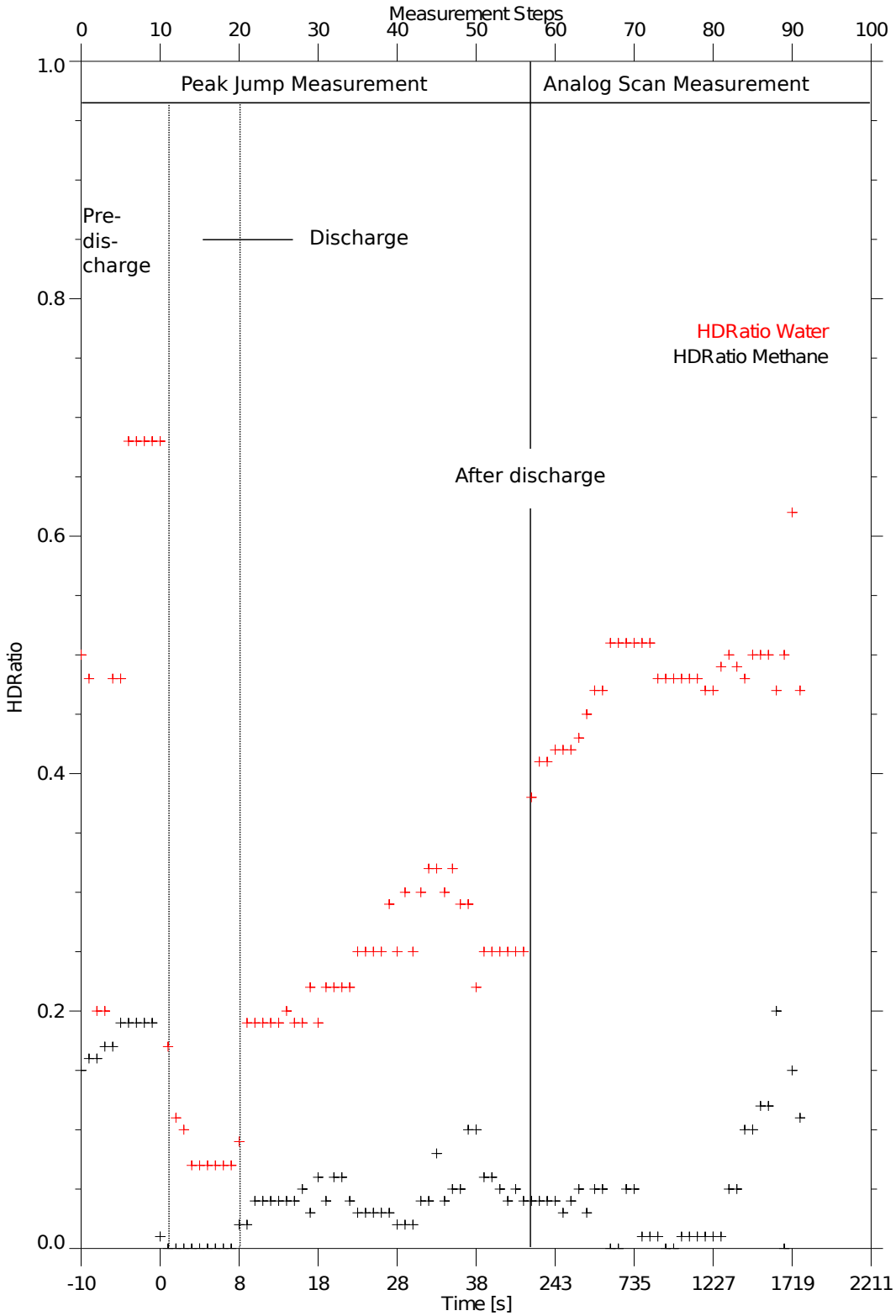

Figure 4.4: *Calcualted HDratios before, during and after non nitrogen seeded H-mode discharge 27082*

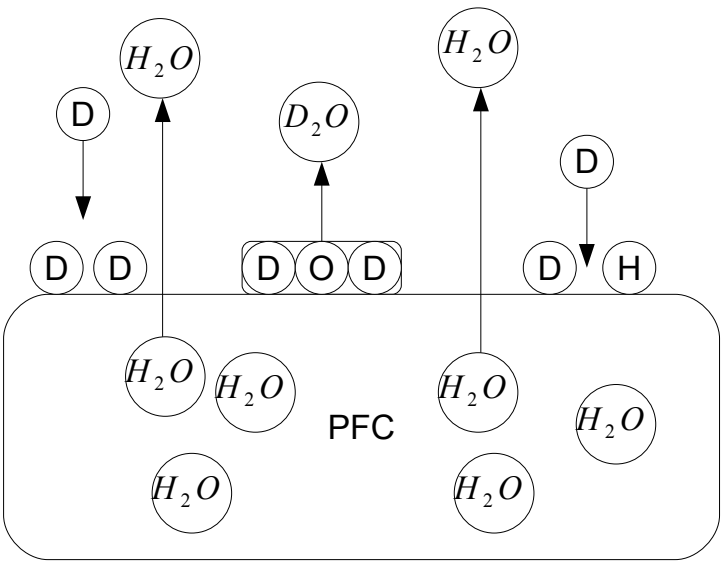

Figure 4.5: *Assumed production mechanism for water molecules found in the residual gas*

4.2.2 Discharge 27169 (nitrogen seeding)

The evolution of the global parameters are illustrated in figure 4.6. Again plasma current, toroidal magnetic field and line averaged density remain constant throughout the discharge. Also their absolute values are similar to the values during discharge 27082 (figures a), b) and c)). The auxiliary heating power shown in figure d) is stepwise increased from 4MW to 14MW. In figure f) the flux of the injected deuterium is depicted. It is roughly equal to the flux injected during discharge 27082, but additionally nitrogen molecules are seeded. The flux of nitrogen is roughly a factor of 7 lower compared to the flux of deuterium. Nitrogen injection starts roughly 2s after the beginning of the discharge. The flux of nitrogen is stepwise increased. Hence also the absolute pressure at the divertor, as shown in figure e) increases stepwise.

The measured intensities before, during and after nitrogen seeded discharge 27169 are depicted in figure 4.7. At the start of the discharge (0s) all measured intensities rise by several orders of magnitude. After about 1 second all intensities beside m/z =28 and m/z =14 decline by a factor of two. During the discharge (0s-10s) the intensities at m/z =28 and m/z =14 clearly dominate the spectrum. The measured intensities at m/z =18 and m/z =20 are almost two orders of magnitude lower than the intensity at m/z =28. Towards the end of the discharge the intensities at m/z =16, m/z =18 and especially m/z =17 and m/z =19 suddenly rise over the level at the beginning of the discharge. While the intensity at m/z =12, m/z =14 and m/z =28 drop at least two orders of magnitude within a few seconds the other depicted intensities decline only gently. The highest intensity is measured at m/z =18, followed by m/z =17, m/z =19, m/z =16 and m/z =20.

Now the composition of the residual gas of discharge 27169 (with nitrogen seeding) has to be determined. In a first step the measured spectrum is compared to the HDratio dependent cracking patterns of pure methane, pure water and pure ammonia (see figures 2.24, A.4, A.5). Pure methane with a HDratio of 0.35, pure water with a HDratio of 0.95 and ammonia with a HDratio of 0.50 show up to be potential candidates. In figure 4.8 the intensities during the 25th measurement step of discharge 27169 are depicted together with the calculated spectra of pure methane (HDratio 0.35), pure ammonia (HDratio 0.50) or pure water (HDratio 0.95). All intensities are normalized to the intensity at m/z =18. Water shows the weakest agreement, whereas ammonia shows the best. For a more elaborated evaluation the partial pressures are now calculated by the fit routine. Figure 4.9 illustrates the calculated partial pressures.

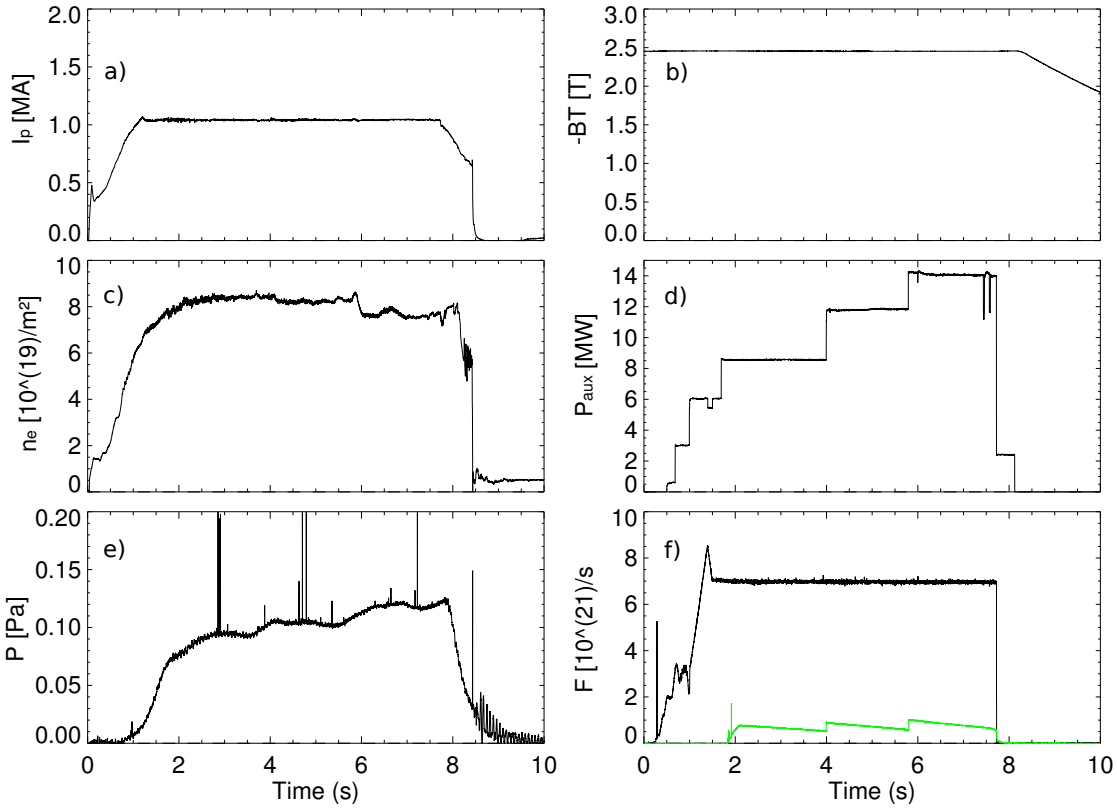

Figure 4.6: *a) Plasma current I_p, b) Toroidal magnetic field BT, c) line averaged density n_e, d) auxiliary heating power P_{aux}, e) Pressure at the divertor p and f) Injected deuterium (black line) flux F_D and nitrogen (green line) flux F_N during nitrogen seeded H-mode discharge 27169*

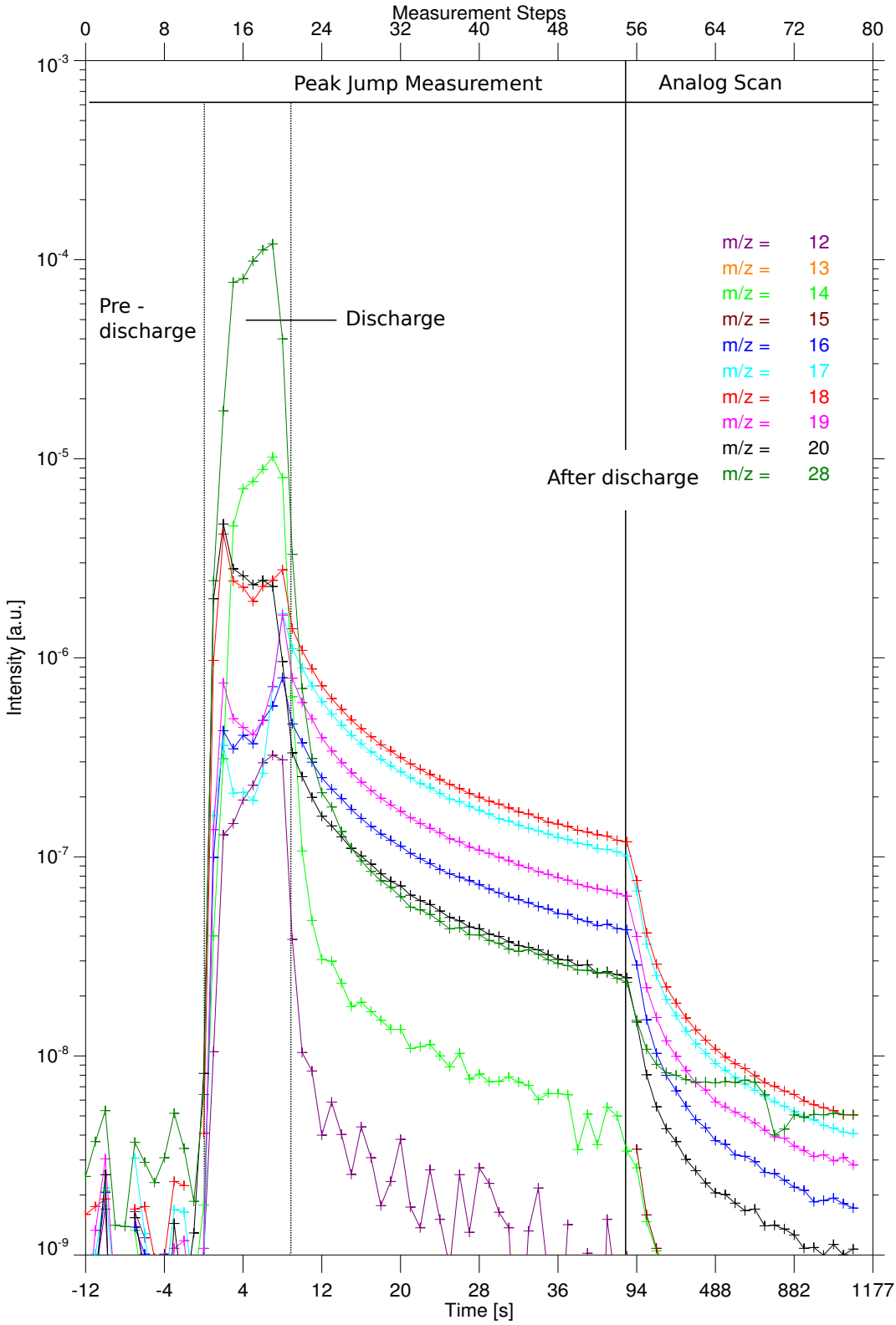

Figure 4.7: *Intensities measured by HPQI before, during and after nitrogen seeded H-Mode discharge 27169*

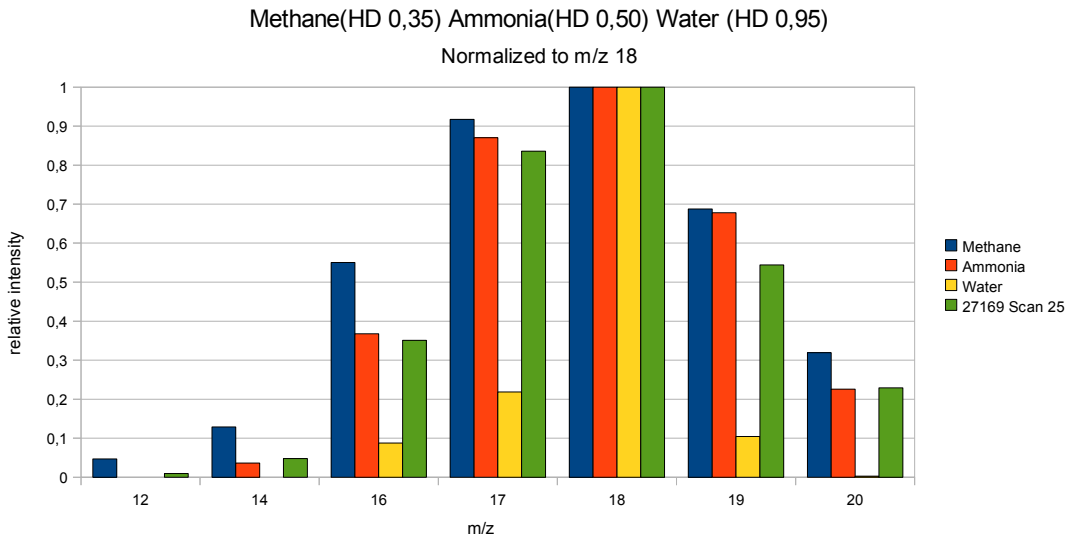

Figure 4.8: *Measured spectra compared with calculated spectra for pure methane (HDratio 0.35), pure ammonia (HDratio 0.50) and pure water (HDratio 0.95) normalized to m/z =18*

During the discharge the partial pressure of nitrogen is about $6 \cdot 10^{-2}$Pa and therefore by far the dominating impurity in the residual gas. The partial pressures of water and methane are almost two orders of magnitude lower, roughly $8 \cdot 10^{-4}$Pa. That no water can be found a few second within the discharge is probably an artifact of the fit routine. The partial pressure of ammonia during the discharge does barely exceed $2 \cdot 10^{-4}$Pa. After the discharge the partial pressures of methane, water and nitrogen decrease by several orders of magnitude within a few seconds, where as the partial pressure of ammonia decreases much slower. After the discharge the partial pressure of ammonia clearly exceeds the partial pressures of methane water and nitrogen. The HDratios of methane and water are again 0.0 and 0.1 respectively during the discharge. After the discharge (10s-1200s) the HDratio of methane rises from 0.0 to about 0.1 and the HDratio of water from 0.1 to 0.85. The HDratio of ammonia stays roughly constant at 0.55, after one minute the HDratio begins to decrease. About 20 minutes after discharge 27169 the HDratio of ammonia is roughly 0.45. During the experiment on 2011-06-20 an ammonia gas mixture was injected into the plasma vessel of ASDEX Upgrade. As shown in figure 3.7 the HDratio of ammonia declined throughout phase VIII when the injection of the gas mixture was stopped. This result was interpreted as the continuous replacement of protium atoms by deuterium within adsorbed ammonia molecules. Assuming that most of the ammonia found in the residual gas after discharge 27169 was formed within the discharge and is adsorbed at the surface of the plasma vessel the same effect could show up for the ammonia in the residual gas of discharge 27169.

4.2.3 Comparison and Discussion

Comparisons of discharges are often hampered by the multiple differences between the different discharges. However discharge 27082 and 27169 are similar enough (see table 4.1) to make valid comparisons. In figures 4.11 and 4.12 the measured intensities and fitted partial pressures for discharges non nitrogen seeded discharge 27082 and nitrogen seeded discharge 27169 are compared. During discharge 27169 the intensities at m/z =28 and m/z =14 exceed the measured intensities during discharge 27082 by at least two orders of magnitude. Consequently nitrogen is determined to be the dominant impurity in the residual gas during the discharge. The distribution of the measured intensities is roughly equal for discharge 27169 and 27082. Nevertheless the behavior of the intensities is a bit different for both discharges. Whereas during discharge 27082 all intensities remain almost constant, during discharge 27169 they drop by a factor of two and then stay roughly constant until the end of the discharge. As the distribution of the intensities measured during discharges 27082 and 27169 is almost equal, the determined gas mixture is also

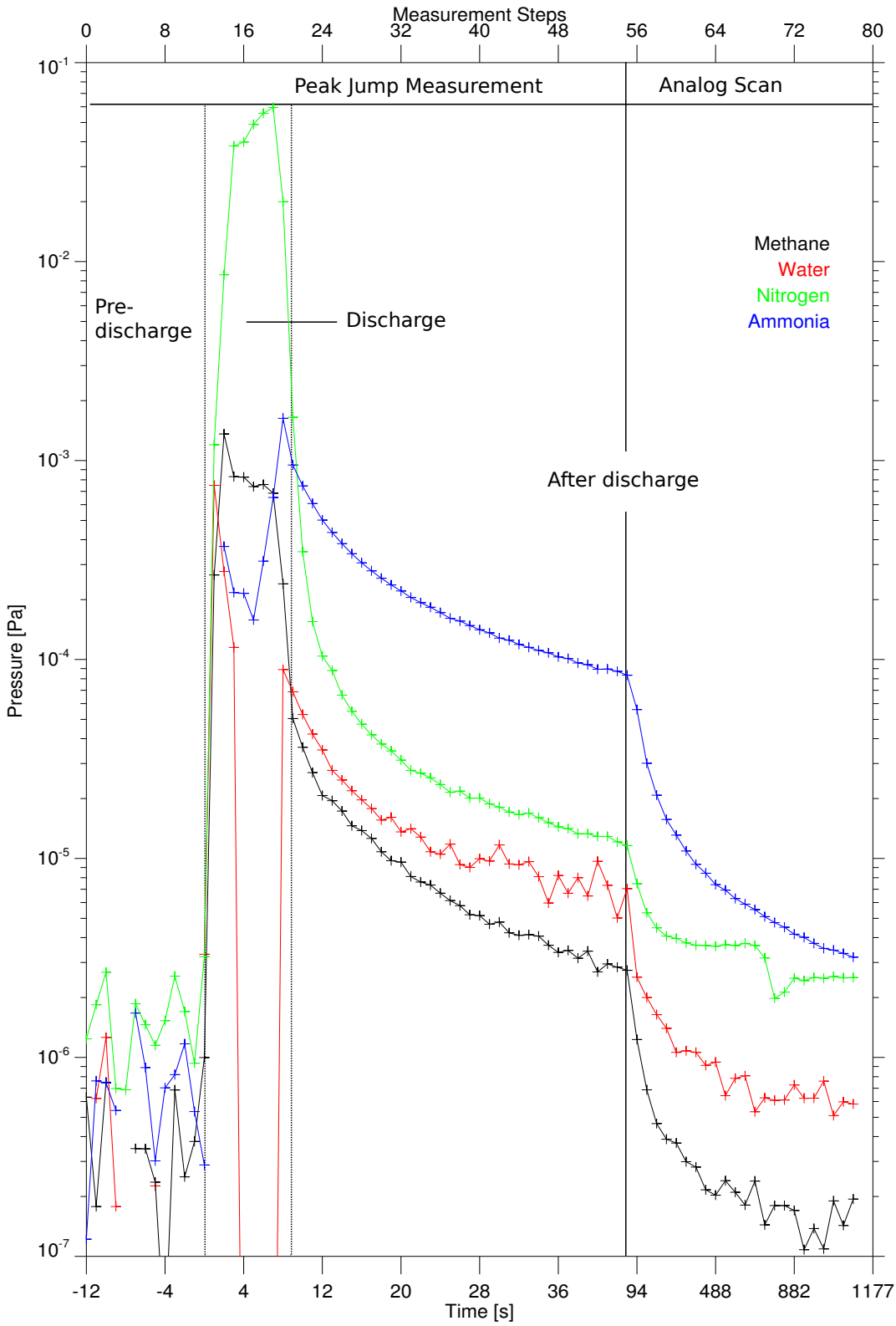

Figure 4.9: *Calculated partial pressures before, during and after discharge nitrogen seeded H-mode discharge 27169*

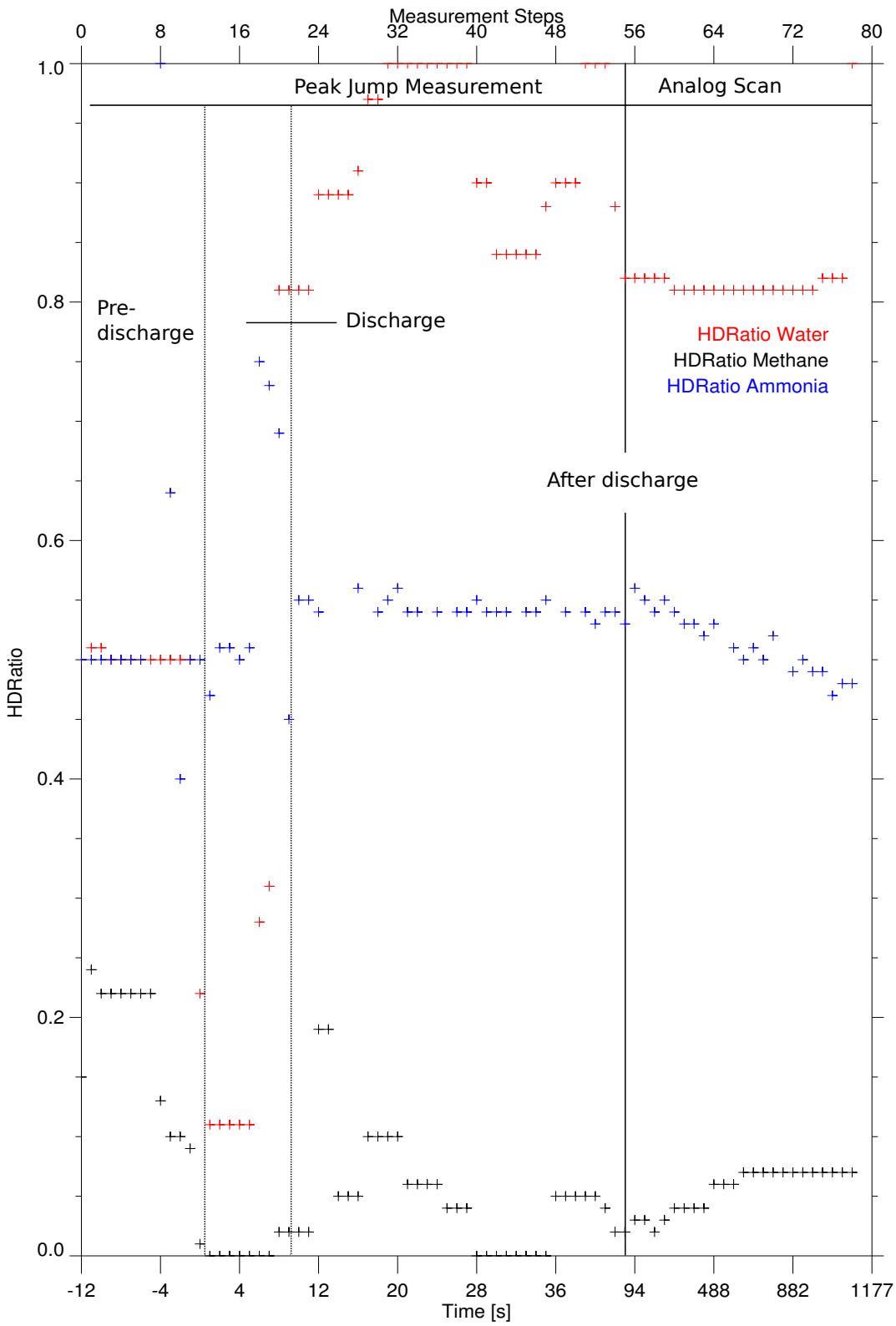

Figure 4.10: *Calculated HDratios before, during and after nitrogen seeded H-mode discharge 27169*

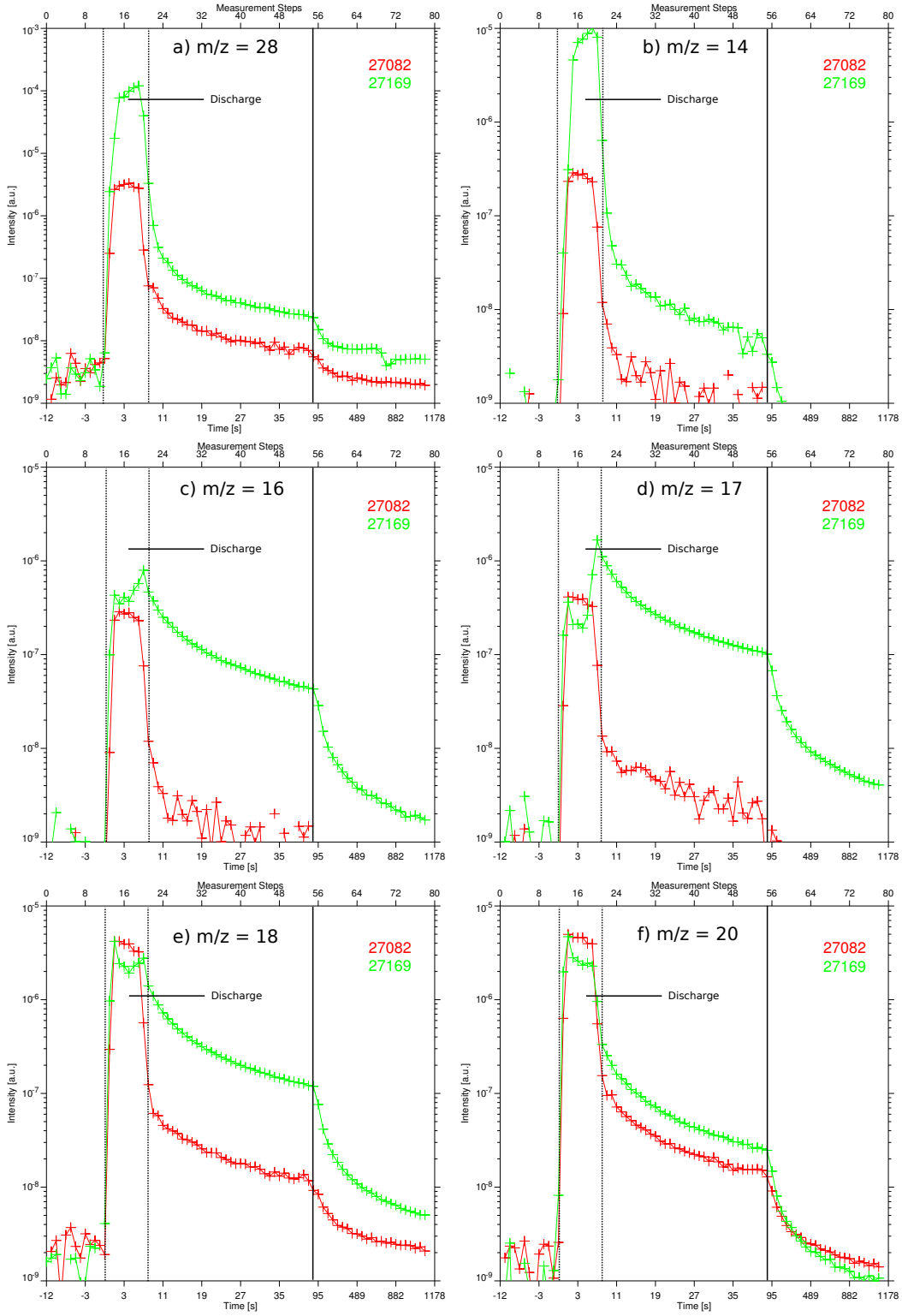

Figure 4.11: *Comparison of the intensities measured by HPQI before, during and after non nitrogen seeded H-mode discharge 27082 and nitrogen seeded H-mode discharge 27169*

similar. During the first two seconds of discharges 27082 and 27169 the determined partial pressures of methane are almost equal. During non nitrogen seeded discharge 27082 the partial pressure of methane remains roughly constant throughout the discharge. As soon as nitrogen is injected during discharge 27169 roughly after 2s the partial pressure of methane drops by a factor of two. This behavior of the partial pressure of methane is a typical feature of discharges with nitrogen seeding. Hence the seeded nitrogen seems to prevent the production of hydrocarbons like methane from the walls of the plasma vessel.

As described above the intensities measured at m/z =17, m/z =19 and, to a lower extent, also at m/z =16 and m/z =18 rise suddenly at the end of the discharge. Consequently the measured intensities at m/z =17 and m/z =19 are at least one order of magnitude higher than after discharge 27082. This behavior is quite surprising as neither deuterated methane (CD_4), water (D_2O) nor ammonia (ND_3) can evoke huge intensities at these mass to charge ratios. After the discharge the intensities at the mentioned mass to charge ratios decline slowly. Therefore it is unlikely that they are evoked by methane, as hydrocarbons can be removed from the plasma vessel quite fast. The distribution of the measured intensities does not fit with the calculated distribution for pure water (see figure 4.8), whereas the measured and the calculated spectrum for ammonia with a HDratio of 0.55 fit quite well. Hence ammonia is the dominant impurity after the discharge, but not during the discharge. As the content of nitrogen in the residual gas after discharge 27169 is only slightly higher than after 27082, it is unlikely that a significant part of the ammonia is formed after the discharge. The formation mechanism of ammonia in hydrogen-nitrogen plasmas have been described by e.g. J.H. van Helden et al. in [JHe07] by a stepwise addition of hydrogen to the nitrogen atom on top of the surface of the plasma vessel. During these experiments the complete surface was covered by nitrogen, the formation itself happened on top of this nitrogen layer. The formed ammonia is then desorbed and enters the plasma again. This formation mechanism is in principle equivalent to the assumed formation mechanism for hydrocarbons and other impurities. From the calibration measurements shown above it is known that ammonia sticks at the wall and has a very slow outgassing. Hence the ammonia produced during the discharge will also be adsorbed at the surface of the plasma vessel. Due to the interest in the growth rate of hydrocarbon layers in fusion experiments the sticking probabilities of hydrocarbons have been investigated (e.g. [KTi09]) but mainly on carbon surfaces. It showed up that the sticking coefficients of hydrocarbons are close to one during the discharge. After the discharge the sticking coefficient declines again.

Ammonia is by far the dominating impurity in the residual gas after discharge 27169 whereas ammonia can hardly be found after discharge 27082. The partial pressure of water is almost equal for both discharges whereas the evolution of the partial pressure shows some variations. After discharge 27169 the decrease of the partial pressure of methane is steeper then after discharge 27082. Indicating again that nitrogen seeding influences the production of hydrocarbons like methane. As a direct consequence the partial pressure of nitrogen is a bit higher after discharge 27169 than after discharge 27082. The HDratio of the ammonia formed after nitrogen seeded discharges is roughly 0.55 and therefore unexpected high. Consequently the formation mechanism as well as where ammonia is actually formed needs closer investigations.

In figures 4.4 and 4.10 the calculated HDratios of methane, water and ammonia molecules are shown. The HDratios for methane during and after discharges 27082 and 27169 are quite equal. But the HDratios of water change dramatically. After discharge 27169 the HDratio of water vapor is between 0.8 and 1.0. One possible explanation is that the seeded nitrogen prevents the formation of water out of oxygen and hydrogen adsorbed at the surface of the PFCs just like it hampered the formation of hydrocarbon. Hence nearly all water in the residual would be gassed out by the PFCs resulting in a HDratio close to one. But it could also be an artifact of the fit routine.

As the partial pressures of the impurities are known, the amount of pumped ammonia and nitrogen molecules can be calculated. Thus the quantity of nitrogen atoms contained in nitrogen molecules and ammonia molecules can be compared to the number of seeded nitrogen atoms. As shown in table 4.1 $8.40 \cdot 10^{21}$ nitrogen atoms were seeded during discharge 27169. During and after discharge 27082 nitrogen was also detected by the fit routine in the residual gas, consequently there is always a certain background of nitrogen in the residual gas. In fact nitrogen is beside water the most important impurity in the evac-

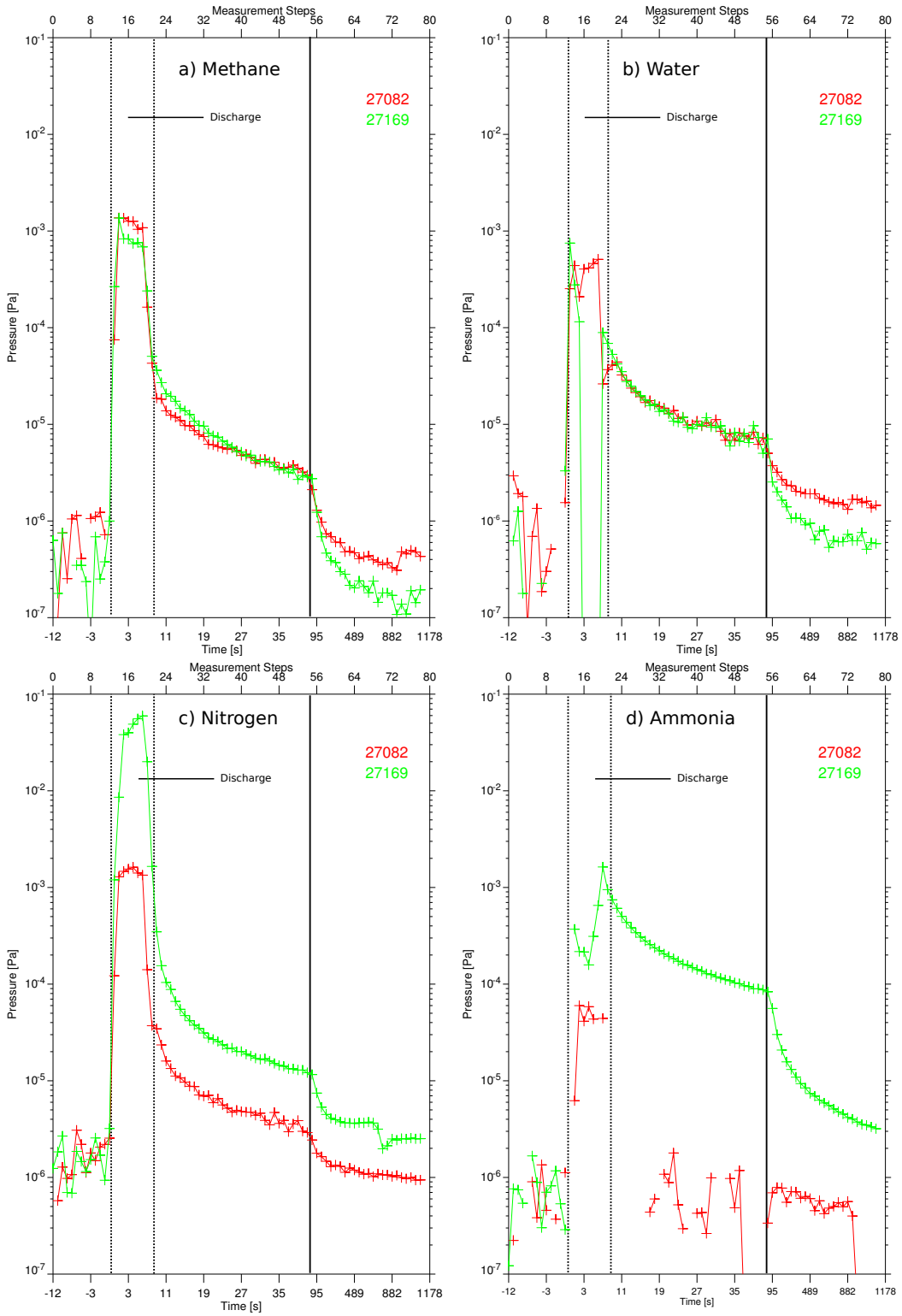

Figure 4.12: *Partial pressures of methane (a), water (b), nitrogen (c) and ammonia (d) before during and after discharges 27082 (without nitrogen seeding) and 27169 (nitrogen seeding)*

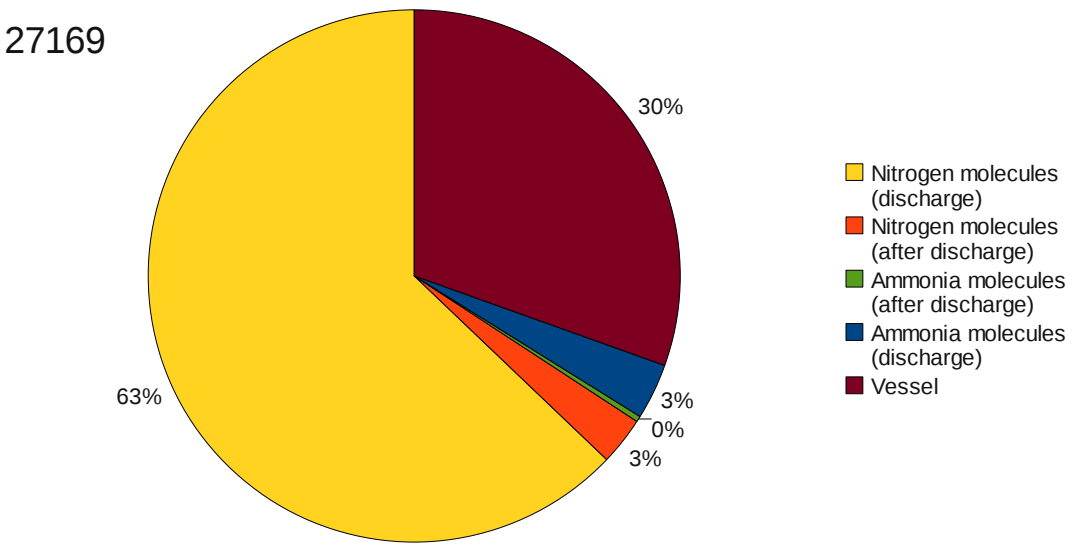

Figure 4.13: *Pumped nitrogen atoms contained in nitrogen molecules or ammonia molecules during and after H-mode discharge 27169 ($8.40 \cdot 10^{21}$ nitrogen atoms seeded)*

uated plasma vessel. The main source for nitrogen is air leakage. Hence to gain the number of nitrogen molecules in the residual gas due to nitrogen seeding, the calculated values have to be corrected by the background. The number of pumped nitrogen molecules during and after discharge 27082 are calculated separately and normalized to the total number of pumped molecules. The concentration of nitrogen in residual gas is roughly 0.6% during the discharge and 2.4% after the discharge. By assuming the same concentration of nitrogen during and after all other discharges a specific background for these discharges can be gained. The values shown in figure 4.13 correlate to the number of pumped nitrogen atoms within the corresponding compound. To get the number of pumped nitrogen molecules (N_2) the shown value has to be divided by two, whereas the shown value for ammonia is equal to the number of pumped ammonia molecules (NH_3). In total 70% of the seeded nitrogen atoms are detected during or after discharge 27169. The waist majority of the pumped nitrogen atoms, about 63% of the seeded nitrogen atoms, are contained in the nitrogen molecules pumped immediately during the discharge. Additionally 3% of the seeded atoms are found in molecular nitrogen contained in the residual gas after the discharge. A total of 3% of the seeded nitrogen atoms have formed ammonia molecules. As stated earlier roughly 90% of the formed ammonia are detected after the discharge. About 30% of the seeded nitrogen atoms can not be found in the residual and are therefore still adsorbed at the surface of the plasma vessel. Consequently to calculate the total amount of formed ammonia during nitrogen seeded discharges the adjacent discharges have also to be taken into account (see chapter 4.3).

During discharge 27092 $5.60 \cdot 10^{21}$ nitrogen atoms are seeded. Again about 68% of the seeded nitrogen atoms are detected during or after the discharge. Roughly 2% of the seeded nitrogen atoms are found in ammonia molecules and 66% are found in nitrogen molecules (see figure 4.14). Similar to discharge 27169, the majority of the ammonia molecules is detected after the discharge and the majority of the nitrogen molecules directly during the discharge. In figure 4.15 the nitrogen atoms found in molecular nitrogen and ammonia molecules are shown for discharges 27169 and 27092. The amount of seeded nitrogen molecules seem to be linked to the amount of formed ammonia molecules. But other factors like the duration of the discharge may also play a role.

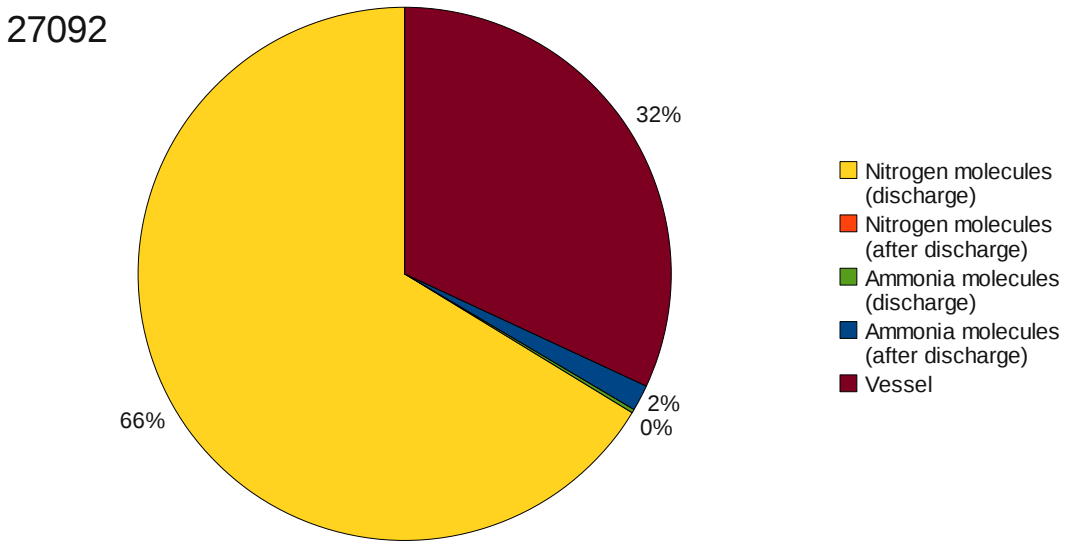

Figure 4.14: *Pumped nitrogen atoms contained in nitrogen molecules or ammonia molecules during and after H-mode discharge 27092 ($5.60 \cdot 10^{21}$ nitrogen atoms seeded)*

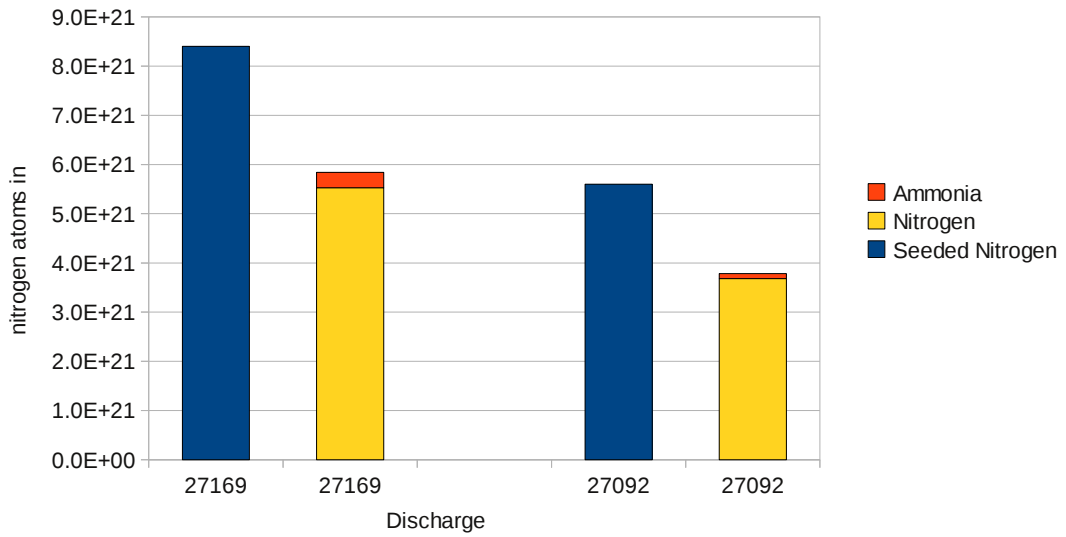

Figure 4.15: *Comparison of pumped nitrogen atoms contained in nitrogen molecules or ammonia molecules for discharges 27169 and 27092*

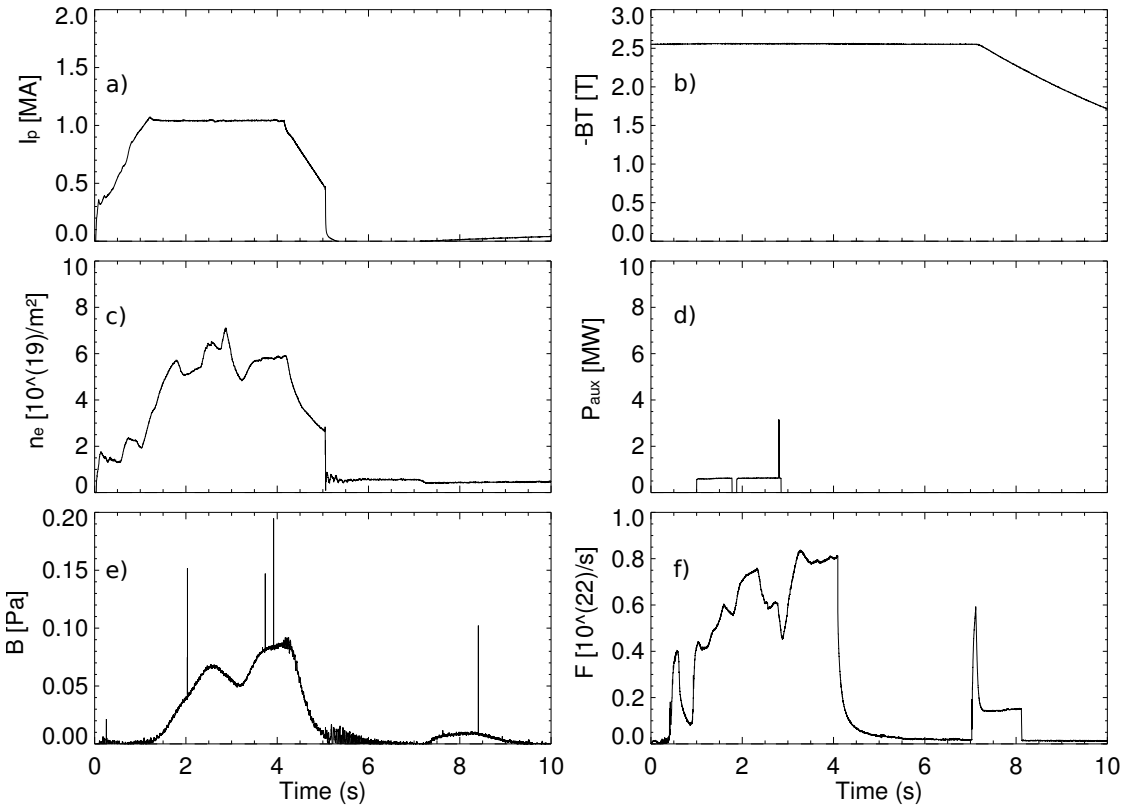

Figure 4.16: *a) Plasma current I_p, b) Toroidal magnetic field BT, c) line averaged density n_e, d) auxiliary heating power P_{aux}, e) Pressure at the divertor p and f) Injected deuterium flux F during non nitrogen seeded H-mode discharge 27171*

4.3 Ammonia inventory in discharges subsequent to discharges with nitrogen seeding

As described above roughly 30% of the nitrogen atoms seeded during discharges 27092 and 27169 are not contained in the residual gases of these discharges. The measurement done on 2011-06-20 showed that ammonia is adsorbed at the tungsten surface of ASDEX Upgrade and hence is retained in the vessel. Furthermore it is known that nitrogen molecules show a similar behavior. Hence at least a part of the missing nitrogen atoms probably stick at the surface of the plasma vessel as adsorbed nitrogen and ammonia molecules. During the next discharges the ammonia and nitrogen molecules are probably released from the surface and thus can be found in the residual gas. To estimate the total number of formed ammonia molecules the discharges subsequent to discharges with nitrogen seeding have to be investigated too.

On the experimental day 2011-06-21 two discharges with nitrogen seeding (27169 and 27172) followed by one (27171) or respectively two discharges (27176 and 27177) without nitrogen seeding were performed. In figure 4.17 the intensities measured during and after discharge 27171 are shown together with the measured intensities of 27082 (reference without nitrogen seeding) and 27169 (nitrogen seeding). As depicted in figure 4.16 again a constant plasma current I_P and toroidal magnet field BT is applied throughout discharge 27171 (figures a) and b)). But compared to discharges 27082 and 27169 the duration of discharge 27171 is lesser. As shown in figures c), e) and f) significant fluctuations of the line averaged density n_e, the pressure at the divertor p and injected deuterium flux F occur. The applied auxiliary heating power is shown in figure d), the heating power is very low compared to discharges 27082 and 27169, probably resluting in a lesser production of impurities.

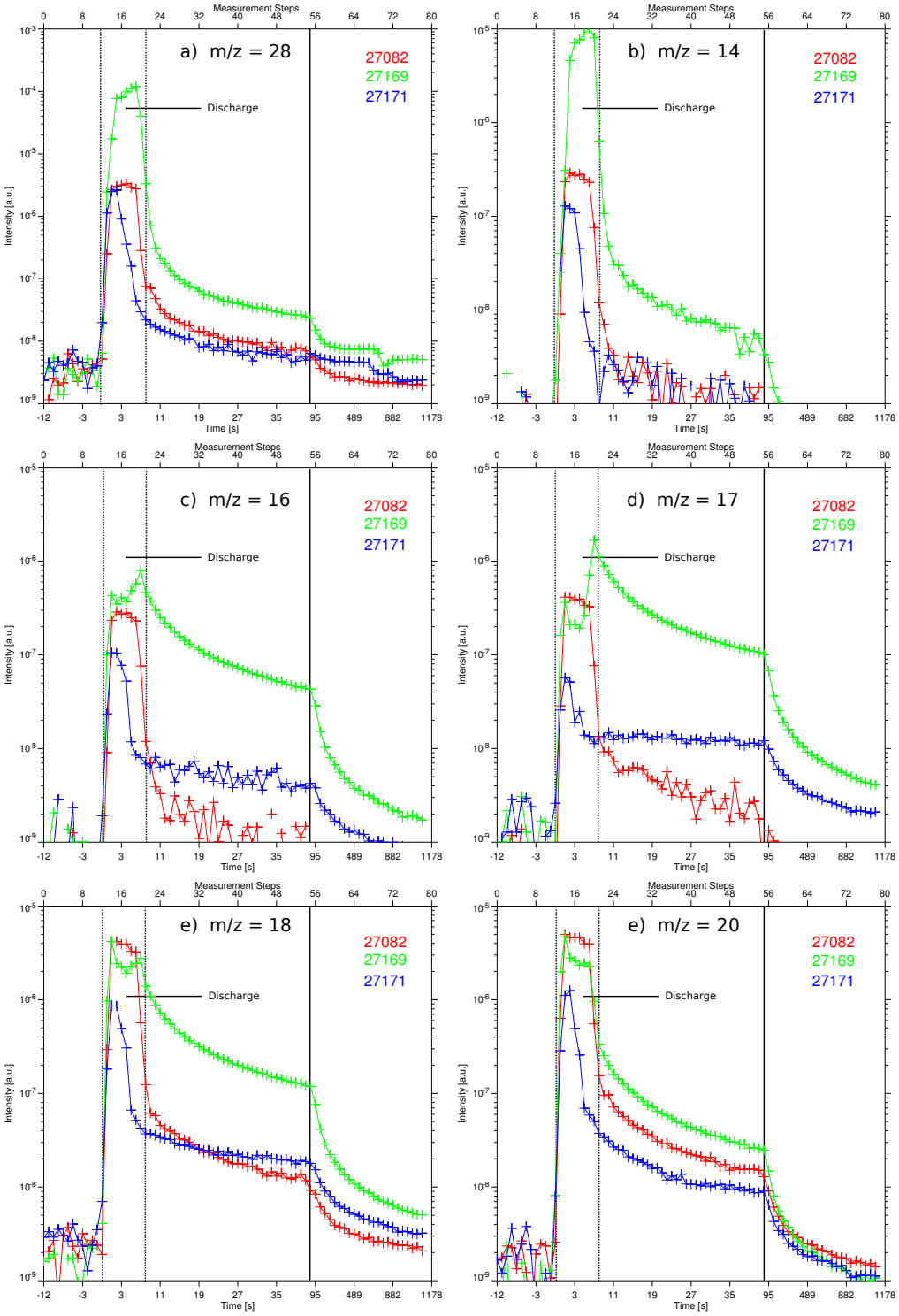

Figure 4.17: *Comparison of the intensities measured by HPQI at m/z =28 (a), m/z =14 (b), m/z =16 (c), m/z =17 (d), m/z =18 (e) and m/z =20 (f) for non nitrogen seeded discharge 27082, nitrogen seeded discharge 27169 and subsequent discharge 27171*

Due to quite different global parameters (e.g. heating power), especially due to lesser heating the measured intensities during discharge 27171 are remarkable lower compared during discharges 27082 and 27169. Furthermore the time dependence of the intensities changes. While the intensities during discharge 27082 and 27169 remain almost stable for a few seconds this is not the case for the intensities measured during discharge 27171. The maximal measured intensities at m/z =28 and m/z =14 are quite equal for discharges 27171 and 27082. After the discharge hardly any difference is visible. The measured intensities at m/z =16, m/z =17, m/z =18 and m/z =20 are clearly lower during discharge 27171 compared to 27169 and 27082, but after the discharge these intensities exceed the intensities after 27082 slightly. The intensities measured at these four mass to charge ratios decline much faster after discharge 27082 than after discharge 27171. Furthermore the distribution of the intensity changes, the highest measured intensity is now located at m/z =18, whereas after discharge 27082 the highest intensity can be found at m/z =20. The intensity distribution after 27171 and 27169 is quite similar, but the measured intensities after 27169 are clearly higher.

These changes in the measured intensities indicate that the composition of the residual gas has changed compared to 27082 and is similar to the composition after 27169. For a more sophisticated evaluation the partial pressures of methane, water and ammonia are again determined by the fit routine (see figure 4.18). It shows up that ammonia is the dominating impurity after discharge 27171. In total $2.0 \cdot 10^{20}$ ammonia molecules can be found in the residual gas during and after discharge 27171 (see figure 4.19). This value is equal to 50% of the ammonia molecules contained in the residual gas of discharge 27169. The HDRatio within the ammonia molecules is slightly lower compared to discharge 27169. Whereas the intensities measured at m/z =16, m/z =17, m/z =18 and m/z =20 are significantly lower during discharge 27171 compared to 27082 this is not the case for the intensity at m/z =14 and m/z =28. Hence surplus nitrogen can be found during the discharge. As the global parameters of 27082 and 27171 are quite different no background correction can be applied. In figure 4.20 the quantity of nitrogen atoms in the residual gases of discharge 27169 and 27171 contained in nitrogen or ammonia molecules is shown. As stated above no background correction can be performed. Therefore the shown values for nitrogen during and after discharge 27171 are too high as nitrogen is always present in the plasma vessel due to air leakage. In total 74% of nitrogen atoms seeded during discharge 27169 are found in the residual gases of discharges 27169 and 27171.

Figure 4.19 illustrates the distribution of nitrogen atoms on nitrogen and ammonia molecules contained in the residual gas. The amount of nitrogen atoms in nitrogen molecules and ammonia molecules is almost equal. The vast majority of the ammonia molecules are found after the discharge whereas the nitrogen molecules are distributed homogeneously during and after the discharge. In figure 4.20 the calculated quantities of nitrogen atoms in nitrogen and ammonia (different scale) for the five discharges are shown. In this figure 'residual gas' refers to the sum of nitrogen atoms found in pumped nitrogen molecules and ammonia molecules. During discharges 27169 and 27172 a total of $1.4 \cdot 10^{22}$ nitrogen atoms have been seeded. In total 84% of the seeded nitrogen atoms can be found in the residual gas contained in nitrogen and ammonia molecules pumped during discharges 27169, 27171, 27172, 27176 and 27177. 76% are pumped in the form of nitrogen molecules. The vast majority of nitrogen molecules can be found in the residual gas of the nitrogen seeded discharges 27169 and 27172. 8% of the seeded nitrogen atoms have formed ammonia molecules. In contrast to nitrogen the quantity of ammonia molecules is roughly equal in all 5 discharges. The amount of ammonia found in the residual gas of nitrogen seeded discharge is only a factor of two higher then the amount found in non nitrogen seeded discharge 27171. 16% of the seeded nitrogen atoms are not found in the residual gas of these five discharges, they are probably still adsorbed at the surface of the vessel or the cryo pump.

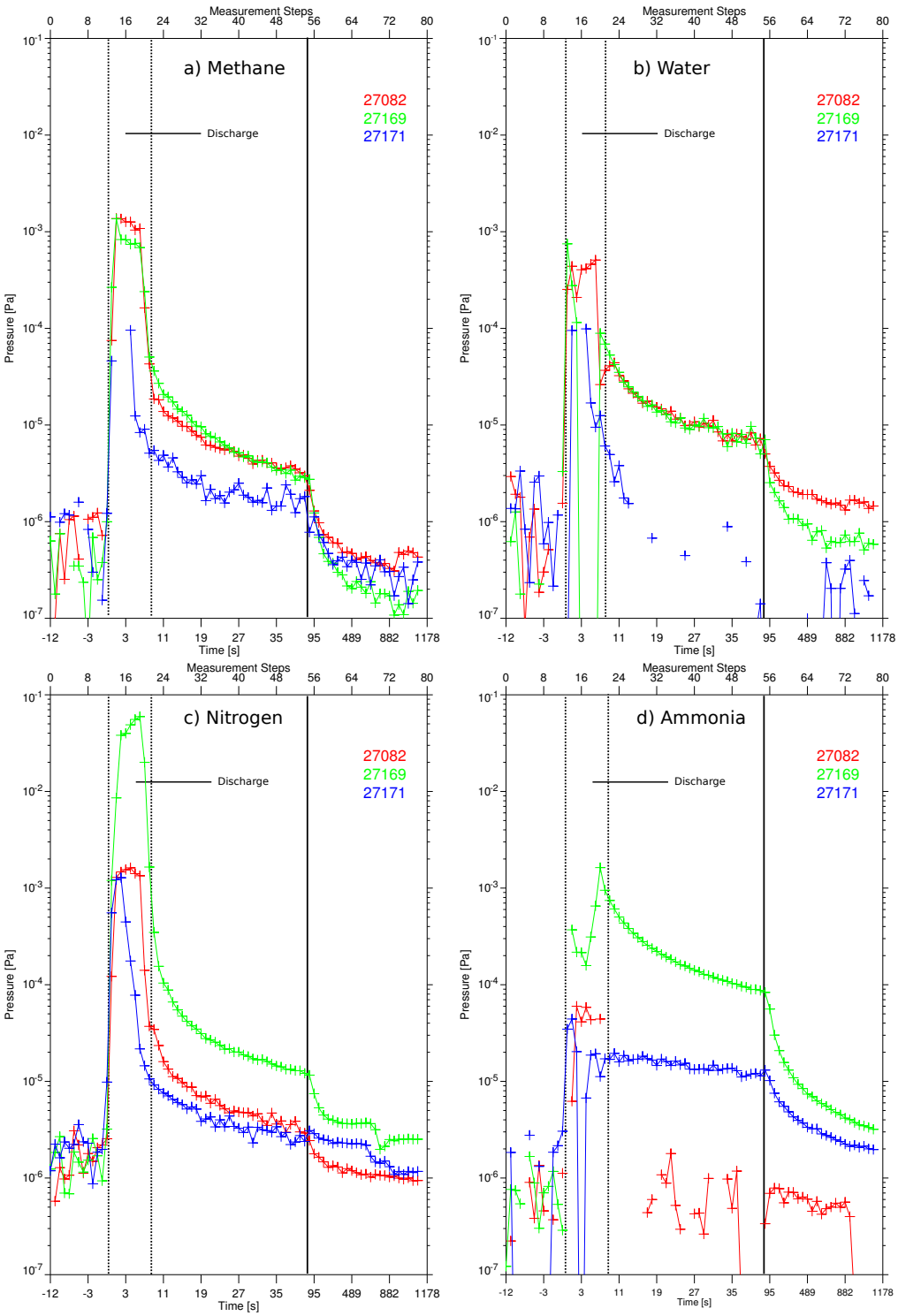

Figure 4.18: *Comparison of the calculated partial pressures of methane, water, ammonia and nitrogen for non nitrogen seeded discharge 27082, nitrogen seeded discharge 27169 and subsequent discharge 27171*

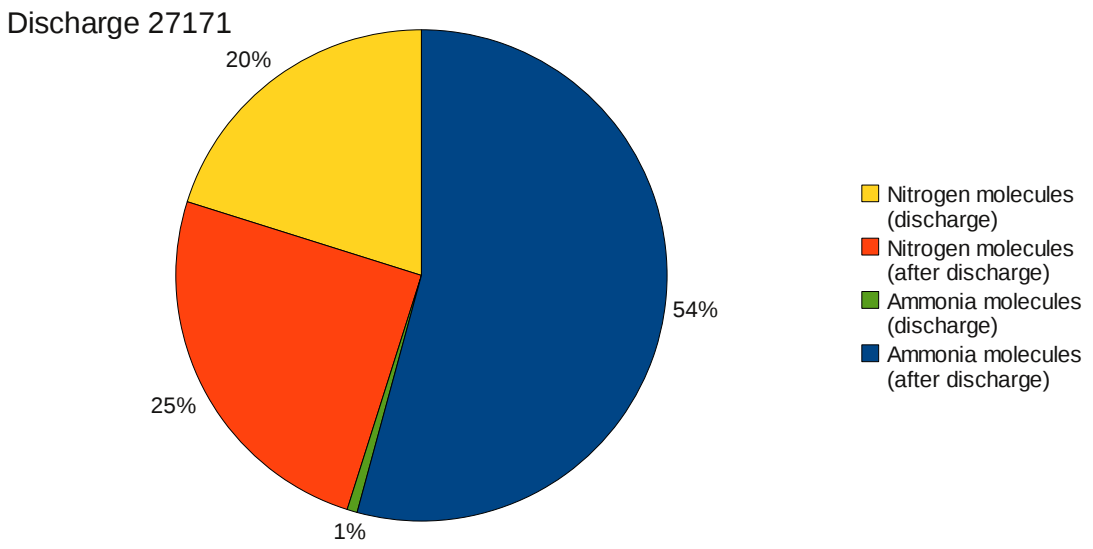

Figure 4.19: *Quantity of nitrogen atoms contained in nitrogen molecules and ammonia molecules for non nitrogen seeded discharge 27171 subsequent to nitrogen seeded discharge 27169*

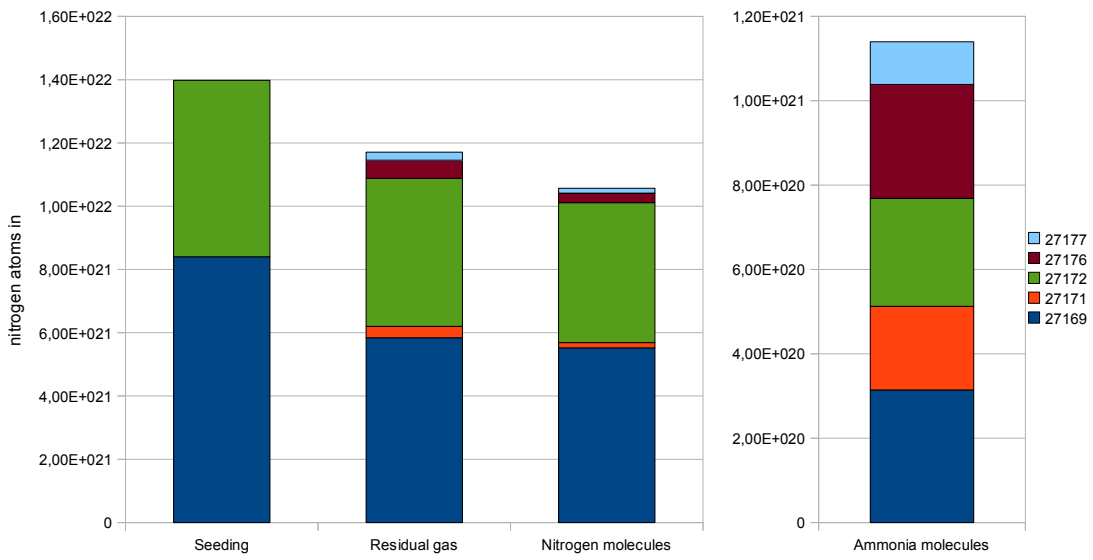

Figure 4.20: *Nitrogen atoms in nitrogen and ammonia molecules (different scale) during and after discharges 27169, 27171, 27172, 27176 and 27177 . Residual gas refers the total number of nitrogen atoms pumped in nitrogen and ammonia molcules*

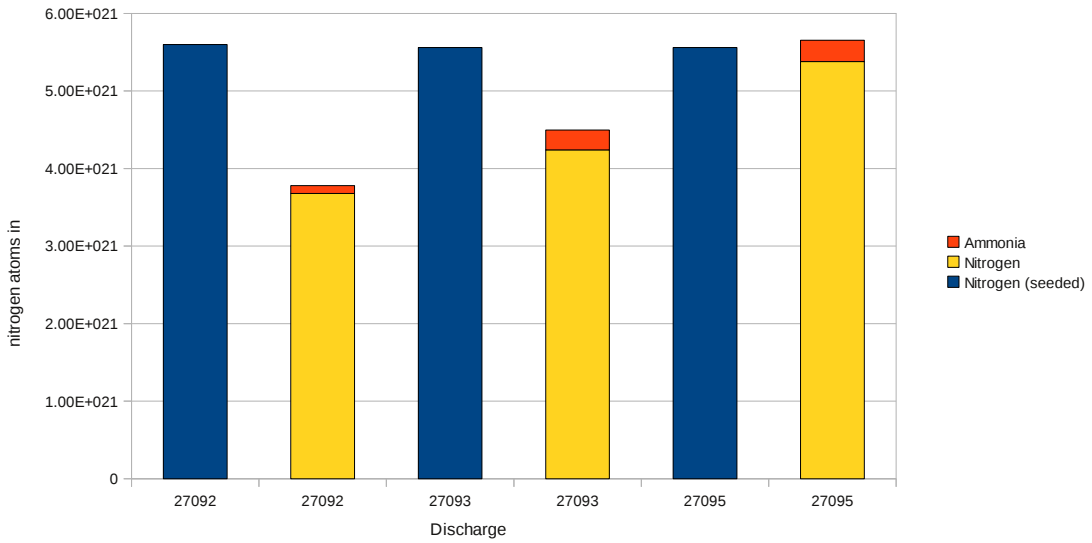

Figure 4.21: *Pumped nitrogen atoms in nitrogen molecules or ammonia molecules during and after discharges 27092, 27093 and 27095*

4.4 Consecutive discharges with nitrogen seeding

During each discharge from 27092 to 27095, with exception of 27094, roughly $2.80 \cdot 10^{21}$ nitrogen molecules were seeded. Discharge 27094 was not successful and therefore can be neglected. Consequently the development of the concentration of molecular nitrogen and ammonia can be examined for consecutive discharges with nitrogen seeding. As shown in table 4.1 the three investigated discharges are quite similar to each other. In figure 4.21 the pumped nitrogen atoms broken down to molecular nitrogen and ammonia are shown. An enrichment of ammonia and nitrogen is clearly visible from 27092 to 27095. While the amount of seeded nitrogen stays approximately constant the amount of ammonia found in the residual rises about by more than a factor of two. The HDratio of ammonia decreased from discharge to discharge as an increasing part of the ammonia is produced in earlier discharges and therefore more and more protium is replaced by deuterium for ammonia molecules adsorbed at the surface of the plasma vessel. It should be noted that after discharge 27095 a glow discharge was performed. While during the glow discharge the partial pressure of ammonia stays rather constant, the partial pressure of nitrogen rises at least one order of magnitude. Therefore roughly $0.26 \cdot 10^{21}$ 'additional' nitrogen molecules can be found in the residual gas. During discharge 27095 the quantity of seeded nitrogen atoms is roughly equal to the number of nitrogen atoms contained in pumped nitrogen molecules and ammonia molecules. Hence the surface of the plasma vessel is saturated with nitrogen and ammonia molecules.

4.5 Nitrogen seeding experiments in hydrogen L-Mode plasmas

Until now the residual gases of discharges with nitrogen seeding in deuterium plasma were analyzed. For the evaluation of the measured data three problems have to solved.

1. The presence of deuterium shifts the base peak of methane, water and ammonia towards m/z =20.
2. There is always a certain background of nitrogen in the plasma vessel due to air leakage.
3. Discharges are often too different to compare them easily.

On the 2011-07-28 a total of eleven discharges with $^{15}N_2$ seeding into hydrogen plasmas were performed. As the natural abundance of ^{15}N is below 0.5% almost the entire content of $^{15}N_2$ in the vessel was due to seeding. Additionally almost no deuterium is expected to be contained within the formed methane, water

Compound	Base peak
$^{12}CH_4$	m/z =16
$^{13}CH_4$	m/z =17
H_2O	m/z =18
$^{15}NH_3$	m/z =18

Table 4.2: *Base peaks of the expected methane, water and ammonia molecules in the residual gas*

or ammonia molecules. But as $^{15}N_2$ was seeded, probably $^{15}NH_3$ will mainly be formed, therefore the expected base peak of ammonia is located at m/z =18. Furthermore $^{13}CH_4$ is seeded, hence two different methane species are probably contained in the residual gas, CH_4 (base peak m/z =16) and $^{13}CH_4$ (base peak m/z =17). Additionally water is present in the plasma vessel of ASDEX Upgrade. The expected base peaks are summarized in table 4.2 But as deuterium is still present in the plasma vessel, some hydrogen atoms will be replaced by deuterium atoms. Therefore different HDratios for methane, water and ammonia have still to be taken into account. In contrast to previously investigated discharge the eleven discharges performed on 2011-07-28 are very similar. Furthermore the amount of seeded nitrogen is almost constant for all eleven discharges. Hence this sequence yields the possibility to investigate the development of the content of ammonia and nitrogen in the residual gas for subsequent discharges with nitrogen seeding. The amount of seeded nitrogen molecules per discharge is roughly $2.30 \cdot 10^{20}$ and thus about one order of magnitude smaller than during discharges 27092, 27093 and 27095. Therefore it is possible to investigate if a certain amount of nitrogen is necessary for a significant production of ammonia. First the measured intensities at m/z =12, m/z =13, m/z =16, m/z =17, m/z =18 and m/z =30 before, during and after L-Mode discharge 27381, 27383, 27387 and 27391 are compared. Then the quantity of formed ammonia molecules is. calculated for all eleven discharges.

4.5.1 Development of the measured intensities at the methane-water-ammonia group

As stated above the intensities at six different mass to charge ratios measured during and after discharges 27381, 27383, 27387 and 27391 are investigated in detail.

- 27381: Reference discharge without $^{15}NH_3$ or $^{13}CH_4$ seeding.
- 27383: 2nd discharge with $^{15}NH_3$ and $^{13}CH_4$ seeding.
- 27387: 6th discharge with $^{15}NH_3$ and $^{13}CH_4$ seeding.
- 27391: 10th discharge with $^{15}NH_3$ and $^{13}CH_4$ seeding.

In total the development of the measured intensities at 6 different mass to charge ratios is presented within this chapter:

- m/z =12: specific for $^{12}CH_4$, which is formed by carbon atoms adsorbed at the surface of the plasma vessel, hence allowing a distinction between both methane species
- m/z =13: evoked by $^{12}CH_4$ and $^{13}CH_4$
- m/z =16: allows a distinction between $^{15}NH_3$ and $^{13}CH_4$
- m/z =17: allows a distinction between $^{15}NH_3$ and H_2O
- m/z =18: base peak of $^{15}NH_3$ and H_2O
- m/z =30: base peak of $^{15}N_2$

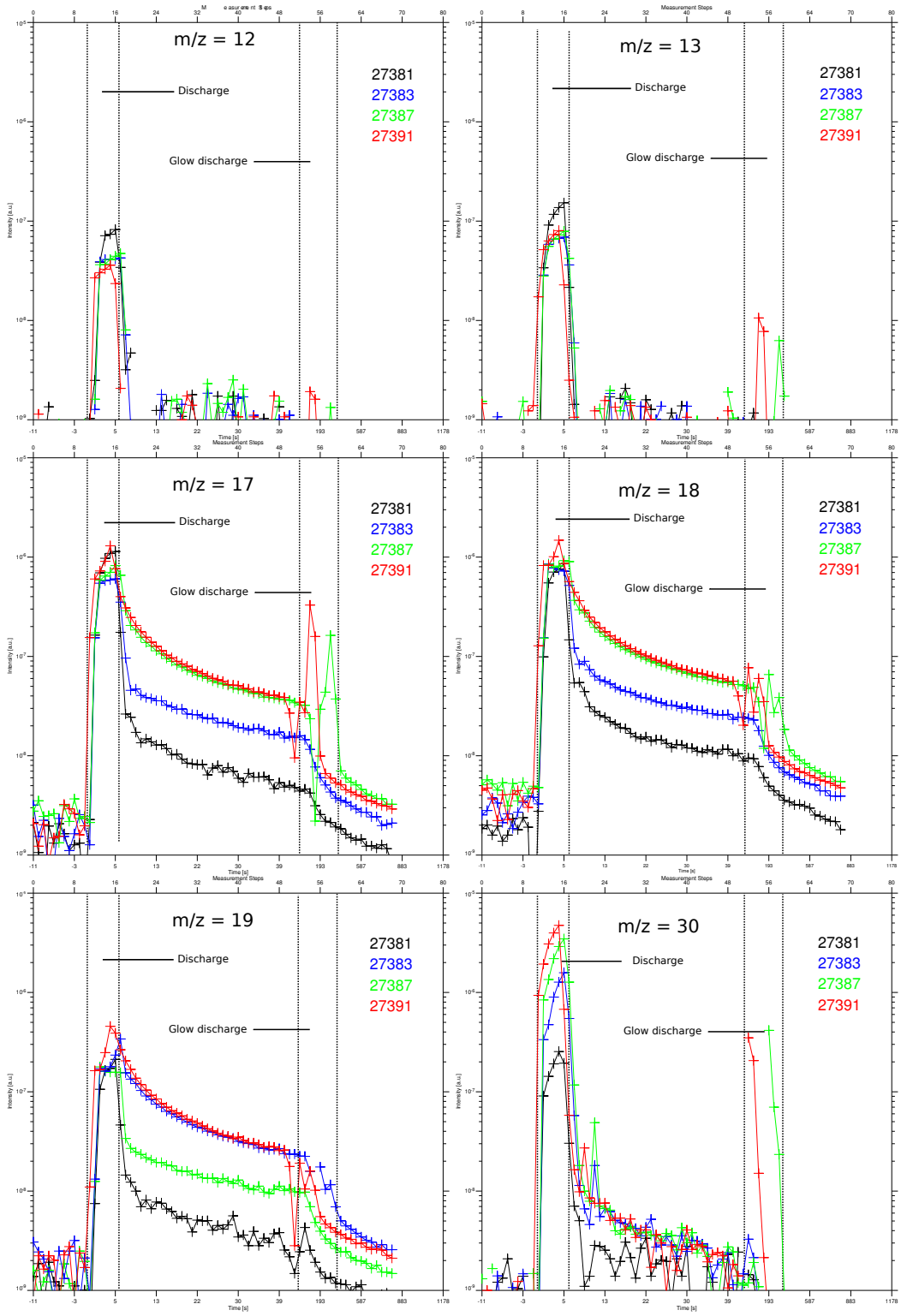

Figure 4.22: *Evolution of the intensities at m/z =12 (a), m/z =13 (b), m/z =16 (c), m/z =17 (d), m/z =18 (e) and m/z =30 (f) for discharges 27381, 27383, 27387, 27391*

The measured intensities for these 6 mass to charge ratios are shown in figure 4.22 In the bottom right corner the development of the intensity at m/z =30 (f) is shown. The intensity during discharge 27381 can hardly be evoked by $^{15}N_2$, but is probably due to ethane. The intensity at m/z =30 increases clearly from discharges 27381 to 27391, at least during the discharge. After the discharge the measured intensities are rather equal for discharges 27383, 27387 and 27391. At the top the intensities measured at m/z =12 (a) and m/z =13 (b) respectively are shown. For m/z =12 a clear decrease between 27381 and 27390 can be seen. The same trend is in principle visible for m/z =13. The intensity at m/z =17 (c), m/z =18 (d) and also m/z =19 (e) show a completely different behavior. After the discharge the measured intensities clearly increase from discharge 27381 to 27383, and from 27383 to 27387. But from discharge 27387 to 27391 the measured intensities show only a small increase. At the begin of the Analog Scan measurement of all discharges, with the exception of 27383, a glow discharge is performed in order to desorb impurities from the surface of the walls of the plasma vessel. As illustrated in 4.22 no clear increase of the intensity at m/z =18 (d) is visible, hence probably almost no ammonia is removed from the walls of the plasma vessel. But a clear reaction at m/z =17 (c) can be seen, probably methane is released into the residual gas.

4.5.2 Development of the content of ammonia ($^{15}NH_3$) and nitrogen ($^{15}N_2$) in the residual gas

As the measured intensities at m/z =12 and m/z =13 show roughly the same development over the four shown discharges it is unlikely that a huge amount of $^{13}CH_4$ can be found in the residual gas. In fact the measured intensity during discharge 27381 (reference shot without $^{13}CH_4$ or $^{15}N_2$ seeding) is the highest for both mass to charge ratios. Hence the desorption of methane molecules from the surface of the plasma vessel seems to be hampered by nitrogen. The development of the intensity at m/z =30 shows a clear trend towards enrichment of nitrogen. The intensity at m/z =17, m/z =18 and m/z =19 are interpreted as ammonia by the fit routine for discharges 27383, 27387, 27391. Hence only a small amount of ammonia can be found in the residual gas of discharge 27383. As during the glow discharge after discharge 27383 the highest intensities at these three mass to charge ratios are measured, it is quite unlikely that during glow discharges a huge amount of ammonia is released from the walls of the plasma vessel. In figure 4.23 the quantity of $^{15}NH_3$ and $^{15}N_2$ molecules in the residual gas is shown. $^{15}N_2$ and also $^{15}NH_3$ detected during the glow discharge is once again neglected, also a background correction for $^{15}N_2$ is not performed. For discharges 27383 to 27386 a enrichment of ammonia in the residual can be observed, after discharge 27386 the quantity of ammonia molecules remains rather constant. The quantity of $^{15}N_2$ increases from discharge to discharge. A remarkable part of the seeded ^{15}N is found in the residual gas during the glow discharge. As stated above is the evaluation during glow discharges hampered by a time resolution of about a minute. The quantity of $^{15}N_2$ molecules in the residual during the glow discharges is roughly evaluated and shown in figure 4.24. After discharge 27383 no glow discharge was performed. Hence the quantity of $^{15}N_2$ molecules in the residual gas of discharge 27384 was exceptional high, and the quantity exceptional low for discharge 27387. During discharges 27383 to 27389 more ^{15}N atoms are seeded that can be found in the residual gas. Thus a enrichment of $^{15}N_2$ molecules and also $^{15}NH_3$ adsorbed at the surface walls is likely. During discharges 27390, 27391 and 27392 ^{15}N atoms seem to be removed from the surface of the plasma vessel. It should be noted that for discharge 27387 to 27391 quantity of seeded ^{15}N atoms is within the expected error margin equal to the quantity of ^{15}N contained in $^{15}N_2$ and $^{15}NH_3$ molecules in the residual gas. But a clear towards more $^{15}N_2$ molecules in the residual gas is visible. By comparing figures 4.23 and 4.24, it gets clear that this trend is mainly due to increase of $^{15}N_2$ molecules during the glow discharges in the residual gas. In total for all eleven discharges 2738 - 27392 have been $5.23 \cdot 10^{21}$ nitrogen atoms seeded and $1.01 \cdot 10^{21}$ ammonia molecules found in the residual gas. Hence roughly 20% of the seeded nitrogen atoms have formed ammonia molecules. Hence the formation of ammonia has been observed for nitrogen seeded deuterium H-mode plasmas as well as for protium L-mode plasmas. No significant differences regarding production rate could be observed. For both types a suppression of the production of methane shows up.

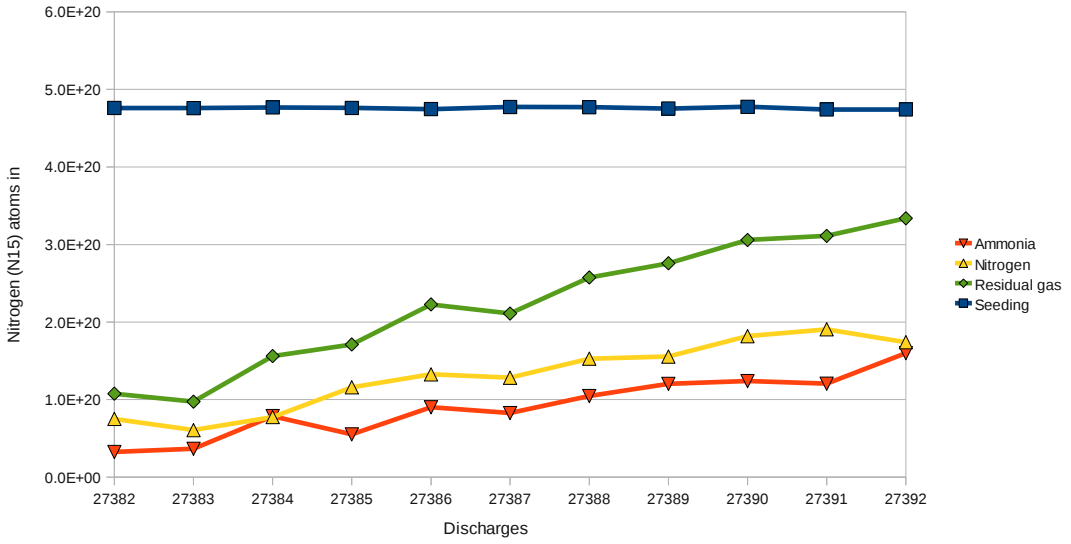

Figure 4.23: *Pumped* ^{15}N *atoms in* $^{15}N_2$ *and* $^{15}NH_3$ *molecules (neglecting the glow discharge). Residual gas refers to the sum of nitrogen atoms pumped in nitrogen and ammonia molecules.*

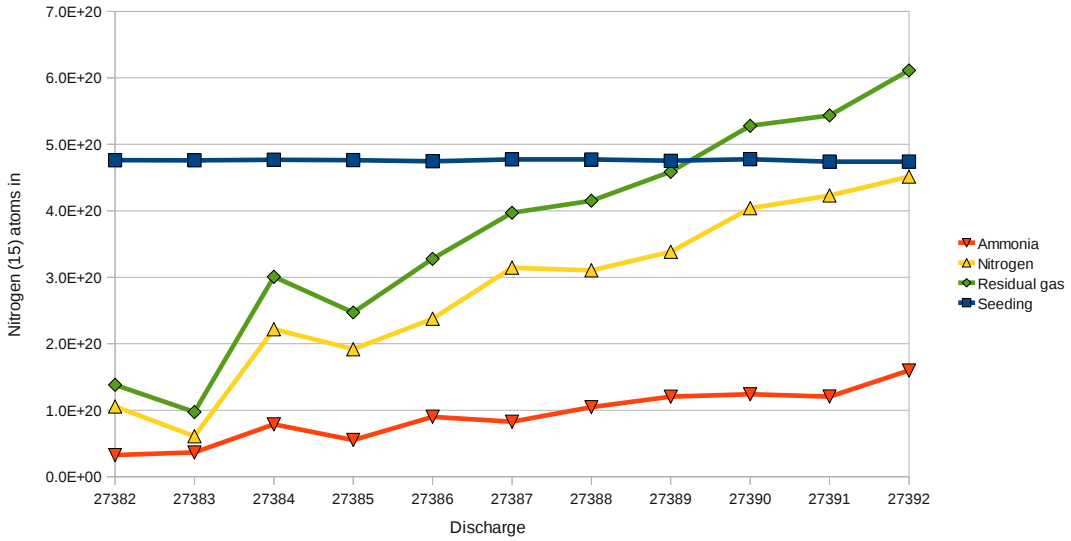

Figure 4.24: *Pumped* ^{15}N *atoms in* $^{15}N_2$ *and* $^{15}NH_3$ *molecules (taking the glow discharge into account). Residual gas refers to the sum of nitrogen atoms pumped in nitrogen and ammonia molecules.*

Chapter 5

Summary and Conclusion

Within this diploma thesis the formation of ammonia during nitrogen seeded discharges was investigated. Mass spectrometry was used as the main diagnostic to analyze the residual gases of several non nitrogen seeded discharges, as well as nitrogen seeded discharges. For the deconvolution of the measured mass spectra a method was developed that takes the different isotopic distributions of protium and deuterium in different impurity molecules into account. It is based on a model proposed by Poschenrieder. By applying this method the residual gases of discharges in an all tungsten fusion device were analyzed quantitatively for the first time.

A significant production of ammonia in nitrogen seeded discharges was observed during deuterium H-mode discharges as well as during protium L-mode discharges. Up to 8% of the seeded nitrogen atoms have formed ammonia during H-mode deuterium discharges. The unexpected high concentration of protium in the ammonia molecules calls for a investigation of the production mechanism of ammonia in detail. A transient behavior of nitrogen seeded discharges have been found. For the applied fluxed of roughly $2 \cdot 10^{20}$ nitrogen molecules per second typically three H-mode discharges were necessary to reach an equilibrium state with a constant inventory of about $3 \cdot 10^{21}$ nitrogen atoms. It was shown that ammonia is still present in subsequent non nitrogen seeded discharges in total amounts that limit the operational space of ASDEX Upgrade. Consequently glow discharges and conditioning discharges were applied in order to reach non nitrogen conditions again. A clear effect of the nitrogen seeding on the production of hydrocarbons was observed. With the beginning of the nitrogen injection the partial pressure of methane dropped by a factor of two.

Even without plasma operation a significant retention of ammonia was observed when protonated ammonia was filled into the plasma vessel of ASDEX Upgrade. The formation of ammonia tungsten complexes at the walls of the tungsten vessel was suggested. A clear indication is the observation of partly deuterated ammonia molecules during the course of the measurement. In contrast to this experiment performed at ASDEX Upgrade no significant retention nor partly deuterated ammonia could be observed when ammonia was filled into a stainless steel vessel. For the applied -unoptimized- partial pressure of 0.01 Pa removal efficiencies comparable to present wall conditioning methods like oxygen glow discharges or ion cyclotron wall conditioning (ICWC) are achieved. At the same time the injection of protonated ammonia may serve as a diagnostic tool for other cleaning methods. As ammonia reaches all surfaces in the vessel, the injection of ammonia could reveal if all surfaces have been conditioned by the applied technique. Therefore further confirmation of the proposed reaction mechanism of ammonia adsorbed at the surface of the plasma vessel is required.

Bibliography

[ABo04] A. H. Boozer, Physics of magnetically confined plasmas, Review of modern Physics 76, 2005

[ASc11] A. Scarabosio et al., 64th IUVSTA Workshop on Practial Applications of Methods of Gas Dynamics for Vacuum Science and Technology, Leinsweiler 2011

[AKa10] A. Kallenbach et al., Divertor power load feedback with nitrogen seeding in ASDEX Upgrade, Plasma Phys. Control Fusion 52, 055002, 2010

[CHo06] C. Hopf et al., Oxygen Glow Discharge Cleaning at ASDEX Upgrade J. Nucl. Mater., 363-365, 882, 2006

[DLe84] D.H. Lenz and WM. C. Conner Jr., Computer Analysis of the cracking patterns of deuterated hydrocarbons, Analytica Chimica Acta 173, 227, 1985

[DMa95] D.P. Mason et al, The sticking and dissociation of NH_3 on W(110): a three-state model, Surface Science 330, 239, 1995

[FRe09] Felix Reimold, Praktikumsberich: Massenspektrometrie am ASDEX Upgrade

[FWa82] F. Wagner et al., Regime of Improved Confinement and High Beta in. Neutral-Beam-Heated Divertor Discharges of the ASDEX Tokamak

[FTa10] F. L. Tabarés et al. Suppression of Tritium Retention in Remote Areas of ITER by Nonperturbative Reactive Gas Injection, Physical Review Letters, 105, 175006, 2010

[GPr89] G. L. Price and E. Iglesia, Matrix Method for Correction of Mass Spectra in Deuterium Exchange Applications, Ind. Eng. Chem. Res. 28, 844, 1989

[HAn] http://www.hidenanalytical.com/index.php/en/cracking-patterns (November 2011)

[HMu09] H.W Müller et al., SOL and divertor inverstigations in Nitrogen seeded discharges, 36th EPS Conference on Plasma Physics Sofia 2009/ ECA Vol33P-1156, 2009

[JHe07] J.H. van Helden et al., Detailed Study Detailed study of the plasma-activated catalytic generation of ammonia in N2-H2 plasmas, Journal of Applied Physics 101, 043305, 2007

[KTi09] K. Tichmann et al., Determination of the sticking probability of hydrocarbons on an amorphous hydrocarbon surface, Phys. Scr. T138, 014015, 2009

[MKa03] M. Kaufmann, Plasmaphysik und Fusionsforschung, Teubner, 2003

[MMa06] M. Mayer et al., Further insight into the mechanism of hydrocarbon layer formation below the divertor of ASDEX Upgrade, Nucl Fusion 46, 914, 2006

[NIST(1)] http://www.nist.gov/pml/data/ionization/index.cfm (November 2011)

[NIST(2)] http://webbook.nist.gov/chemistry/ (November 2011)

[PDa68] P. T. Dawson and R. S. Hansen, Field Emission Study of the Adsorption of Ammonia on Tungsten, The Journal of Chemical Physics Volume 48, Number 2, 623, 1968

[PMi86] Phillip E. Miller, M. Bonner Denton, The Quadrupole Mass Filter: Basic Operating Concepts, Journal of Chemical Education 63 No 7, 617, 1986

[PEs68] P. J. Estrup and J. Anderson, Adsorption and Decomposition of Ammonia on a Single-Crystal Tungsten (100) Surface, The Journal of Chemical Physics Volume 49, Number 2, 523, 1968

[TWa07] J. Throck Watson, O. David Sparkman, Introduction to Mass Spectrometry, Wiley, 2007

[TWa10] T. Wauters at al., J. Nucl. Mater. (2010), doi:10.1016/j.jnucmat.2010.11.072

[VRo09(1)] V.Rohde et al. Wall retention of deuterium and gaseous impurities in all tungsten ASDEX Upgrade, Plasma Phys. Control. Fusion 51, 124033, 2009

[VRo09(2)] V. Rohde et al., Dynamic and static deuterium inventory in ASDEX Upgrade with tungsten first wall, Nucl. Fusion 49, 085031, 2009

[WPo90] W. Poschenrieder et al., Recycling of gaseous impurities in ASDEX, Journal of Nuclear Materials 176 & 177, 381, 1990

[WPo95] W. Poschenrieder et al. Molecular impurities in ASDEX UPGRADE plasma discharge, Journal of Nuclear Materials 220-222, 36, 1995

[WAt87] W. P. Atkinson, Physikalische Chemie, VCH, 1987

[WCo] Wikimedia Commons

Appendix A

Appendix

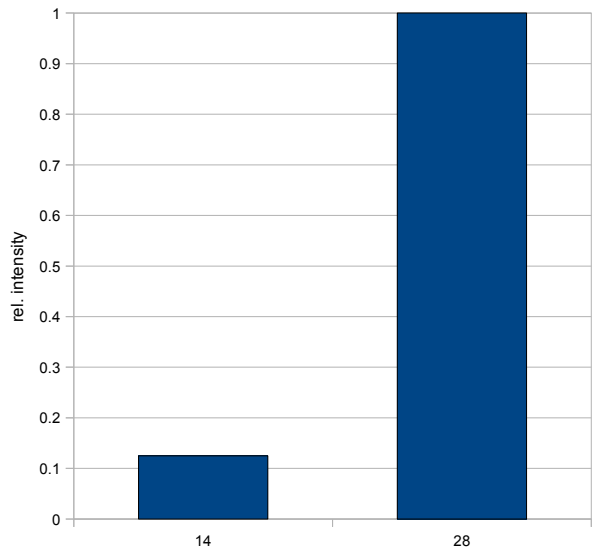

Figure A.1: *Used cracking pattern of nitrogen normalized to the intensity at m/z =28*

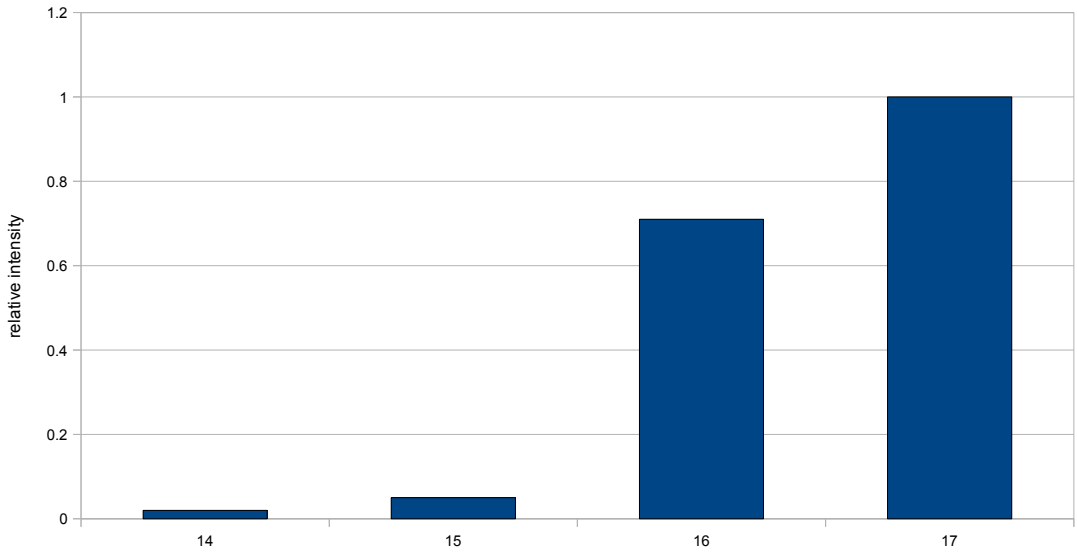

Figure A.2: *Used cracking pattern of protonated ammonia normalized to the intensity at m/z =17*

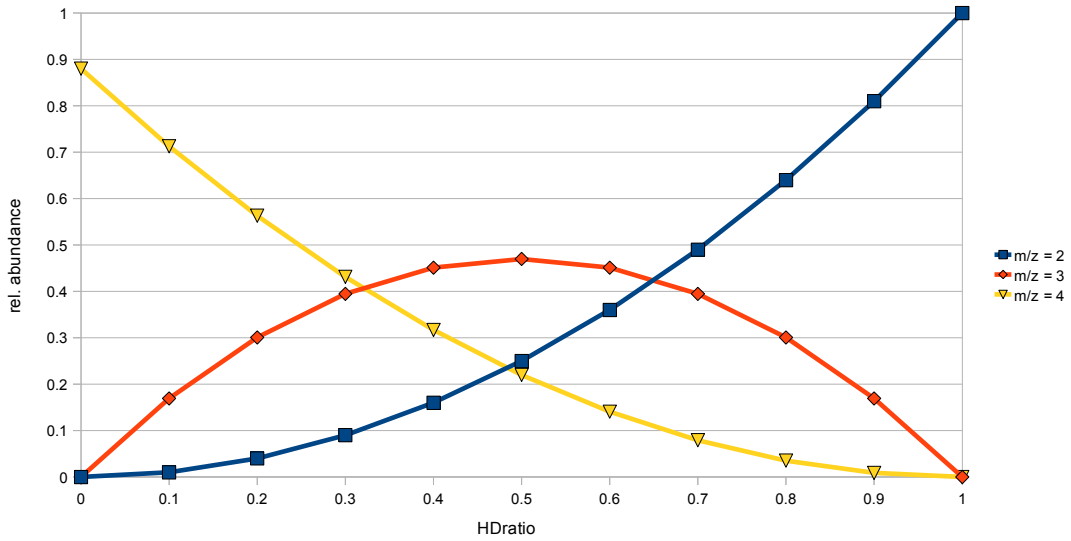

Figure A.3: *Calculated cracking pattern of hydrogen as a function of the HDratio*

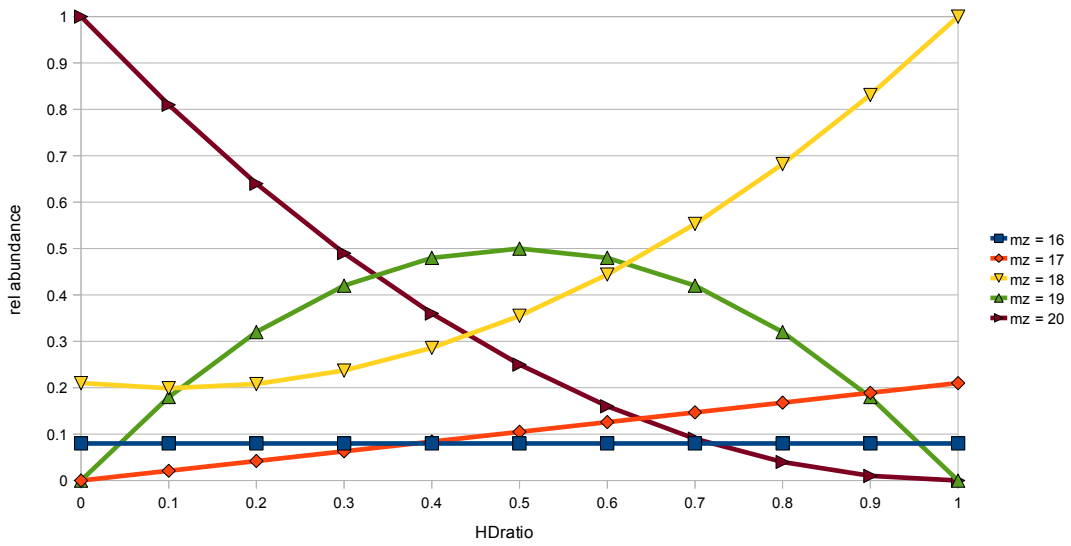

Figure A.4: *Calculated cracking pattern of water as a function of the HDratio*

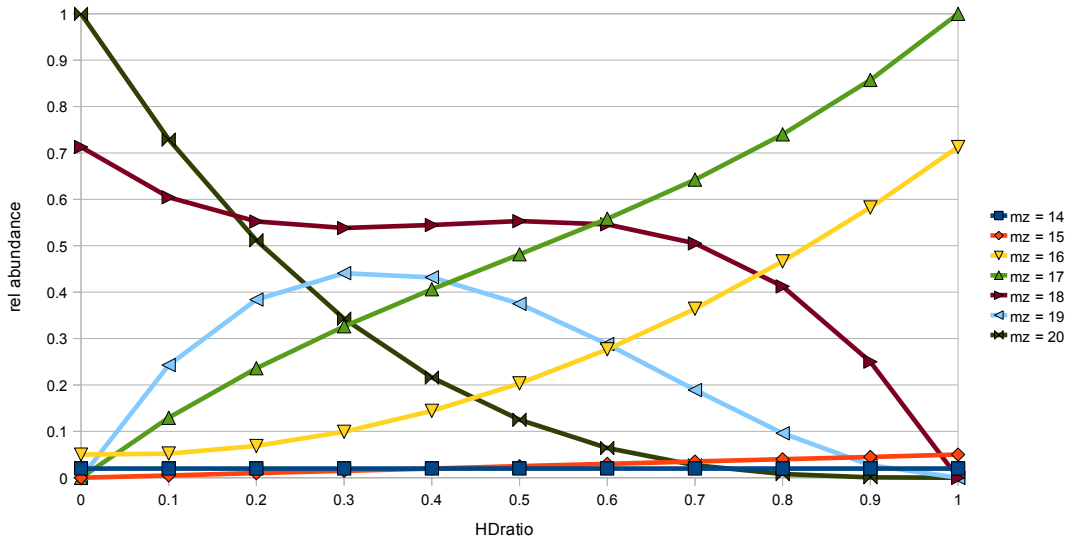

Figure A.5: *Calculated cracking pattern of ammonia as a function of the HDratio*

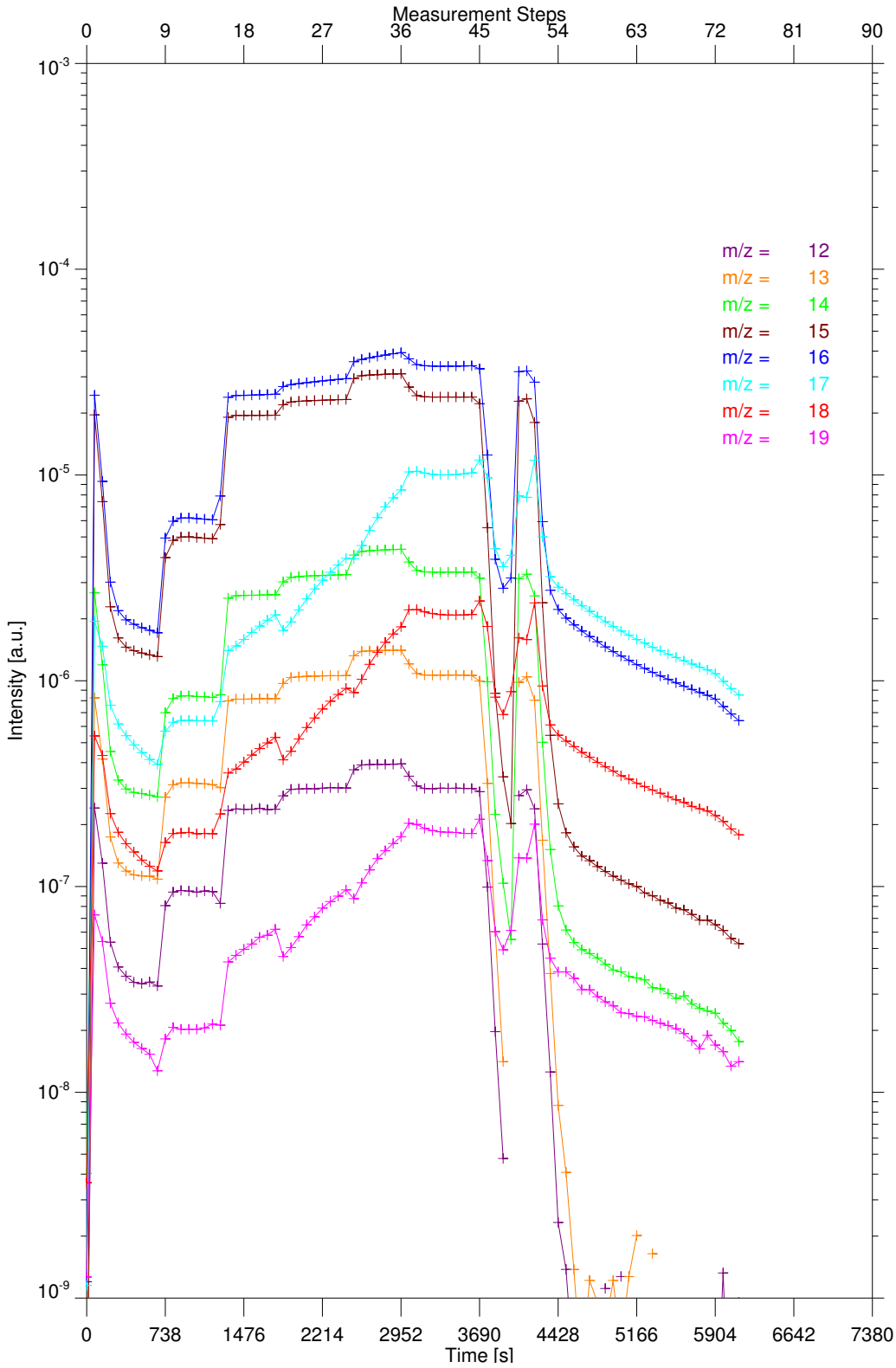

Figure A.6: *Intensities measured by HPQO at m/z =12 to m/z =19 for the injection of a methane and ammonia containing gas mixture into ASDEX Upgrade on 2011-06-20*

Acknowledgements

During my diploma thesis at the Max Planck Institut für Plasma Physik I experienced a lot of help, support and interest. Therefore I owe thanks to everybody.

In particular I would like to thank

- **Prof. Dr. Sibylle Günter** for giving me the opportunity to perform my diploma thesis at the Max Planck Institut für Plasma Physik

- My supervisor **Dr. Volker Rohde** for his patience, his expertise, the encouraging discussions and for offering me a helping hand whenever a problem occured

- **Dr. Thomas Schwarz-Selinger** for his advice, the fruitful discussions and all the time and work he invested

- **Dr. Rudolf Neu** for his interest and his uplifting commentary

- My family, especially my parents **Anneliese** and **Franz**, my aunt **Maria** and my uncle **Fritz** for the support that enabled me so much. I would also like to thank for the encouragement and advice throughout my studies.

- **Tamara and Alexander Naumann** for offering me a home for the last year

- **Anna** for being there for me, her encouraging believe in me and for giving me so much joy.

Erklärung

des Diplomanden

Name:

Vorname:

Mit der Abgabe der Diplomarbeit versichere ich, dass ich die Arbeit selbständig verfasst und keine anderen als die angegebenen Quellen und Hilfsmittel benutzt habe.

....

(Ort, Datum) (Unterschrift)